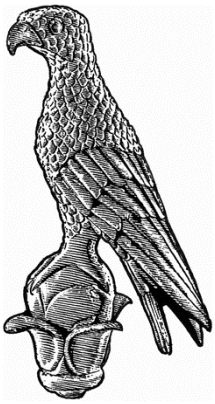

UNIVERSITY OF IOANNINA
SCHOOL OF PHYSICAL SCIENCES
DEPARTMENT OF PHYSICS

Study of (n,x) reactions for Erbium isotopes at energies higher than 17 MeV

MASTER THESIS

ELEME Zinovia

ACADEMIC SUPERVISOR

PATRONIS Nikolas, Assistant Professor, University of Ioannina

IOANNINA
MARCH 2017

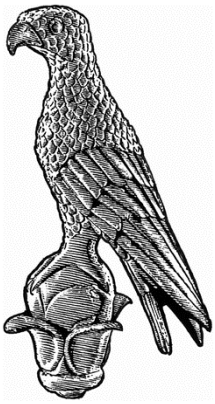

ΠΑΝΕΠΙΣΤΗΜΙΟ ΙΩΑΝΝΙΝΩΝ
ΣΧΟΛΗ ΘΕΤΙΚΩΝ ΕΠΙΣΤΗΜΩΝ
ΤΜΗΜΑ ΦΥΣΙΚΗΣ

Μελέτη των αντιδράσεων (n,x) σε ισότοπα του Ερβίου για ενέργειες μεγαλύτερες των 17 MeV

ΜΕΤΑΠΤΥΧΙΑΚΗ ΔΙΠΛΩΜΑΤΙΚΗ ΕΡΓΑΣΙΑ

ΕΛΕΜΕ Ζηνοβία

ΑΚΑΔΗΜΑΙΚΟΣ ΕΠΙΒΛΕΠΩΝ

ΠΑΤΡΩΝΗΣ Νικόλας, Επίκουρος Καθηγητής, Πανεπιστήμιο Ιωαννίνων

ΙΩΑΝΝΙΝΑ
ΜΑΡΤΙΟΣ 2017

"I have passed through fire and deep water, since we parted. I have forgotten much that I thought I knew, and learned again much that I had forgotten."

— *J.R.R. Tolkien, The Lord of the Rings*

Acknowledgment

First of all, I would like to thank Assis. Prof. Nikolas Patronis of the Physics Department of the University of Ioannina, who supervised the present thesis and gave me an insight of an appealing world, that of Nuclear Physics. He guided patiently my steps in the research field and gave me the opportunity to work on a distinctive, challenging and fascinating project by letting me take active roles and initiatives during both experimental and analysis process. Also, he supported me countless times with countless meetings and discussions, trying to find solutions to any incident that troubled me. I feel very grateful for all that I have learned from him over these years in personal, scientific and professional level and I could not imagine a better cooperation. Thank you Nikolas!

Moreover, I owe special thanks to my teacher Xenofon Aslanoglou, Assoc. Prof. of the University of Ioannina because he transmits me enthusiasm for this science. His office door was always open and he was always willing to share his experience with us and answer in a variety of queries that occasionally puzzled me. He is a teacher in the fullest sense of the word!

I am grateful to Roza Zanni-Vlastou, Prof. of the N.T.U.A. of the Department of Physics for the trust and the support that she shows me, as well as for the positive energy that always makes sure to carry around throughout the critical period of the experiment conduction. Along the same lines, I would like to express to Michael Kokkoris, Assoc. Prof. of the same Department, my gratitude for his meaningful instructions and advice, not to mention my joy, every time that he welcomes me to work among his team.

Furthermore, I owe special thanks to PhD candidate of the N.T.U.A. Antigoni Kalamara, for her valuable assistance while carrying out the experiments and everything else that arose along the way of the analysis process. I also want to thank Varvara Foteinou, Post doc Researcher of the Institute of Nuclear and Particle Physics N.C.S.R. “Demokritos”, for her help in the preparation of the Erbium Targets.

Additionally, I consider it my duty to thank Anastasios Lagoyannis, Senior Researcher and Michael Axiotis, Post doc Researcher of the Institute of Nuclear and Particle Physics N.C.S.R. “Demokritos”, for their assistance in carrying out the experiments and in data acquisition. Of course, this work became possible thanks to all the operators and the staff of the Tandem Accelerator Laboratory!

For my friend and colleague Efstathia Georgali, MSc student of the Physics Department of the University of Ioannina, I have only to say that she is the most optimistic person that I have ever known in my life and thus I thank her for the beautiful time we had within and outside the office. Working in such a pleasant atmosphere I found out that teamwork can indeed make the dreamwork!

In closing, I want to say thanks my family for the support that shows me in what I want to do and guides me and advises me when needed. Finally, I feel the need to thank my friends who supported me during the ups and downs on the path to this thesis work, directly or indirectly, with or without my notice, with large effort, with a smile or just a hug! I will not name them not because they are many but because they know. Thank you all!

Abstract

The aim of this work is the experimental study of the $^{162}Er(n,2n)^{161}Er$ and $^{167}Er(n,p)^{167}Ho$ nuclear reactions. The cross sections have been measured by means of the activation technique by using as reference reactions $^{197}Au(n,2n)^{196}Au$, $^{27}Al(n,a)^{24}Na$ and $^{93}Nb(n,2n)^{92m}Nb$. The quasi-monoenergetic neutron beams at 17.1, 18.1 and 19 MeV, were produced in the Tandem Van der Graaf 5.5 MV accelerator of the Institute of Nuclear and Particle Physics of N.C.S.R. “Demokritos”, by using the reaction $^{3}H(d,n)^{4}He$. The Erbium targets along with the reference foils were irradiated for each neutron beam energy for 10 h. For the measurement of the γ-ray activity of the samples, two HPGe detectors with 100% and one with 16% relative efficiency were used. After the energy calibration of the detection setup in the desired geometry, the absolute peak efficiency for the three HPGe detectors was estimated. From these data, the cross sections of the $^{162}Er(n,2n)^{161}Er$ and $^{167}Er(n,p)^{167}Ho$ nuclear reactions were determined for the first time at three neutron energies.

Περίληψη

Σκοπός αυτής της εργασίας είναι η πειραματική μελέτη των πυρηνικών αντιδράσεων $^{162}Er(n,2n)^{161}Er$ και $^{167}Er(n,p)^{167}Ho$ των οποίων η ενεργός διατομή μετρήθηκε μέσω της μεθόδου της ενεργοποίησης συγκριτικά με τις αντιδράσεις αναφοράς $^{197}Au(n,2n)^{196}Au$, $^{27}Al(n,a)^{24}Na$ και $^{93}Nb(n,2n)^{92m}Nb$. Οι ενεργές διατομές προσδιορίστηκαν για τρεις ενέργειες νετρονίων στα 17.1, 18.1 και 19 MeV. Τα πειράματα πραγματοποίθηκαν στις εγκασταστάσεις του επιταχυντή Tandem Van der Graaf 5.5 MV του Ινστιτούτου Πυρηνικής και Σωματιδιακής Φυσικής του Ε.Κ.Ε.Φ.Ε. “Δημόκριτος”. Οι ημι-μονοενεργειακές δέσμες νετρονίων και στις τρεις περιπτώσεις παράχθηκαν χρησιμοποιώντας την αντίδραση $^{3}H(d,n)^{4}He$. Για τις μετρήσεις των ενεργών διατομών χρησιμοποιήθηκαν δύο παστίλιες Ερβίου που αποτελούνται από σκόνη Er_2O_3. Οι στόχοι του Ερβίου μαζί με τους στόχους αναφοράς ακτινοβολήθηκαν για κάθε ενέργεια νετρονίων για 10 h. Για την μέτρηση της ενεργότητας των δειγμάτων, χρησιμοποιήθηκαν δύο HPGe ανιχνευτές με σχετική απόδοση 100% και ένας HPGe ανιχνευτής με 16%. Μετά την ενεργειακή βαθμονόμηση του ανιχνευτικού συστήματος στην επιθυμητή γεωμετρία, υπολογίστηκε η απόλυτη απόδοση για τους τρεις HPGe ανιχνευτές. Από τα δεδομένα, προσδιορίστηκαν για πρώτη φορά οι ενεργές διατομές των πυρηνικών αντιδράσεων $^{162}Er(n,2n)^{161}Er$ και $^{167}Er(n,p)^{167}Ho$ στις παραπάνω τρεις ενέργειες νετρονίων.

Contents

CHAPTER 1
INTRODUCTION

1.1 Motivation

The study of nuclear reactions is a research field with exceptional interest both for the Application field of Nuclear Engineering, Medicine and Energy but also for other areas such as the Nuclear Astrophysics, Cosmology and the Basic Research in Nuclear Physics. The problem of the dynamics of nuclear reactions can not be solved analytically in a mathematical way and therefore different standards and theoretical models have now been developed in an attempt to describe as accurately as possible the phenomenon. Given the complexity of the description of nuclear reactions depending on the energy regions and the types of the participant nuclides, there are different standards and calculation methods. Today, despite sub-dividing the problem, there are still considerable scopes to improve the accuracy of both theoretical calculations and experimental data.

Therefore, the study of neutron nuclear reactions and the comparison of experimental results with the corresponding theoretical calculations can help in improving the existing nuclear models such as that of the compound nucleus, both in terms of method but also as regards their parameterization. In this way, useful conclusions will arise for a variety of queries related both to Nuclear Astrophysics and Cosmology as well as to open issues concerning the investigation of the nucleus structure and its role in theoretical calculations of nuclear reactions as for example the parameters describing the binding energy, the density of excited states of the nucleus and its moment of inertia.

In the Applications field, the scientific community has unanimously agreed that the energy production in the coming years should be done with zero greenhouse gas emissions. Nuclear energy may contribute in this direction only if the existing nuclear facilities will be replaced by next generation reactors which produce as far a possible minimum nuclear waste or even better produce energy by incineration of the already existing nuclear waste, while the probability of an accident is almost zero. Technologically, in this era such an attempt is feasible as it has already begun the development of the fourth- generation of nuclear reactors of fast neutron reactors and the ADS systems (Accelerator Driven Systems). In this direction, the development of Nuclear Data Bases in the fast neutron region is crucial given that the scopes for improving of data accuracy, yet remain vast. For a significant number of isotopes used or produced in thermal power reactors, the cross sections for induced reactions by fast neutrons remain unexplored. The same applies also for isotopes used as structural materials of reactors and/or neutron economy control materials.

One category of these materials that have a particular role in the development of the absorbers and control rods are the rare earths such as Erbium. Erbium is one of the most important elements in Nuclear Technology where due to the high neutron absorption cross section is widely used as a neutron absorber. In fact it has emerged as one of the suitable

materials for manufacturing consumable neutron absorbers (burnable neutron absorbers), which limit the available number of neutrons per fission when the nuclear fuel is newly installed and stop working negative in the neutron production- loss balance as the fuel is used. In this way, the production- loss neutron rate is maintained constant despite the decrease of the initial amount of nuclear fuel.

Erbium in its natural composition consists of six stable isotopes.

Nuclide	$T_{1/2}$ of the State	Isotopic Abundance (%)
^{162}Er	STABLE	0.139 ± 0.005
^{164}Er	STABLE	1.601 ± 0.003
^{166}Er	STABLE	33.503 ± 0.036
^{167}Er	STABLE / 2.269 s	22.869 ± 0.009
^{168}Er	STABLE	26.978 ± 0.018
^{170}Er	STABLE	14.910 ± 0.036

Table 1.1: Isotopic composition of natural Erbium.

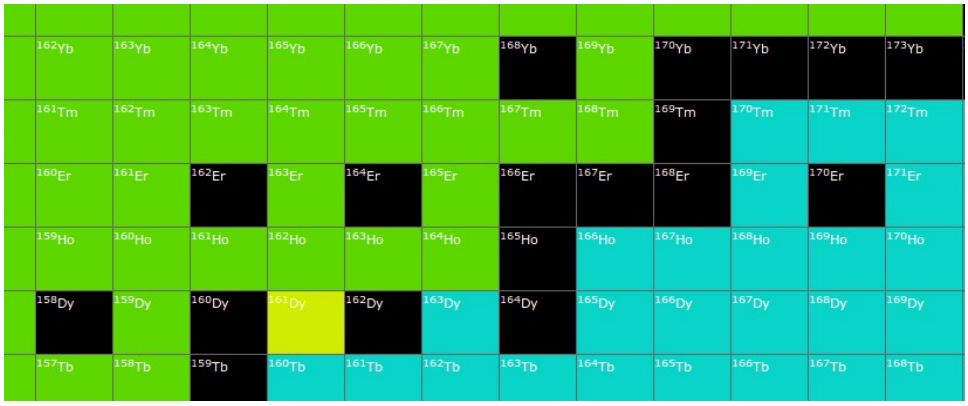

Figure 1.1 : Location of Erbium Isotopes in the nuclide chart.

In the present thesis, cross sections of (n,x) reactions for Erbium isotopes at energies higher than 17 MeV will be discussed. The cross section is usually given in barns (1 barn=10^{-24} cm^2) and is a function of the energy of the incident particle. The plot of σ (E) against E is called excitation function. For excitation function measurements, monoenergetic neutrons are required. For this purpose, mainly accelerator based monoenergetic neutron sources are employed.

Within the present work, the reaction cross section in all cases was determined by means of the activation technique. The activation technique offers the advantage of high sensitivity and selectivity. In this experiment, the samples were placed in front of the neutron production

target (solid TiT) of the Tandem Van der Graaf 5.5 MV accelerator of the Institute of Nuclear and Particle Physics of N.C.S.R. “Demokritos” in order to achieve high neutron fluxes.

The main goal of the present work, is the study of ^{162}Er(n,2n)^{161}Er and ^{167}Er(n,p)^{167}Ho nuclear reactions for the first time at neutron beam energies higher than 17 MeV given that the existing experimental information for both reactions is limited at neutron energies between 14 and 15 MeV.

1.2 Previous Experimental Data

The measurement of the ^{162}Er(n,2n)^{161}Er nuclear reaction was motivated by severe discrepancies among the existing data (up to 30%). On the other hand, almost all the experimental data points in the excitation function of the ^{167}Er(n,p)^{167}Ho are inaccurate mainly for two reasons. Firstly, *Prasad and Sarkat 1971,* in the cross section determination used as half-life of the ^{167}Ho nucleus the value 2.8 h and not 3.1 h (which is the currently adopted value). Secondly, *Wille and Fink 1960*, *Liljavirta and Tuurnala 1978*, *Prasad and Sarkat 1971*, *Lakshmana Das et al. 1978* and *Kong et al. 1998* did not consider the contribution of the interfering reaction ^{170}Er(n,a)^{167}Dy in their cross section calculations. All the results of the previous researchers are presented in the following figures.

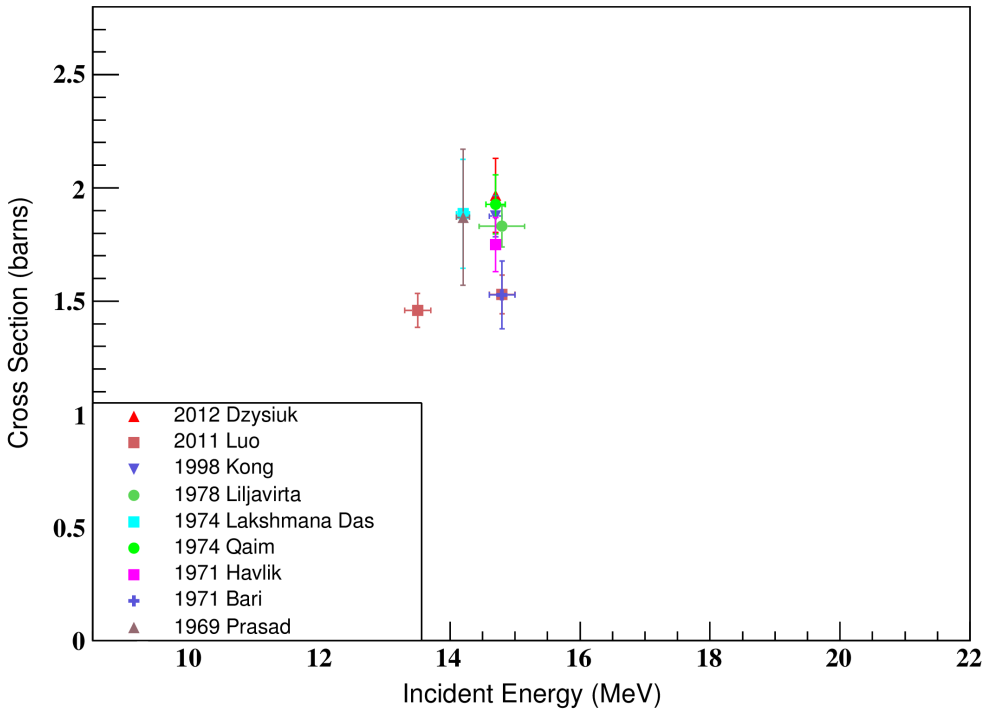

Figure 1.2: Experimental data of previous studies of the ^{162}Er(n,2n)^{161}Er nuclear reaction concerning the EXFOR data base [Dzy12] [Luo11] [Kon98] [LT78] [Lak74] [Qai74] [Hav71] [Bar71] [Pra69].

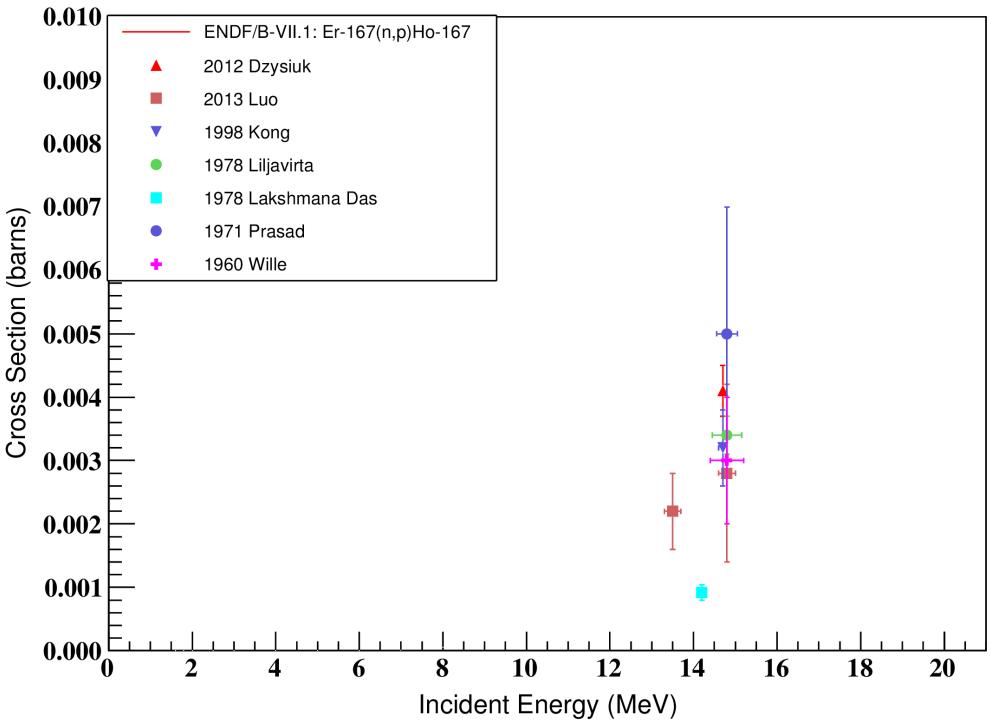

Figure 1.3: Experimental data of previous studies of the ^{167}Er(n,p)^{167}Ho nuclear reaction concerning the EXFOR data base [Dzy12] [Luo13] [Kon98] [Lak78] [PS71] [WF60].

CHAPTER 2
THEORY

2.1 Nuclear Reaction Mechanisms

The phenomenon of interaction between nuclei, is called nuclear reaction. This is a process which is accompanied by mass/energy exchange resulting in energy production or absorption depending of the masses of the involved nuclei [BW91]. The process in its general form, is described schematically as follows:

$$a + A \rightarrow B + b \qquad (2.1)$$

In the above relation, a could match any nucleon, or any nucleus while the b stands for the emission of one or more particles or nuclei. In fact, the nuclear reactions are not only processes leading to the creation of a new nucleus. Each time that the particle a interacts with the nucleus A, all of the following procedures are possible to occur:

$$a + A \rightarrow A + a \qquad (2.2)$$
$$a + A \rightarrow A^{*} + a$$
$$a + A \rightarrow B + b$$
$$a + A \rightarrow C + c + d$$

The asterisk (*) indicates that the initial nucleus after interacting with the incident particle, was found in excited state.

The description of nuclear reactions mechanism is a very complex open issue of nuclear physics. Thus, has prevailed, a separation of nuclear reactions, based on the time of the interaction between the projectile and the target nucleus. Although that the existence of different excitation mechanisms is experimentally confirmed, the way of this separation is based on theoretical estimates of the time of interaction, since experimentally is not possible to observe periods on the oder of 10^{-22} seconds, which is the time required for a nucleon to cross the field of the nucleus. Thus in the first case of “long” interaction time, the projectile and the target supposedly create a compound nucleus, which has reached a state of thermodynamic equilibrium after the projectile has stimulated the maximum possible number of degrees of freedom of the target. In the second case, the projectile makes a direct interaction with the target nucleus stimulating only some of the degrees of it's freedom. In practice, the reactions that last as long as the time of crossing the nuclear field (10^{-22} s) are considered to be direct, while those lasting a few orders of magnitude longer (10^{-16} s), are considered to result in the formation of the compound nucleus. Between these two extreme mechanisms, lie the reaction mechanisms that the nucleus has not had time to reach in full thermodynamic equilibrium, but in state of partial equilibrium (pre-equilibrium) is reached [GH92].

The interaction of the particle-projectile with the target-nucleus, regardless of the time scale at which occurs, in most cases, leaves the system in an excited state, from which is de-excited with emission of γ-rays or particles. The possible methods, are defined in the first approach, from the energy, the angular momentum and the deformation of the nucleus. At low excitation energies, dominates the de-excitation via emitting gamma radiation. As the excitation energy increases, the emission of particles from the nucleus becomes important given that energetically is favored. For even higher excitation energies, the great deformation caused in the nucleus, may even lead to fragmentation of the nucleus into fragments of smaller mass which then in turn are de-excited by gamma emission and particles. In very heavy nuclei may be caused significant distortion even at low excitation energies (e.g. thermal neutron incidence), resulting in the fission of the nucleus into two fragments [Col00].

Typically, the mechanism of excitation and de-excitation of the nucleus, can be described considering that the nucleus ground state consists of a number of particles filling all the energy levels of the nucleus up to the Fermi energy. When the core is excited, a number of particles rises energy levels, leaving behind an equal number of holes. The particles and holes, are called quasiparticles. This description through the image of quasiparticles, is particularly important for the explanation of the mechanism of thermodynamic equilibrium of the nucleus, and especially for the description of the density of states of a nucleus.

2.1.1 The Compound Nucleus Reaction Mechanism

The nuclear reaction process through the compound nucleus, is described schematically from the interaction:

$$a + X \rightarrow C^{*} \rightarrow Y + b \qquad (2.3)$$

The particle a, interacts with the nucleus X and after multiple scattering within the nucleus, a compound nucleus C* is formed, which is in thermodynamic equilibrium. Then the nucleus de-excites by emitting a particle b, and thus creating the nucleus Y. Assuming that the compound nucleus has reached thermodynamic equilibrium, the basic idea the compound nucleus reaction mechanism is that its behavior does not depend on the manner in which it was created. Thus, a nucleus which has reached a state of equilibrium, will be de-excited independently from the way of its excitation. The cross section of the reaction X(a, b)Y, is given by the formula:

$$\sigma(a,b) = \sigma_{c^*}(a) \cdot P_{c^*}(b) \qquad (2.4)$$

where, $\sigma_{c^*}(\alpha)$ is the cross section for the creation of the compound nucleus and $P_{c^*}(b)$ is the probability of decay with emission of particle b. The independent probability of de-excitation of how to create the nucleus, is reflected in relation (2.4), and is the essence of "The Assumption of Independence" of Bohr. The way of decay of the nucleus, is a process of competition among the various possible types of radiation or particle emission, towards to the de-excitation of the compound nucleus. Assuming that the overall probability of decay of the compound nucleus in any way is P, then it is given by the formula:

$$P = \sum_{v} \int P_v(\varepsilon_v)\, d\varepsilon_v \qquad (2.5)$$

where, the index v corresponds to the different ways of de-excitation of the compound nucleus. Thus, the probability of decay with emission of the particle b in case of reaction X(a,b)Y, will be given by a relation of the form:

$$P_{c^*}(b) = \frac{P_b(\varepsilon_b)}{\sum_{v} \int P_v(\varepsilon_v)\, d\varepsilon_v} \qquad (2.6)$$

expressing the statistical nature of the competition between the possible decay channels. During the process of a compound nucleus reaction, all allowable energy decay channels can be performed with a certain probability. Thus the compound nucleus can be de-excited either by emitting γ-rays or particles or by fission. At low energies, it is possible for a particle of the same type as the original projectile of the reaction, to be reemitted (inelastic scattering via compound nucleus) and indeed the ejectile may further have the same energy with the projectile so that it is elastic scattering via the compound nucleus [BW91] [Col00].

2.1.2 Direct Reaction Mechanism

The opposite extreme of the compound nucleus mechanism, is the direct reaction mechanism. In the time it takes for the incident particle to travel along the field of the nucleus, it is possible to undergo through different ways of interaction, without creating a compound nucleus. The incident particle, in the case of direct reactions, does not react with many nucleons as in the case of compound nucleus reactions. On the contrary, in direct reactions the incident nucleon or nuclei are transferring their energy to one or to few target nucleons driving them to an excited state or even to an unbound state.

The simplest case of direct reaction is the **elastic scattering,** in which the projectile interacts with the target nucleus without exchanging any nucleons and without causing any kind of excitation. If the incident particle excites the target nucleus, this reaction is called **inelastic scattering**. Many times, the energy of the projectile is sufficient enough to have a nucleon transferred from the projectile to the target or vice versa. These reactions are called **transfer reactions**. If the incident particle gives a nucleon sufficient energy to come out of the nucleus, we have **knock-out reaction**.

There are some basic observable characteristics of direct reactions differentiating them with respect to the corresponding compound nucleus reactions that produce the same products. The processes of excitation and de-excitation of the compound nucleus, produce different angular distributions of reaction products and different energy dependence of cross section. Reactions of compound nucleus because of the thermodynamic equilibrium of the compound system, lead to isotropic distribution of products, while direct reactions lead to strong

preferred emission guidelines generally toward the forward angles.

2.1.3 Pre-equilibrium Nuclear Reactions

Apart from the mechanisms of the formation of compound nucleus and the direct reaction, there is an intermediate mechanism of early de-excitation of the compound nucleus. In the period between the time it takes the projectile to travel the field of the nucleus target and the time required to bring about thermodynamic equilibrium of the compound nucleus, may be excited by the incident particle a limited number of degrees of freedom of the compound system.

This mechanism becomes obvious experimentally in several ways. In the emission spectra of the particles from nuclear reactions where the projectile has a high energy, for different masses of nuclei targets, there is a region without a structure with loose dependence on the mass of the target, between the regions which are dominated by two other mechanisms of nuclear reactions. While with the change in mass of the target, the emission of particles due to the mechanism of compound nucleus or due to direct reactions can be varied even by an order of magnitude, in the unstructured region because of pre-equilibrium reactions, the emission of particles remains almost constant. Moreover, the angular distributions of the products of pre-equilibrium reactions, while showing preference to the forward angles, however, no change to their characteristics for different mass targets is observed [GH92].

2.1.4 Exothermic and Endothermic Nuclear Reactions

In order for the compound nucleus to be de-excited with a reaction channel, the excitation energy should be energetically allowable. One of the fundamental quantities defining the released or the absorbed energy of a nuclear reaction is the Q-value. The Q-value is equal to the mass difference between the nuclei participating in a nuclear reaction minus the total mass of the reaction products. If this value is positive, then the reaction is exothermic. If the Q-value is negative, the reaction can only take place if this amount of energy is available in the center of mass system (CMS). Based on the equation 2.3, the Q-value of the reaction X(a,b)Y is given by the form:

$$Q=(m_a+m_X-m_Y-m_b)\cdot c^2 \qquad (2.7)$$

or as a function of the mass deficit: $\Delta=m-A$ (2.8)

where, m is the mass of the neutral atom in atomic units (amu) and
A is the mass number of the atom in atomic units (amu)

Eventually, the Q-value can be written as: $Q=\Delta_a+\Delta_X-\Delta_Y-\Delta_b$ (2.9)

A nuclear reaction is characterized as:

- **Exothermic** when Q>0,
- **Endothermic** when Q<0 and
- **Elastic scattering** when Q=0, where the nuclei before the reaction takes place are the same with the reaction products.

2.2 The Nuclear Reactions $^{162}_{68}Er_{94}(n,2n)^{161}_{68}Er_{93}$ and $^{167}_{68}Er_{99}(n,p)^{167}_{67}Ho_{100}$

Very important feature and a direct consequence of the thermal equilibrium inside a compound nucleus is the fact that the mode decay of the compound nucleus does not depend on the way the nucleus is formed. The large number of collisions between nucleons leads to the loss of the information on the entrance channel from the system. The decay mechanism (exit channel) that dominates the decay of C* is determined by the excitation energy in C* and by the law of probability.

2.2.1 Energy Diagram of the Interaction n+^{162}Er

The n+^{162}Er is a compound nucleus reaction. In order to present the energy diagram of this interaction the possible reaction channels have to be depicted accordingly. For this reason as a reference energy level, the compound nucleus ground state was considered.

For example, for the reaction $n+^{162}_{68}Er_{94} \rightarrow ^{163}_{68}Er^{*}_{95} \rightarrow 2n+^{161}_{68}Er_{93}$, the energy level will be:

$$Q = \Delta(^{163}_{68}Er_{95}) - 2\Delta(^{1}_{0}n_{1}) - \Delta(^{161}_{68}Er_{93}) \Rightarrow$$
$$Q(MeV) = (-65.1663) - 2(8.0713) - (-65.1992) \approx -16.11\ MeV$$

The sign "-" indicates that considering as a reference level the ground state of the compound nucleus ^{163}Er*, 16.1 MeV energy is required for populating the ^{162}Er(n,2n)^{161}Er reaction channel. Similarly, for all interactions, the following table results (Table 2.1).

Entry Interaction	Channel Output	Q-value (MeV)	Energy Level (MeV)
$n+{}^{162}_{68}Er_{94} \rightarrow {}^{163}_{68}Er^{*}_{95}$	$n+{}^{162}_{68}Er_{94}$	0.00	6.90
	$2n+{}^{161}_{68}Er_{93}$	-9.20	16.11
	$3n+{}^{160}_{68}Er_{92}$	-16.42	23.32
	$4n+{}^{159}_{68}Er_{91}$	-25.99	32.89
	$p+{}^{162}_{67}Ho^{g}_{95}$	0.49	6.42
	$p+{}^{162}_{67}Ho^{m}_{95}$	0.38	6.52
	$pn+{}^{161}_{67}Ho^{g}_{94}$	-6.42	13.33
	$pn+{}^{161}_{67}Ho^{m}_{94}$	-6.66	13.54
	$2p+n+{}^{160}_{66}Dy_{94}$	-11.24	18.14
	$a+{}^{159}_{66}Dy_{93}$	8.48	-1.57
	$na+{}^{158}_{66}Dy_{92}$	1.65	5.26
	$d+{}^{161}_{67}Ho^{g}_{94}$	-4.20	11.11
	$d+{}^{161}_{67}Ho^{m}_{94}$	-4.41	11.32

Table 2.1: Potential Output Channels of the interaction n+^{162}Er [1] [2].

Also, the neutron separation energy S_n which is the amount of energy that is needed to remove a neutron from a nucleus ${}^{A}_{Z}X_{N}$ and equal to the difference in binding energies between ${}^{A}_{Z}X_{N}$ and ${}^{(A-1)}_{Z}X_{(N-1)}$, should be calculated. So, for the reaction under study:

$$S_n = \Delta({}^{1}_{0}n_1) + \Delta({}^{162}_{68}Er_{94}) - \Delta({}^{163}_{68}Er_{93})$$
$$S_n(MeV) = 8.0713 + (-66.3329) - (-65.1663) = 6.9047 \approx 6.9\ MeV$$

By knowing with good precision the energy of the neutron beam in the laboratory system using the NeuSDesc-2008 programme [Lov02] (see next chapter), it can be calculated the energy of the neutron beam in the center of mass through the following relation.

$$E_{n,CMS} = \frac{A_{target\ nucleus}}{A_{compound\ nucleus}} \cdot E_{n,LAB} \qquad (2.10)$$

where, $A_{target\ nucleus}$ is the atomic number of the irradiated nucleus (here equal to 162),

$A_{compund\ nucleus}$ is the atomic number of the compound nucleus (here equal to 163) and

$E_{n,LAB}$ is the neutron beam energy in the laboratory system

Combining the above, the excitation energy of the compound nucleus can be obtained.

$$E_X = S_n + E_{n,CM} \qquad (2.11)$$

$E_{n,LAB}$ (MeV)	$E_{n,CMS}$ (MeV)	E_x (MeV)
17.1	17	23.9
18.1	18	24.9
19	18.9	25.9

Table 2.2: The correspondence of the monoenergetic neutron beam between the LAB and the CM system, coupled with the excitation energy of the compound nucleus ^{163}Er* for each irradiation.

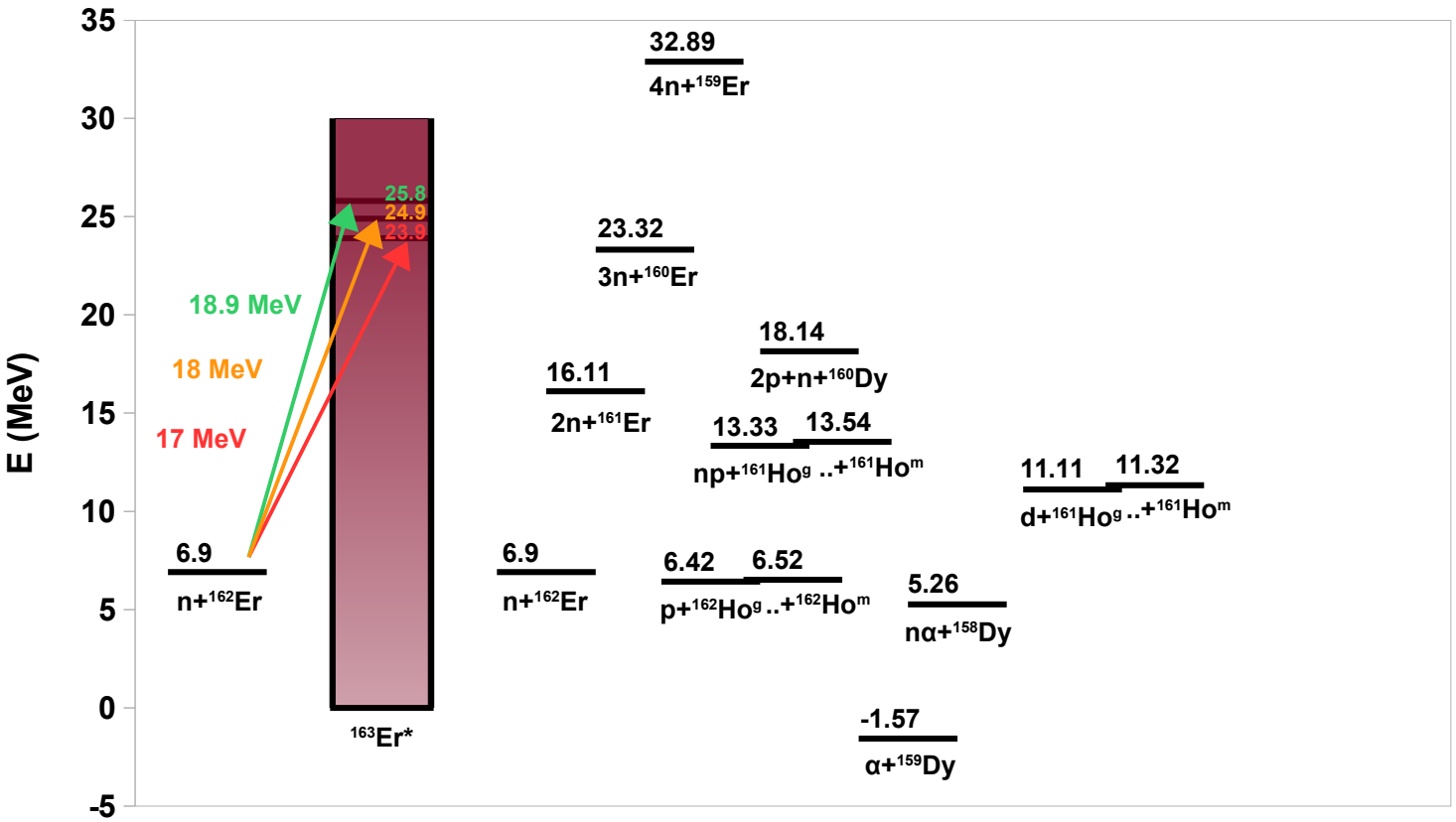

Figure 2.1: Energy diagram of the interaction n+^{162}Er.

2.2.2 Reaction Channels for the Interaction n+^{162}Er

Below all the possible reaction channels are discussed one by one for the three neutron irradiations performed at the Tandem Van der Graaf 5.5 MV accelerator of the Institute of Nuclear and Particle Physics of N.C.S.R. “Demokritos”.

- $n+{}^{162}_{68}Er_{94}$: The channel of elastic scattering would be very interesting to be investigated but it requires a different experimental setup for the study of the scattered neutrons in space.

- $2\mathrm{n}+{}^{161}_{68}Er_{93}$: This is the channel under study and is suitable for the conduction of the current experiment using the activation method [Pat04]. The product nucleus ^{161}Er has half-life $T_{1/2}=3.21h$ and the gamma-ray that will be studied and by which the cross section of the reaction ^{162}Er(n,2n)^{161}Er will be extracted, has energy $E\gamma=826.6keV$ and intensity $I\gamma=64\%$. In the figure below (Figure 2.2), the the gamma-rays emitted from the unstable nucleus ^{161}Er can be seen.

- $3\mathrm{n}+{}^{160}_{68}Er_{92}$ **:** The gamma-rays that are emitted from the the de-excitation of the unstable nucleus ^{160}Er are not recorded in the spectrum because have energy below 80 keV, which is the window threshold of the germanium detectors.

- $4\mathrm{n}+{}^{159}_{68}Er_{91}$: This reaction channel is energetically not allowed.

- $p+{}^{162}_{67}Ho^{g}_{95}$: The nucleus ^{162}Ho in the ground state, has a $T_{1/2}=15min$ so it cannot be studied with the current irradiation conditions (10h of irradiation and 35-45 min waiting time).

- $p+{}^{162}_{67}Ho^{m}_{95}$: The same nucleus has a metastable state with $T_{1/2}=67min$ and emits a gamma-ray with energy $E\gamma=184.99keV$ and intensity $I\gamma=23.94\%$ but it cannot be measured due to the fact that in the same area there is a background radiation.

- $pn+{}^{161}_{67}Ho^{g}_{94}$: During the de-excitation of the nucleus ^{161}Ho from the ground state, the gamma-rays that are emitted have no sufficient intensity so as be recorded in the spectrum.

- $pn+{}^{161}_{67}Ho^{m}_{94}$: The nucleus ^{161}Ho in the metastable state has a very short half live $T_{1/2}=6.76s$ and thus it cannot be studied.

- $2\mathrm{p}+n+{}^{160}_{66}Dy_{94}$: The produced nucleus ^{160}Dy is stable and therefore is impossible to be studied.

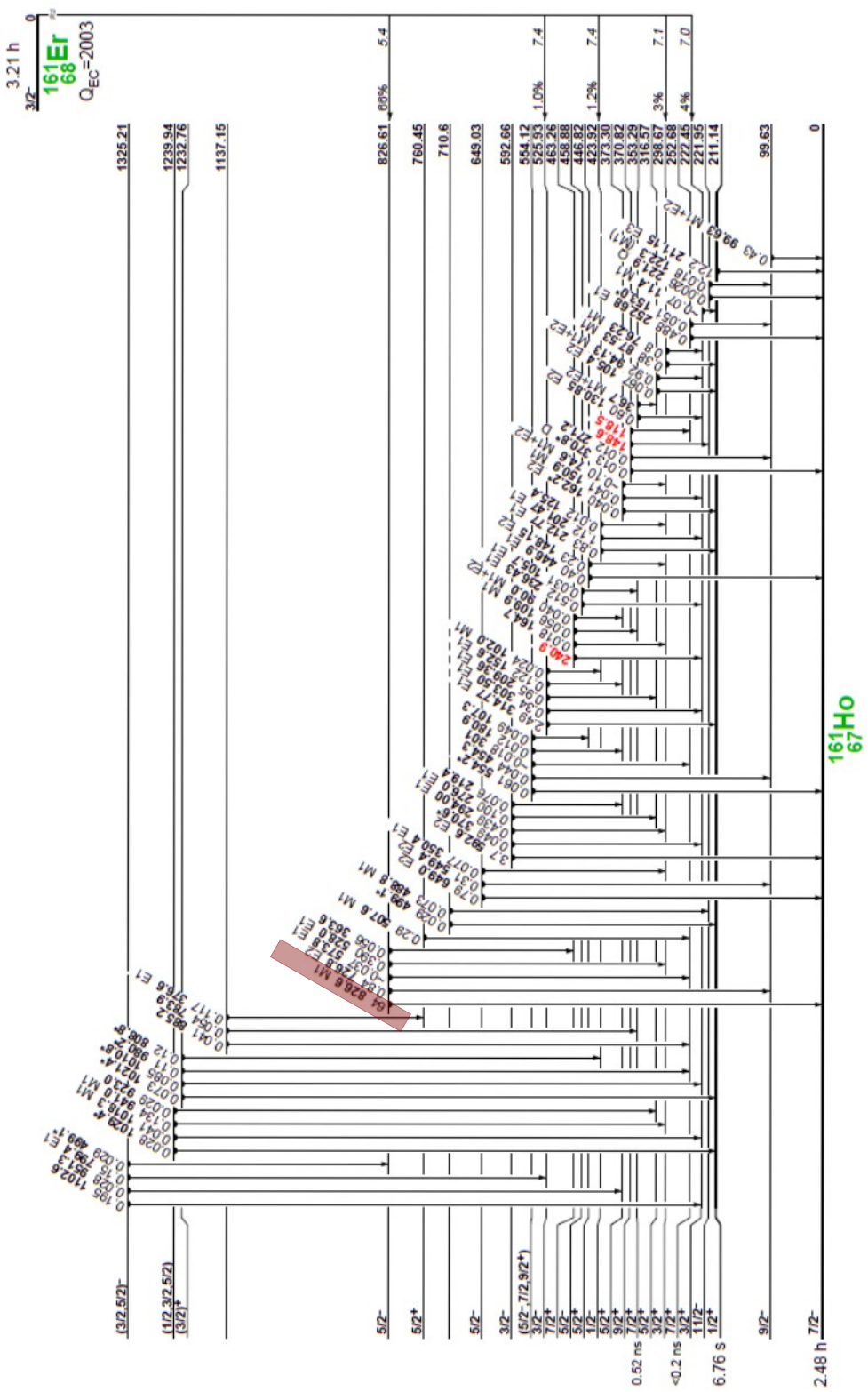

Figure 2.2: Decay scheme of the ^{161}Er.

- $a + {}^{159}_{66}Dy_{93}$: This channel with $Energy\,level = -1.57\,MeV$, has very low cross section value given that an alpha particle has to be formed and to be emitted from the compound nucleus through the Coulomb barrier.

- $na + {}^{158}_{66}Dy_{92}$: The produced nucleus ^{158}Dy is stable.

- $d + {}^{161}_{67}Ho^{g}_{94}$: The de-excitation of the nucleus ^{161}Ho from the ground state has been mentioned above.

- $d + {}^{161}_{67}Ho^{m}_{94}$: The same applies on this channel too.

2.2.3 Energy Diagram of the Interaction n+^{167}Er

For the reaction $n + {}^{167}_{68}Er_{99} \rightarrow {}^{168}_{68}Er^{*}_{100} \rightarrow p + {}^{167}_{67}Ho_{100}$, the energy level will be:

$$Q = \Delta\left({}^{168}_{68}Er_{100}\right) - \Delta\left({}^{1}_{1}p_{0}\right) - \Delta\left({}^{167}_{67}Ho_{100}\right) \Rightarrow$$
$$Q(MeV) = (-62.9897) - (7.2889) - (-62.2799) \approx -8\,MeV$$

and the neutron separation energy S_n will be:

$$S_n = \Delta\left({}^{1}_{0}n_{1}\right) + \Delta\left({}^{167}_{68}Er_{99}\right) - \Delta\left({}^{168}_{68}Er_{100}\right)$$
$$S_n(MeV) = 8.0713 + (-63.2897) - (-62.9897) = 7.7713 \approx 7.77\,MeV$$

Likewise, for all the interactions the following table results (Table 2.3).

Entry Interaction	Channel Output	Q-value (MeV)	Energy Level (MeV)
$n+{}^{167}_{68}Er_{99} \rightarrow {}^{168}_{68}Er^{*}_{100}$	$n+{}^{167}_{68}Er_{99}$	0.00	7.77
	$2n+{}^{166}_{68}Er_{98}$	-6.44	14.21
	$3n+{}^{165}_{68}Er_{97}$	-14.91	22.68
	$4n+{}^{164}_{68}Er_{96}$	-21.56	29.33
	$p+{}^{167}_{67}Ho_{100}$	-0.23	8
	$pn+{}^{166}_{67}Ho^{g}_{99}$	-7.51	15.28
	$pn+{}^{166}_{67}Ho^{m}_{99}$	-7.52	15.29
	$2\,p+n+{}^{165}_{66}Dy^{g}_{99}$	-14.26	22.03
	$2\,p+n+{}^{165}_{66}Dy^{m}_{99}$	-14.36	22.14
	$a+{}^{164}_{66}Dy_{98}$	8.32	-0.55
	$na+{}^{163}_{66}Dy_{97}$	0.66	7.11
	$d+{}^{166}_{67}Ho^{g}_{99}$	-5.28	13.05
	$d+{}^{166}_{67}Ho^{m}_{99}$	-5.29	13.06

Table 2.3: Potential Output Channels of the interaction n+^{167}Er [1] [2].

$E_{n,LAB}$ (MeV)	$E_{n,CMS}$ (MeV)	E_x (MeV)
17.1	17	24.77
18.1	18	25.77
19	18.9	26.67

Table 2.4: The correspondence of the monoenergetic neutron beam between the LAB and the CM system, coupled with the excitation energy of the compound nucleus ^{168}Er* for each irradiation.

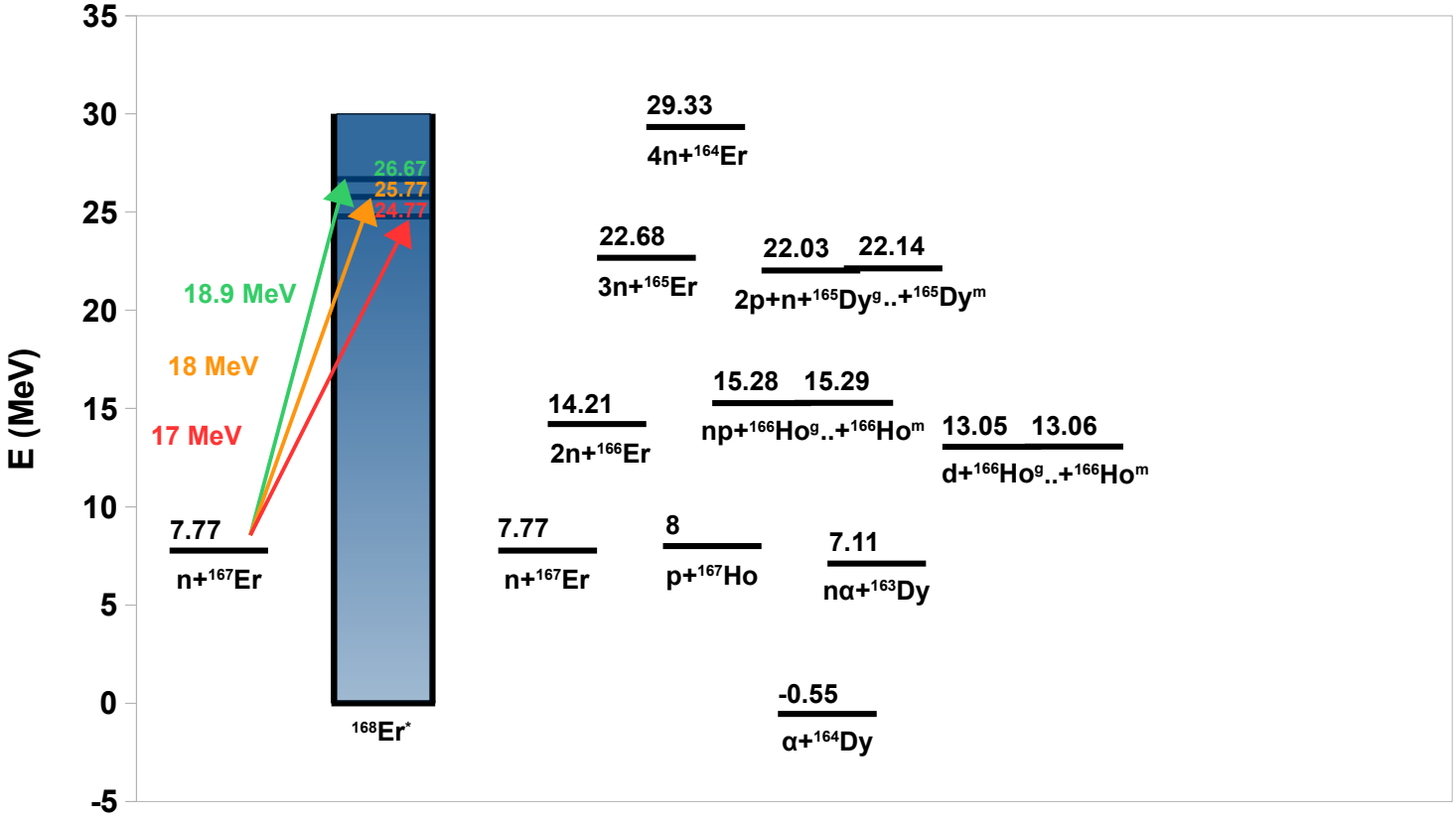

Figure 2.3: Energy diagram of the interaction n+^{167}Er.

2.2.4 Reaction Channels for the Interaction n+^{167}Er

- $n+{}^{167}_{68}Er_{99}$: The channel of elastic scattering would be very interesting to be investigated but it requires a different experimental setup for the study of the scattered neutrons in space.
- $2n+{}^{166}_{68}Er_{98}$: The produced nucleus ^{166}Er is stable, therefore is impossible to be studied.
- $3n+{}^{165}_{68}Er_{97}$: The produced nucleus ^{165}Er is de-excited with ec :100% directly to the ground state of the stable nucleus ^{165}Ho without the emission of gamma-rays.
- $4n+{}^{164}_{68}Er_{96}$: This reaction channel is energetically not allowed.

- $p + {}^{167}_{67}Ho_{100}$: This is the channel under investigation. The product nucleus ^{167}Ho has half-life $T_{1/2} = 3.1h$ and the gamma-ray that will be studied and by which the cross section of the reaction ^{167}Er(n,p)^{167}Ho will be extracted, has energy $E\gamma = 346.5\,keV$ and intensity $I\gamma = 57\%$. In the figure below (Figure 2.4), the the gamma-rays emitted from the unstable nucleus ^{167}Ho can be seen.

- $pn + {}^{166}_{67}Ho^{g}_{99}$: The nucleus ^{166}Ho in the ground state has a half-life equal to $T_{1/2} = 26.82h$ therefore considering the current irradiation and measuring conditions as well as the small reaction cross section, the expected counting rate is bellow the detection limits.

- $pn + {}^{166}_{67}Ho^{m}_{99}$: The same nucleus lives in the metastable state for a very long time $T_{1/2} = 1.20 \times 10^{3}\,y$ therefore it is practically impossible to be studied.

- $2\,p + n + {}^{165}_{66}Dy^{g}_{99}$: Even though the nucleus ^{165}Dy in the ground state has a $T_{1/2} = 2.334h$ it cannot be studied because all the gamma rays which are emitted during the de-excitation have intensities less than 4%.

- $2\,p + n + {}^{165}_{66}Dy^{m}_{99}$: The same nucleus has a metastable state with a very short half-life $T_{1/2} = 1.257m$ and is not possible to observe its decay.

- $a + {}^{164}_{66}Dy_{98}$: This channel with $Energy\,level = -0.55\,MeV$,has very low cross section value given that an alpha particle has to be formed and to be emitted from the compound nucleus through the Coulomb barrier.

- $na + {}^{163}_{66}Dy_{97}$:The produced nucleus ^{163}Dy is stable.

- $d + {}^{166}_{67}Ho^{g}_{99}$: The de-excitation of the nucleus ^{166}Ho from the ground state has been mentioned above.

- $d + {}^{166}_{67}Ho^{m}_{99}$: The same applies on this channel too.

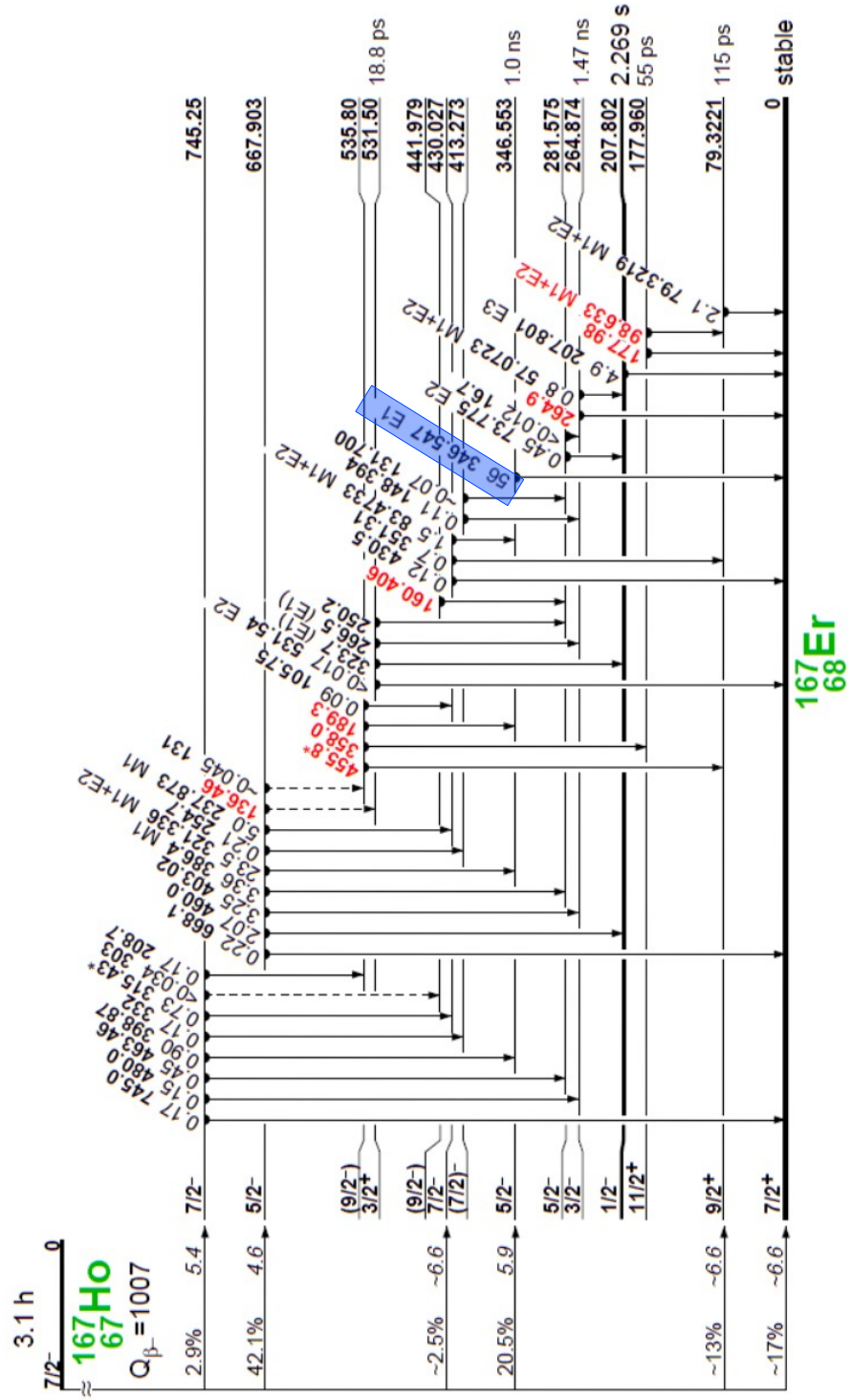

Figure 2.4: Decay scheme of the ^{167}Ho.

CHAPTER 3
EXPERIMENTAL METHOD AND SETUP

3.1 The Activation Technique

The activation technique is an established method for both basic research purposes as well as for Nuclear Physics Applications. It can be adopted for the accurate determination of cross sections as well as for analytical purposes. The sensitivity of the activation technique promotes this method in many scientific and technological disciplines, in which there is a need for trace detection. Therefore, the activation technique is the adopted method in applications in medicine, archeometry, as well as in environmental studies. The sensitivity of the method in detecting trace elements, is achieved by exposing the sample, to the large available neutron fluxes, normally provided in nuclear reactors.

The method relies on the fact that many times the nuclei produced by a nuclear reaction are unstable and de-excitated with half-lives long enough (from minutes to several months). Thus it is possible to determine the number of nuclei produced by nuclear reaction, detecting the radiation which accompanies their decay, after the irradiation process. In a reaction of the form:

$$x + X \rightarrow y + Y \qquad (3.1)$$

particle beam type x interacts with the nucleus X of the target and produces the unstable nucleus Y with cross section for the interaction σ. The production rate of the nuclei $\frac{dN}{dt}$ of type Y, is given by the formula (3.2), which describes the competition between the creation of particles of type Y from the beam flux f(t) and the decay rate determined by the constant λ.

$$\frac{dN}{dt} = \sigma \cdot f(t) \cdot N_{\tau} - \lambda \cdot N \qquad (3.2)$$

This differential equation, in which the number of nuclei of the target is represented by N_{τ}, has the general solution:

$$N(t) = \frac{\int e^{\int \lambda dt} \cdot \sigma \cdot N_{\tau} \cdot f(t) + C}{e^{\int \lambda dt}} \qquad (3.3)$$

according to which, the number of nuclei, $N(t_{act})$ produced during an irradiation with duration t_{irr}, is given by the formula:

$$N(t_{act}) = \sigma \cdot N_{\tau} \cdot \Phi \cdot \frac{\int_0^{t_{irr}} e^{\lambda t} \cdot f(t)\, dt}{\int_0^{t_{irr}} f(t) dt} \cdot e^{-\lambda t_{irr}} \qquad (3.4)$$

In the last equation, the total flux Φ in which the sample was exposed is given by the formula:

$$\Phi = \int_0^{t_{irr}} f(t)\,dt \qquad (3.5)$$

The fractional term in relation (3.4), denotes the percentage of the nuclei created but de-excited until the end of the irradiation. The integral in the numerator of this term depends on the fluctuations of the beam. For the ideal case of a constant flux of particles during irradiation, the relation (3.4) takes the simplest form:

$$N(t_{act}) = \sigma \cdot N_\tau \cdot \Phi \cdot \frac{1 - e^{-\lambda t_{irr}}}{\lambda t_{irr}} \qquad (3.6)$$

Generally speaking both relations (3.4) and (3.6) can be summarized in the following:

$$N(t_{act}) = \sigma \cdot N_\tau \cdot \Phi \cdot f_b \qquad (3.7)$$

At the end of the irradiation, the events per second or counts per second that are recorded by the detector are given by the relation:

$$cps = \varepsilon \cdot I \cdot \frac{dN}{dt} \qquad (3.8)$$

The interval of the above relation from the start of the measurement t_0 till the end of the measurement t_m gives:

$$counts = \int_0^{t_m} \left(\lambda \cdot N_0 \cdot e^{-\lambda t} \cdot \varepsilon \cdot I \right) dt \qquad (3.9)$$

that leads to the form:

$$counts = \varepsilon \cdot I \cdot N_0 \left(1 - e^{-\lambda t_m}\right) \qquad (3.10)$$

Between the end of the irradiation and the beginning of the measurement the nucleus is de-excited through the relation :

$$N_0 = N_{act} \cdot e^{-\lambda t_w} \qquad (3.11)$$

where t_w is the waiting time.

Thus, the relation (3.10) takes the following form:

$$counts = \varepsilon \cdot I \cdot N_{act} \cdot e^{-\lambda t_w} \left(1 - e^{-\lambda t_m}\right) \qquad (3.12)$$

Combining the relations (3.7) and (3.12) the formula of the cross section is given as:

$$\sigma = \frac{counts}{\varepsilon \cdot I \cdot \Phi \cdot N_T \cdot e^{-\lambda t_w} \left(1 - e^{-\lambda t_m}\right) \cdot f_b} \qquad (3.13)$$

Actually, during the irradiation of the sample, the particle beam is not stable in intensity, therefore it is important to use some method of recording these fluctuations, as they significantly affect the activation counts, especially when they involve short-lived isotopes.

Determining the number of Y nuclei produced by measuring in some way (e.g. γ-ray

spectroscopy) their decay, it is possible to determine from the relation (3.7), any of the three quantities Φ, N_T, σ providing that two out of three of them are known. The fact that in the activation technique the measurement of the induced activity of the sample takes place after the irradiation (off-line measurements), has a number of **advantages** in comparison with the measurement during the irradiation (on-line measurements).Some of these advantages are:

- ✔ Lower background and less complexity of the spectra in the absence of the spectra of the interaction of the beam with the rest of the ingredients and the target device.
- ✔ Less stress on detection systems of the radiation generated by the interaction of the beam.
- ✔ Generally lower energy radiation produced, due only to decay of standard or metastable levels of the nucleus, and is independent of the energy of the radiating beam.
- ✔ Ability to use simpler detection devices with generally lower costs.
- ✔ Ability to use natural target to measure cross sections.
- ✔ In many cases, simultaneous measurement of multiple cross sections, with properly prepared target.

However, these measurements have some significant **limitations** in their application.

- ✗ If the sample has isotopes that can be populated with different reactions resulting to the same nucleus, then it is not possible to determine their contribution to the production of this nucleus.
- ✗ Too small and too long half-lifes are extremely difficult to be used in the method of activation. The lower limit is of the order of ms and is determined by the time interval between the discontinuation of the irradiation until the end of the measurement of the activity of the target, while the upper limit is mainly determined by the activity that is likely to result in very long measurement periods.
- ✗ In many cases, the irradiation creates increased activity of the samples, which may require the use of individual radiation protection measures.

In neutron induced reaction studies, the accurate determination of the total neutron flux Φ, is of prime importance. For this reason the appropriate reference reaction has to be used with the following **characteristics**:

- Fairly large, smoothly varying and very accurately known cross section, in the region of interest.
- Half-life that allows the creation of significant activity in the target during irradiation.
- The detected radiation from the reaction, is such that in the experimental spectrum is the minimum possible background, and minimal interference from natural radiation and from activation of the impurities in the material of the target.
- The isotope of interest should be easily available in large quantities in high purity samples. Furthermore, the accurate determination of the content of the isotope in the

target is of great importance.

- The sample has to be stable both mechanically and chemically. In general, the handling of a fragile sample or a sample that is rapidly oxidized is an issue.

3.2 Application of the Activation Method in the Cross Section Measurement

In neutron physics experiments performed by means of the activation technique, the accurate determination of the neutron flux across the sample is important. For this reason, the sample-target of the reaction of interest is placed among two others sample-foils used as reference reactions. The purpose to this, is that both the reference targets and the target nucleus should receive the same flux of particles during irradiation. This technique is the one that was applied in these experiments to study the nuclear reactions ^{162}Er(n,2n)^{161}Er and ^{167}Er(n,p)^{167}Ho. Within the present work, the reference foils Au, Al and Nb were used and the neutron flux for each irradiation was determined through the equation:

$$\Phi = \frac{counts \cdot CF_{SA} \cdot CF_{DT}}{\varepsilon \cdot I_{\gamma} \cdot \sigma \cdot N_T \cdot e^{-\lambda t_w}\left(1 - e^{-\lambda t_m}\right) \cdot f_b} \qquad (3.14)$$

where, $counts$ originate from the daughter's nucleus induced activity
CF_{SA} is the sample's self-attenuation correction factor
CF_{DT} is the detector's dead time correction factor
ε is the efficiency of the detector for the emitted γ-ray
I_{γ} is the intensity of the γ-ray emitted
σ is the reference reaction cross section
N_T is the number of parent nuclei in the target sample
t_w is the waiting time between the end of the irradiation and the start of the measurement
t_m is the measuring time of the daughter's induced activity
f_b is the correction factor due to the decay of the daughter nucleus during the irradiation

The number of parent nuclei inside the sample of the target is given by the form:

$$N_T = a \cdot n \cdot \frac{m \cdot N_A}{mw} \qquad (3.15)$$

where, a is the natural abundance of the parent nucleus inside the sample
n is the number of the atoms in the molecule compound that is used as target material
m is the mass of the sample target
N_A is the Avogadro number and
mw is the molecular weight of the molecule compound used as target material

Finally, the cross section of the reaction under study can be calculated using the inverse solution of the above equation as:

$$\sigma = \frac{counts \cdot CF_{SA} \cdot CF_{DT}}{\varepsilon \cdot I_{\gamma} \cdot \Phi \cdot N_T \cdot e^{-\lambda t_w}\left(1 - e^{-\lambda t_m}\right) \cdot f_b} \qquad (3.16)$$

where now Φ is the flux deduced from the equation (3.14).

3.3 Accelerator

Nuclear reactions is a complex physical process and their study is directly connected with the development of the accelerators. Through the acceleration of the particles, the required energy can be achieved as to overcome the Coulomb barrier when charged particles are considered. Furthermore, through the particle acceleration of the initial nuclei, the requires conditions with respect the initial momentum and beam purity can be met. In this way the experimentalist can decrease the degrees of freedom of the system under study. In any form of accelerator, the creation of energetic particles takes place by exploiting the electric charge of the nucleus. In an ion source, by adding or removing electrons in the corresponding neutral atom, the ions of the nucleus that is about to be accelerated, are formed. Afterwards, they are directed into an area with electric field E and possibly magnetic field B and thus Lorentz force is exerted on ions.

$$\vec{F_L} = q\vec{E} + q(\vec{u} \times \vec{B}) \qquad (3.17)$$

Depending on the mode of application of the electric field, the accelerators can be divided into three categories: electrostatic, linear and cyclotrons. The simplest form of an electrostatic accelerator consists of a capacitor with flat armors.

Ions with a positive charge q which are entering from a small hole in the positive armor the space between the armors, are accelerated towards the negative armor from the force $\vec{F} = q\vec{E}$. Thereby, from the corresponding hole of the negative armor, an ion beam with kinetic energy qV is coming out, where V is the potential difference between the two armors of the capacitor.

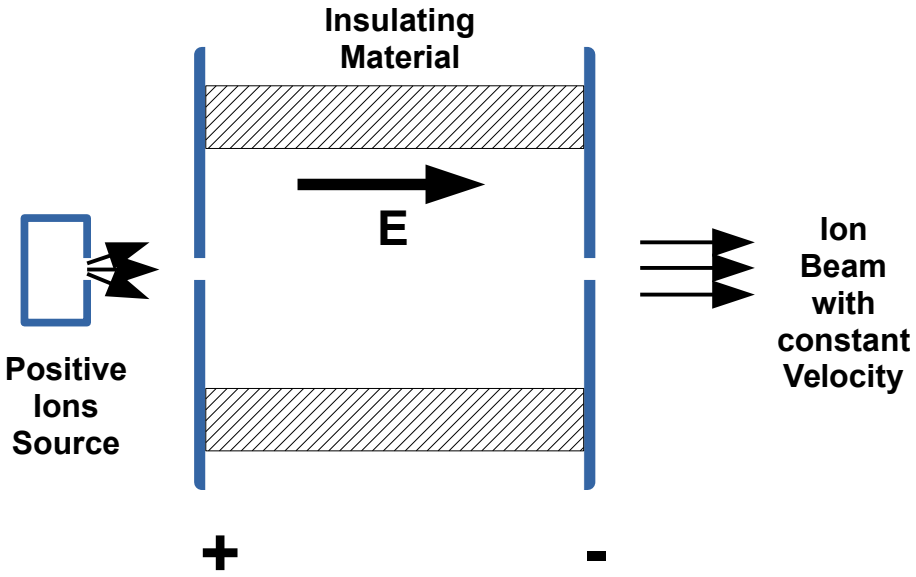

Figure 3.1: Positive Ion acceleration in capacitor with flat armors.

The layout of the capacitor with flat armors gives energies up to some tens of keV while is unable to provide an ion beam with energies of a few MeV required for the excitation of a nuclear system. If however this basic configuration is repeated several times in an array of alternative electrodes in the form of metal discs and rings of insulating material, an accelerating tube is generated. This constitutes the most important part of each electrostatic accelerator.

The functional principle of an accelerator tube from where the positive ions enter, is a DC power supply that generates a positive potential V relative to the right end of the accelerator which is grounded. The sequential electrodes are connected to identical resistances R, so as to ensure the uniform decline of the potential $V = I \cdot R$ at each stage of the layout. In this way and by using hundreds of electrodes in the modern accelerators the maintenance of the potential difference of the order of MV is achieved.

Various types of electrostatic accelerators differ in relation to the way of development of the potential V at the ends of the accelerator tube. The experiments of the present work were performed at the Tandem Van der Graaf 5.5 MV electrostatic accelerator of the Institute of Nuclear and Particle Physics N.C.S.R. “Demokritos”.

The Van der Graaf generator achieves the development of high-voltage with the mechanical transfer of electrical charge on a belt between two rotating rollers. The charge is delivered to the outer surface of the belt by a pin connector arrangement at the bottom of the layout and is discharged towards the high-voltage electrode by a second pin complex on the upper part

(Figure 3.2). The layout creates a potential difference: $V = \frac{Q}{C}$

where, Q is the total charge that accumulates in the electrode and
C is the capacitive connection of the high-voltage electrode relative to the ground

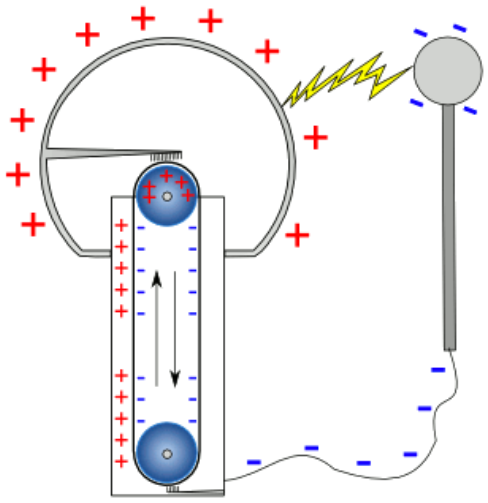

Figure 3.2: Schematic depiction of the Van der Graaf Generator.

The layout of this accelerator is located in the center of a tank containing SF_3 gas at a pressure of 4.5 bar, in order to prevent electrical discharges from the high-voltage electrode to the closest object in the ground potential. The kinetic energy of the particles that an electrostatic accelerator produces is equal to $n \cdot e \cdot V$ where n is the number of electrons removed from the corresponding neutral atom in the ion source.

In this experiment, was used a tandem accelerator (Figure 3.3). This accelerator consists of two simple electrostatic accelerators in series. The two ends of the accelerator system are grounded and high positive voltage is applied in the center of the layout where the two accelerating tubes meet. The ion source is located outside the main accelerator at ground potential.

The procedure adopted is as follows: the negative ions are injected into the first accelerating tube and are accelerated up to an energy equal to $e \cdot V$. After that the negative ions are accelerated through a multi-step process up to the center of the tank where the higher voltage is. In the electrode's region, the ions are going through a thin carbon film, called Carbon Stripper. In this way, one or more electrons are stripped resulting in n positive ions (charge $n \cdot e$), which are accelerated to the other end of the system with total kinetic energy $e \cdot V + n \cdot e \cdot V$ [Ass81].

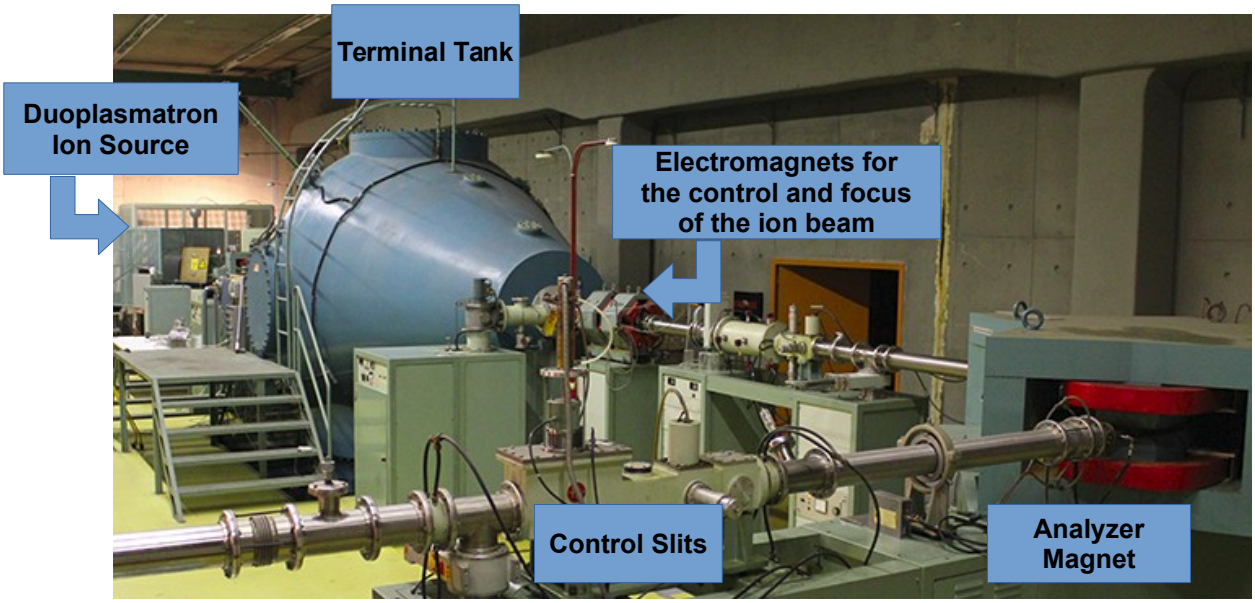

Figure 3.3: Part of the Tandem Van der Graaf accelerator complex.

3.4 Neutron Production from the Accelerator

Beside the ion beams, neutron beams are of special interest for the Basic Research purposes as well as for Nuclear Astrophysics Applications. Considering the absence of electric charge in neutron along with the fact that neutrons are unstable particles outside the nuclear field, the neutron beams cannot be produced are directed directly as in the case with stable ion beams. Usually, a nuclear reaction is used, which has a high neutron yield. The accelerator beam (primary beam) is directed and focused on the primary target. In this way, a neutron field is produced (secondary beam), with an azimuthally symmetric angular distribution with respect the original beam. The angular distribution of the neutron beam depends on the reaction used and on the kinetic energy of the primary beam.

The monoenergetic neutron beams are widely used in the last fifty years in Nuclear Physics, with great success. In fact, the term “monoenergetic” is not always precise. The actual energy distribution of the neutron beam is affected by several factors. For the production of monoenergetic beams, are typically used reactions that are not populating excited states of

the residual nucleus. This ensures the mono-energeticity of neutrons for a fixed emission angle. In practice, this is achieved by using Hydrogen isotopes as a target. The projectile is again usually a hydrogen isotope, normally a proton or a deuterium.

For the study of the $^{162}Er(n,2n)^{161}Er$ and $^{167}Er(n,p)^{167}Ho$ nuclear reactions , quasi-monoenergetic neutron beams were produced by means of the $^{3}H(d,n)^{4}He$ (D-T reaction). The primary deuteron beam was provided by the Tandem accelerator of N.C.S.R. "Demokritos".

3.5 The Reaction $^{3}H(d,n)^{4}He$

The $^{3}H(d,n)^{4}He$ reaction is frequently used to produce high energy neutrons, because of the relatively high Q-value equals to 17.589 MeV. This is also the main reaction used for neutron beam production in small-scale devises as "neutron generators". Given that a small acceleration of the deuteron beam (~keV) can be enough to reach the resonance region at 107 keV, which allows the production of high intensity neutron beams at energies ~14.5 MeV.

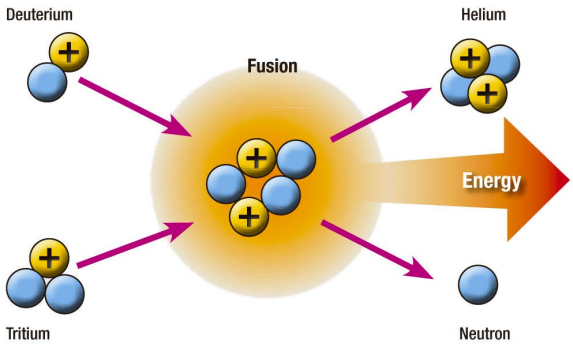

Figure 3.4: The D-T reaction by which the neutron beam is produced.

Deuterium beam is directed through a transmission line (Figure 3.5) which is maintained at high vacuum, towards a CuTiT solid tritium target. In front of the tritium target a Mo foil 5μm in thickness was placed as to de-accelerate the deuteron beam towards to lower energies where the cross section of the D-T reaction is higher (Figure 3.6). Furthermore, it has to be mentioned, that the transmission efficiency of the "Demokritos" 5.5 MV Tandem Van der Graff Accelerator is reduced for energies lower than ~2 MeV and this is an additional reason for operating the accelerator at higher terminal voltage.

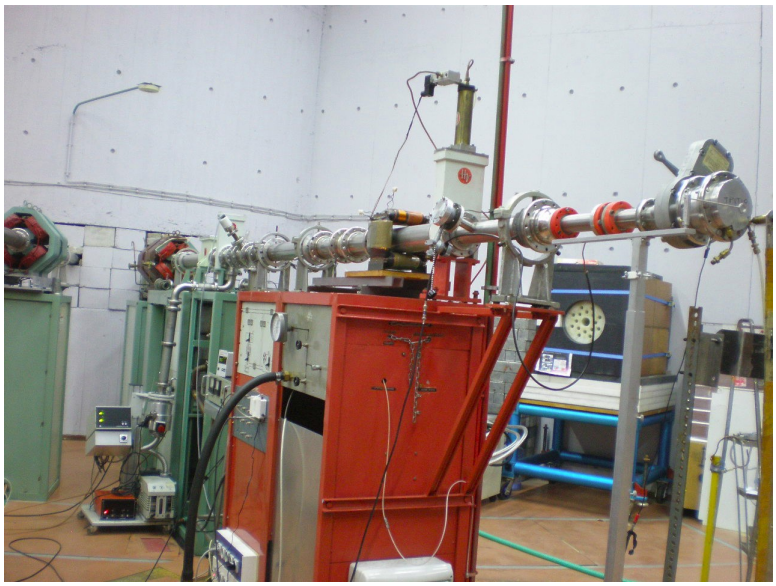

Figure 3.5: Deuterium Beam Transmission Line.

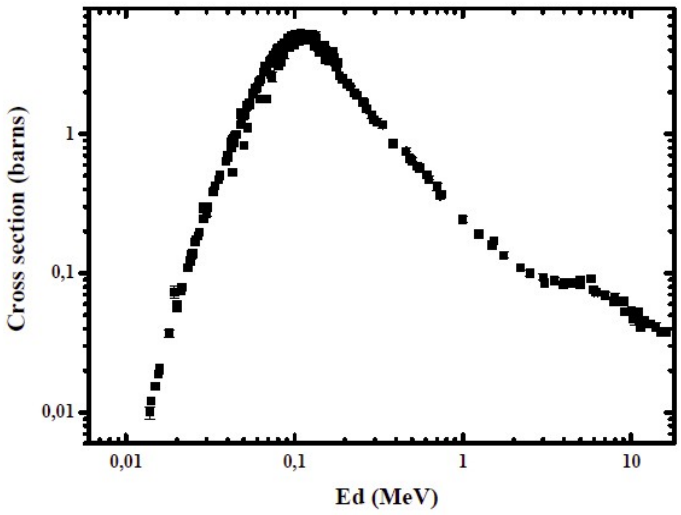

Figure 3.6: Cross section of the D-T reaction in relation with the deuteriums' energy [Kal13].

The tritium target consists of a copper foil Cu, 28.5 mm in diameter and 1 mm thickness, over which is deposited a thick titanium Ti layer, 25.4 mm in diameter. Inside the titanium lies absorbed the tritium with nuclei ratio T/Ti=1.543. The activity of the Tritium is 373 GBq (Figure 3.7).

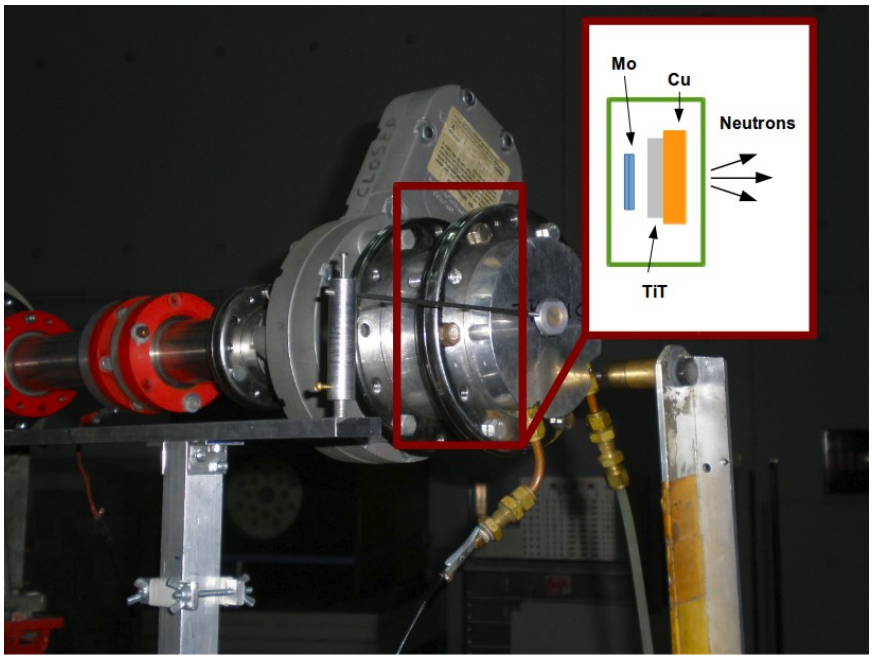

Figure 3.7: Depiction of the tritium target in the end of the experimental line.

In front of tritium target, was used a molecular turbo-compressor pump. The exhaust of the pump was directed in an control area outside the experimental hall. This configuration is crucial for radio-protection reasons in case of tritium gas diffusion.

The neutron beams produced by the reaction of $^{3}H(d,n)^{4}He$, are monoenergetic up to the energy of deuteriums of 3.7 MeV [IAE87]. At higher deuteron energies the break-up of the deuteron as well as the population of excited states in the residual nucleus becomes important. Therefore, the production of neutron beam for E_d> 3.7 MeV is not monoenergetic.

3.6 Determination of the Neutron Beam Energy Using the NeuSDesc Code

The NeuSDesc code (**Neu**tron **S**ource **Des**cription) [Lov02] is a neutron beam simulation toolkit. This code offers a variety of software tools specialized for detailed Monte-Carlo calculations of commonly used nuclear reactions for neutron beam production. The code was developed in the research center JRC- IRMM (Joint Research Centre) which is located in Belgium.

For the determination of neutron energy distribution in an accurate way the physics information with respect the excitation function and differential cross section for each nuclear reaction is taken into account.

Among the calculations that are performed within the NeuSDesc toolkit is also the energy loss and energy strangling of the charged particles within the material of the primary target. For this calculation the different target configurations can be taken into account as well as the different structural materials. The NeuSDesc stopping power calculations are performed by means of the SRIM-TRIM [Zie08] code which is one of the most accurate codes of this kind. For this reason the installation of SRIM-TRIM is one of the prerequisites for the full functionality of the NeuSDesc code.

The SRIM-2008 software, in order to perform simulations makes use of the statistical method of Monte Carlo. It creates and monitors the trajectory of an ion in the target material and then performs detailed calculations of the energy that is attributed to the atoms of the target for each atom-ion collision (BCA - Binary Collision Approximation).

The outgoing flux of neutrons is calculated by Monte Carlo integration on a circular surface. This integration is performed by setting a few random points on the circular disc surface, and then calculating the mean flux of neutrons at each of these points. To perform the calculation the user must enter the radius of the circular disk in mm, and the desired number of points. At the same time is given the opportunity to the user to select the use of SRIM-2008 software as option to "Calculate spectrum software, full angle, including energy straggling". In the Appendix lies the full neutron beam distribution using the NeuSDesc code together with the chosen settings for the three irradiations.

Below can be seen the simulations for the energy distribution of neutrons as derived from the NeuSDesc code [Lov02] for each deuterium bombarding energy.

- **For E_d=2500 keV**

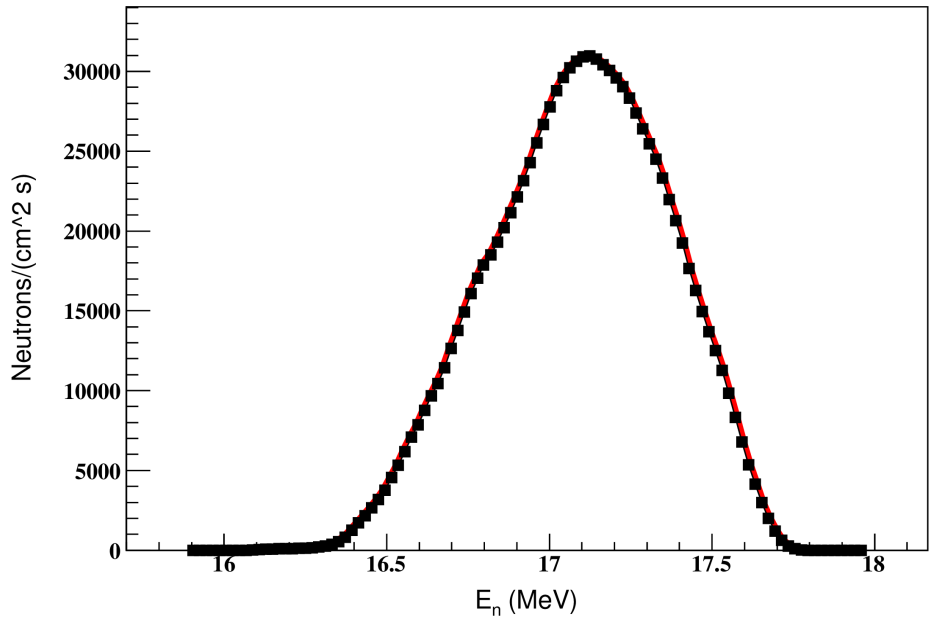

Figure 3.8: Calculation of neutron energy distribution using NeuSDesc code for deuterium incident energy Ed=2.5 MeV.

- **For E_d=3000 keV**

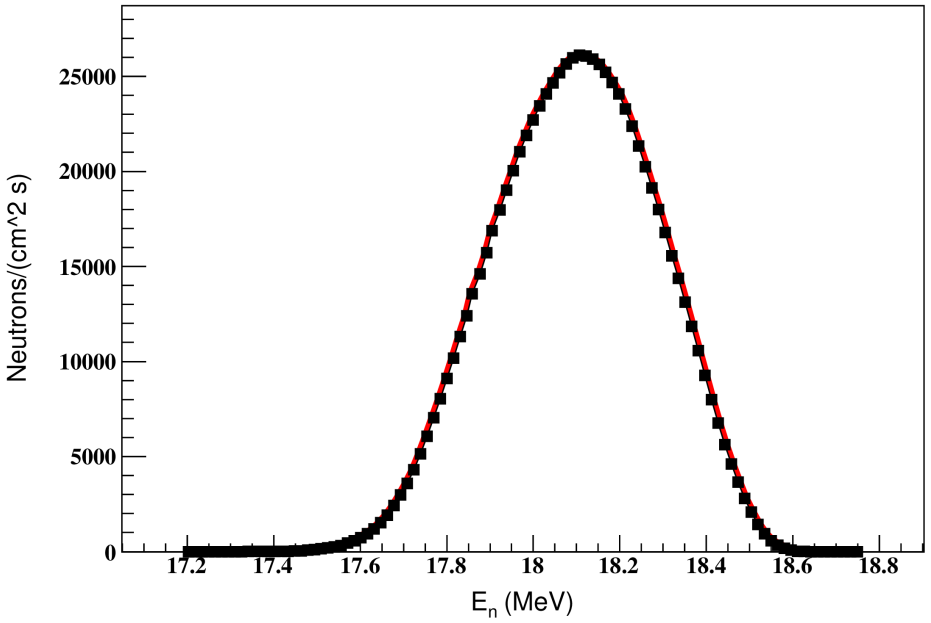

Figure 3.9: Calculation of neutron energy distribution using NeuSDesc code for deuterium incident energy Ed=3.0 MeV.

- **For E_d=3550 keV**

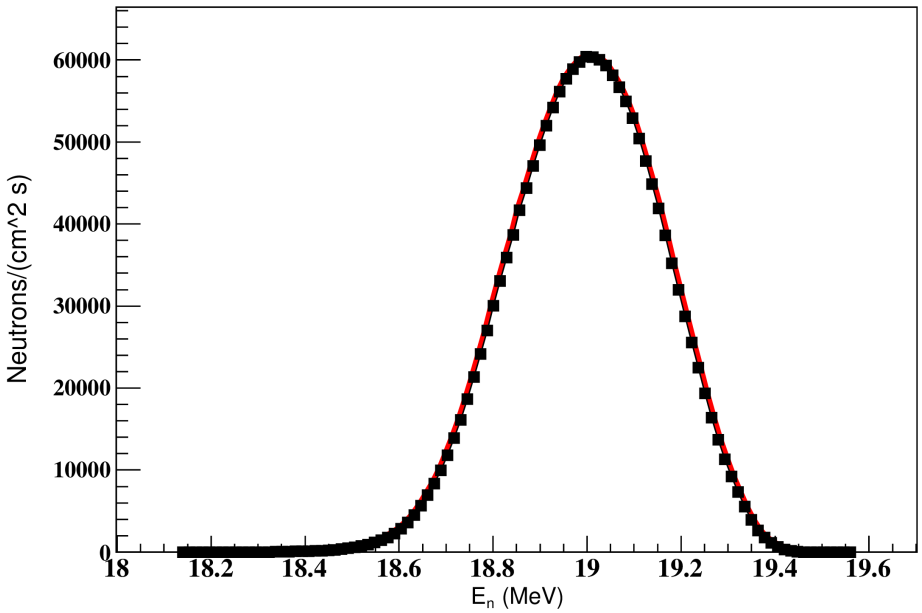

Figure 3.10: Calculation of neutron energy distribution using NeuSDesc code for deuterium incident energy Ed=3.55 MeV.

The Table 3.1, summarizes the results from the above graphs.

Reaction	Target	Ed (MeV)	En (MeV)
T(d,n)^{4}He	T/Ti	2.50	17.1 ± 0.3
		3.00	18.1 ± 0.2
		3.55	19.0 ± 0.2

Table 3.1: Math between deuterium and neutron beam energy.

3.7 Neutron Detection

During the irradiations, a BF_3 neutron counter was used so as to record the fluctuations of the neutron beam (Figure 3.11). The neutron beam intensity fluctuations were taken into account for the accurate determination of the correction factor f_b which corresponds to the decay process during the irradiations. Due to the fact that neutron is neutral, their detection occurs in an indirect way, by detecting the products of the interactions in which they participate.

Figure 3.11: BF3 detector.

A typical BF_3 detector consists of a cylindrical aluminum (brass or copper) tube filled with a BF_3 fill gas at a pressure of 0.5 to 1.0 atmospheres. The boron trifluoride gas accomplishes two things:

- it functions as the proportional fill gas
- it undergoes an (n,a) interaction with thermal neutrons

		Q-value
${}^{10}_{5}B + {}^{1}_{0}n \rightarrow$	${}^{7}_{3}Li + {}^{4}_{2}\alpha$	2.792 MeV (ground state)
	${}^{7}_{3}Li^* + {}^{4}_{2}\alpha$	2.310 MeV (excited state)

Pulse Formation by Neutrons:

When a (thermal) neutron reacts with the ^{10}B component of the gas, an alpha particle and a recoil ^{7}Li nucleus are produced that travel off in opposite directions. The movement of the

alpha particle and ^{7}Li nucleus create primary ion pairs in the gas. The size of the resulting pulse depends on whether the lithium nucleus was left in the ground state or an excited state. When the lithium nucleus is left in the ground state (about 6% of the time), the pulse is larger than if the nucleus was left in an excited state (about 94% of the time) because the alpha particle and ^{7}Li nucleus have more kinetic energy (2.792 MeV vs 2.310 MeV) with which to create ion pairs [Kno00].

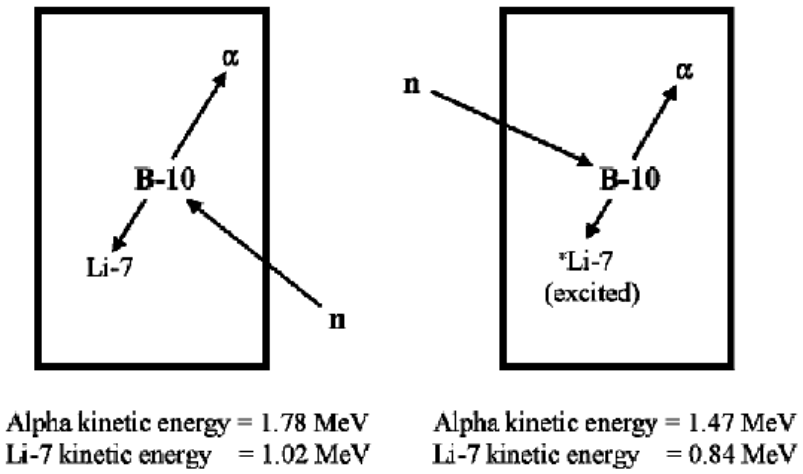

Figure 3.12: Alpha particle and ^{7}Li nucleus create primary ion pairs with different kinetic energies depending if the ^{7}Li was left in an excited or ground state.

When neutrons interact with the ^{10}B of the detector, the produced ^{7}Li and ^{4}He are detected as they lose energy in the gas. This reaction has particularly high cross section for the thermal neutrons (~0.025 eV), which means that the detector has very high yield at low neutron energies. In contrast, for high neutron energies , the yield decreases inversely with the speed of the neutrons. For this purpose, the BF_3 counter is placed in the center of a paraffin barrel which is very rich in hydrogen. Neutrons are scattered in the light nuclei of paraffin losing much of their original energy in each impact. In this way the initial energy of the incident neutron is drastically decreased or even thermalized.

In this experiment, three irradiations took place for energies 17.1, 18.1 and 19 MeV. Below can be seen the fluctuations of the neutron beam for each irradiation as recorded from the BF_3 counter.

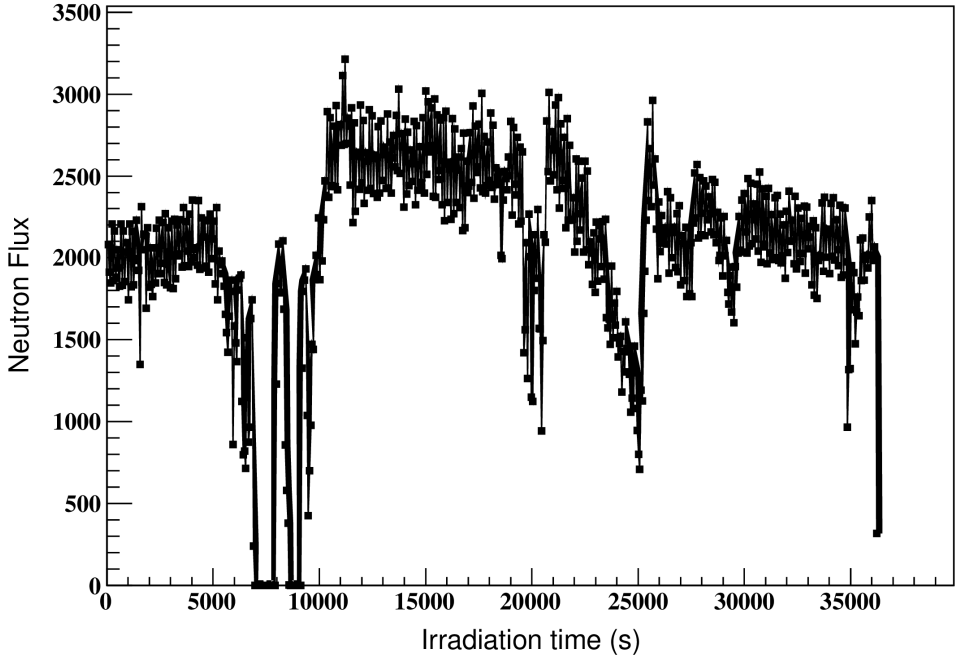

Figure 3.13: Neutron Flux Spectrum during irradiation for En=17.1 MeV.

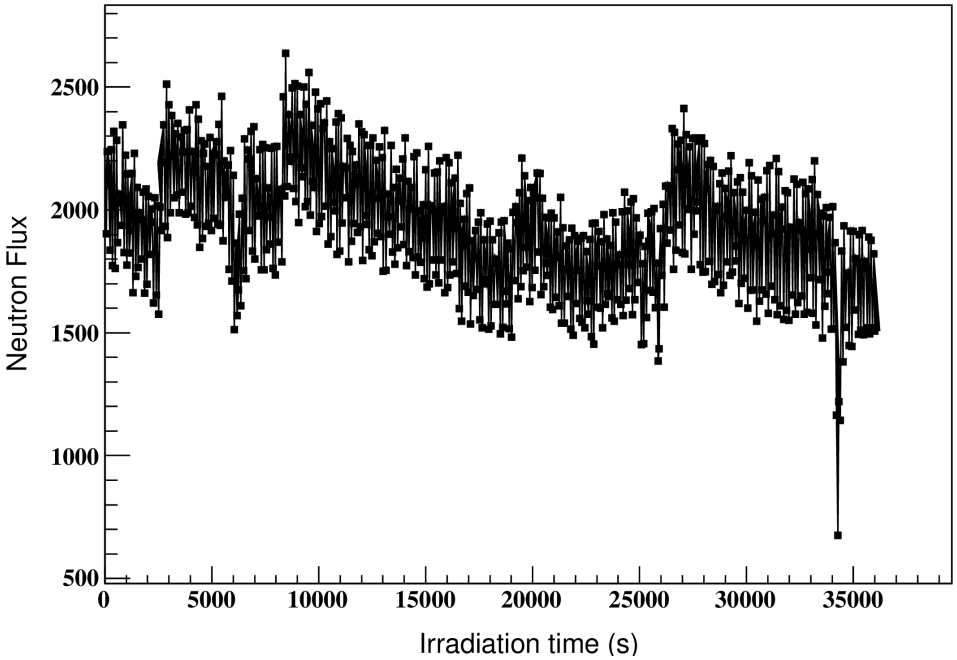

Figure 3.14: Neutron Flux Spectrum during irradiation for En=18.1 MeV.

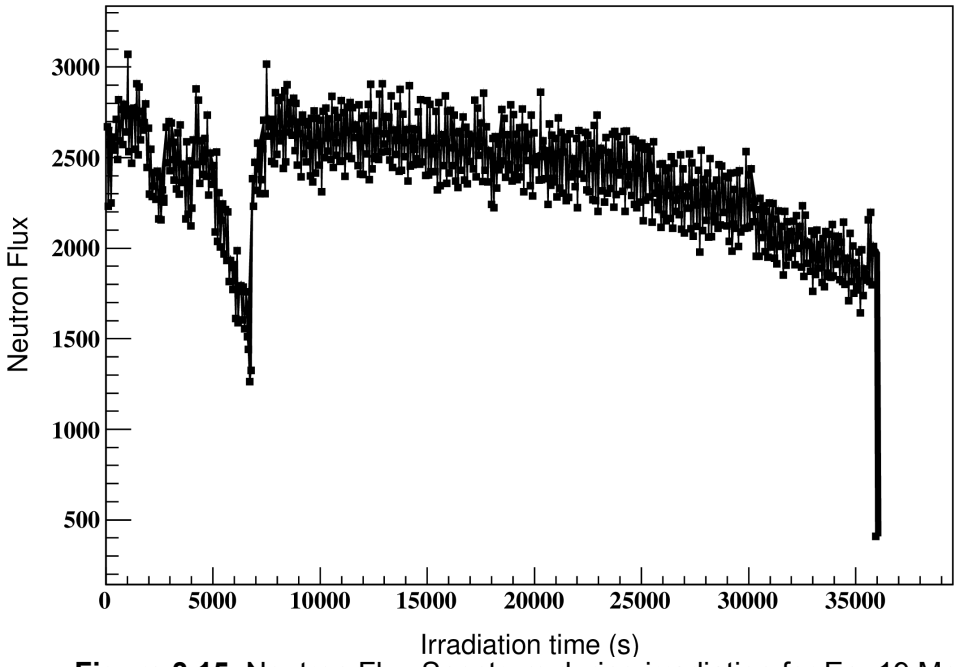

Figure 3.15: Neutron Flux Spectrum during irradiation for En=19 MeV.

3.8 Irradiation Setup

The irradiations were carried out in the neutron beam facility of TANDEM accelerator of the Institute of Nuclear and Particle Physics, N.C.S.R. “Demokritos”. The irradiations of the present work were carried out within the same experimental station, using the setup of the Solid Tritium target for energies at 17.1, 18.1 and 19 MeV.

The targets were placed in a specially designed low-mass holder at the same position for all irradiations at a distance of 1.5 cm with respect the tritium target flange. The duration of each irradiation was three times the half-life time of the (n,2n) reaction product (~10 h).

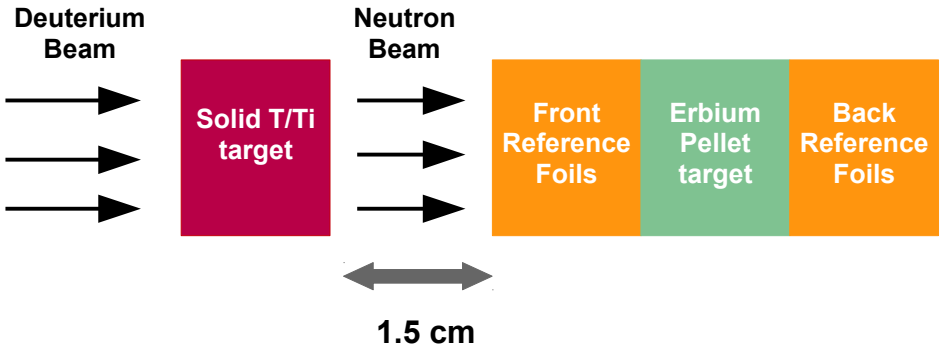

Figure 3.16: The irradiation setup depicting the "Sandwich Technique".

The determination of the neutron beam intensity is of prime importance and in the present and work three different reference reactions were used :

- $^{27}Al(n,a)^{24}Na$
- $^{93}Nb(n, 2n)^{92m}Nb$
- $^{197}Au(n,2n)^{196}Au$

3.9 γ-Ray Activity Measurements

Following the irradiation of the erbium samples and the monitor foils as described previously, the induced activity of the samples was determined by using three coaxial High Purity Germanium (HPGe) detectors.

- Two of them had a relative efficiency 100%. For the γ-ray activity measurements were used in a closed geometry in the configuration that can be seen in Figure 3.17. Each detector was kept in a distance of around 1 cm from the erbium sample which was properly attached in a stable holder.
- The third had a relative efficiency 16%. The samples were placed in front of the detector, in an aluminum holder movable along the axis of the detector. In this way, the source to detector distance could be adjusted. The adopted source to detector window distance from the monitor foil activity measurements was 7 cm (Figure 3.18).

Figure 3.17: Er sample activity measurement.

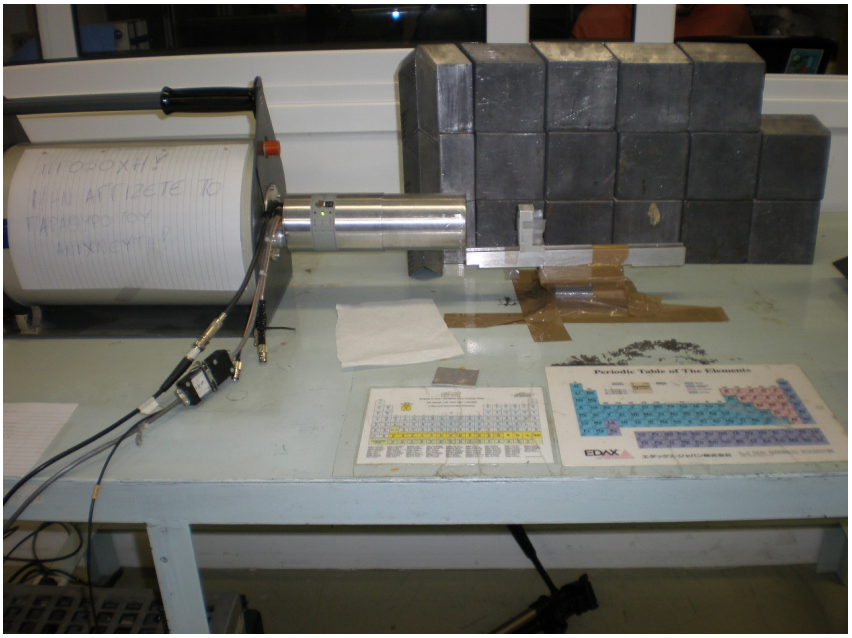

Figure 3.18: 16% HPGe detector.

Prior to the samples activity measurements, the efficiency calibration of the HPGe detectors was performed by using a calibrated ^{152} Eu point source. Several measurements were performed for different distances as to fully characterize the detectors and of course a measurement at the actual source to detector distance. More specifically for the efficiency calibration of the two 100% relative efficiency detectors a ^{54}Mn point source was used.

^{54} Mn source decays through electron capture to the 2^+ state at 835 keV of ^{54}Cr that de-excites to the ground state by emitting a single γ-ray at the same energy, very close to the 826.6 keV γ-ray which is emitted during the de-excitation of the ^{161}Er nucleus. At close detection geometry, the efficiency calibration cannot be performed by using γ-ray sources emitting photons with multiplicity higher than 1. In that case for the close geometry adopted in erbium sample measurements and considering also the high relative efficiency of each detector (100%), important corrections for coincidence summing effects had to be applied. On the other hand, by using single γ-ray sources, as in the present work, the absolute peak efficiency can be experimentally determined without applying important corrections. Additionally, the fact also that the energy of the calibration source is very close to the region of interest allows further simplification of the data analysis.

3.10 Electronics

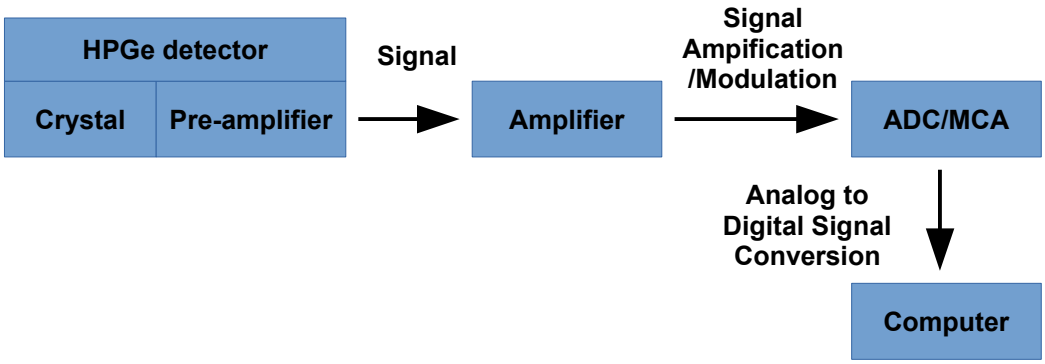

Figure 3.19: Scheme of electronic configuration for the HPGe detectors.

The interaction of a γ-ray with the germanium crystal is accompanied by the generation of electrons and holes in the stripping area. The electons-holes are collected through a strong electric field (~kV) that is applied through the depleted semiconductor material. This results in the creation of a detectable electric signal. Then, the small signal which is about to be amplified, enters the preamplifier and comes out as signal of the order of mV. Afterwards, the signal enters the amplifier as a signal of the order of Volt, while at the same time passes through a process of Differentiation - Integration and ends up having the form of Gaussian

curve. Finally, the ADC / MCA system converts the analog signal into digital information using a Multi-Channel Analyzer. This information is disposed in a memory location of the computer (channel) and eventually a spectrum is created. The calibration of the spectrum is achieved through the assignment of the channels to energies.

3.11 Preparation of the Targets

The sample of natural Er is available in powder-form of Er_2O_3. The pellets constructed with diameter 13 mm are consist of a mixture of 90% powder-form of Er_2O_3 and 10% of Cellulosepulver D as to improve the mechanical properties of the pellets.

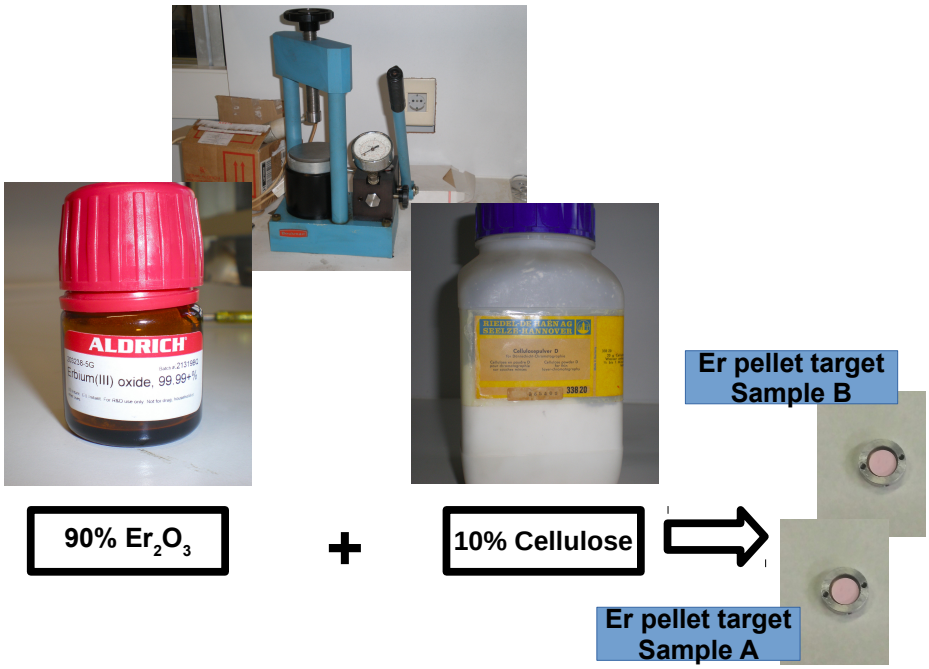

Figure 3.20: Preparation of the Erbium pellet targets using a press machine.

Before the beginning of the irradiations, all the foils were carefully cleaned up to remove any impurities from their surface. Afterwards, the masses and the dimensions of the reference foils and the erbium pellets were measured. The following table summarize these informations.

En=17.1 MeV					
Foils-Targets	**Mass (gr)**	**Diameter (mm)**	**Thickness (mm)**	**Volume (mm^3)**	**Density (gr/mm^3)**
Er_2O_3 (Sample A)	**1.0597**	**12.95**	**2.00**	**263.4265**	**0.0040**
Au_11 (front)	**0.6791**	**13.32**	**0.27**	**37.6238**	**0.0180**
Al_A (front)	**0.2207**	**14.31**	**0.55**	**88.4569**	**0.0025**
Al_B (back)	**0.2210**	**14.26**	**0.59**	**94.2288**	**0.0023**
Au_2 (back)	**1.4374**	**14.34**	**0.50**	**80.7529**	**0.0178**

Table 3.2: Table with the characteristics of targets for the first irradiation.

En=18.1 MeV					
Foils-Targets	**Mass (gr)**	**Diameter (mm)**	**Thickness (mm)**	**Volume (mm^3)**	**Density (gr/mm^3)**
Er_2O_3 (Sample B)	**0.9944**	**12.95**	**1.99**	**262.1093**	**0.0038**
Au_92 (front)	**0.6466**	**13.40**	**0.25**	**35.2565**	**0.0183**
Al_10 (front)	**0.1808**	**13.07**	**0.53**	**71.1077**	**0.0025**
Al_1 (back)	**0.1817**	**13.03**	**0.59**	**78.6739**	**0.0023**
Au_62 (back)	**0.6548**	**13.51**	**0.25**	**35.8377**	**0.0183**

Table 3.3: Table with the characteristics of targets for the second irradiation.

En=19 MeV					
Foils-Targets	**Mass (gr)**	**Diameter (mm)**	**Thickness (mm)**	**Volume (mm^3)**	**Density (gr/mm^3)**
Er_2O_3 (Sample A)	**1.0597**	**12.95**	**2.00**	**263.4265**	**0.0040**
Nb_2 (front)	**0.3026**	**13.26**	**0.33**	**45.5712**	**0.0066**
Al_F (front)	**0.1662**	**11.99**	**0.59**	**66.6163**	**0.0025**
Al_8 (back)	**0.1918**	**13.31**	**0.58**	**80.7001**	**0.0024**
Nb_11 (back)	**0.3375**	**14.15**	**0.34**	**53.4665**	**0.0063**

Table 3.4: Table with the characteristics of targets for the third irradiation.

CHAPTER 4
DATA ANALYSIS

4.1 Calibration of the 16% HPGe Detector

For the energy calibration of the 16% HPGe detector a ^{152}Eu point source was used that emits photons in an extended energy region. The ^{152}Eu source was placed at 7, 10 and 13.4 cm distance with respect to the detector's window. Below can be seen a typical energy spectrum of the ^{152}Eu decay.

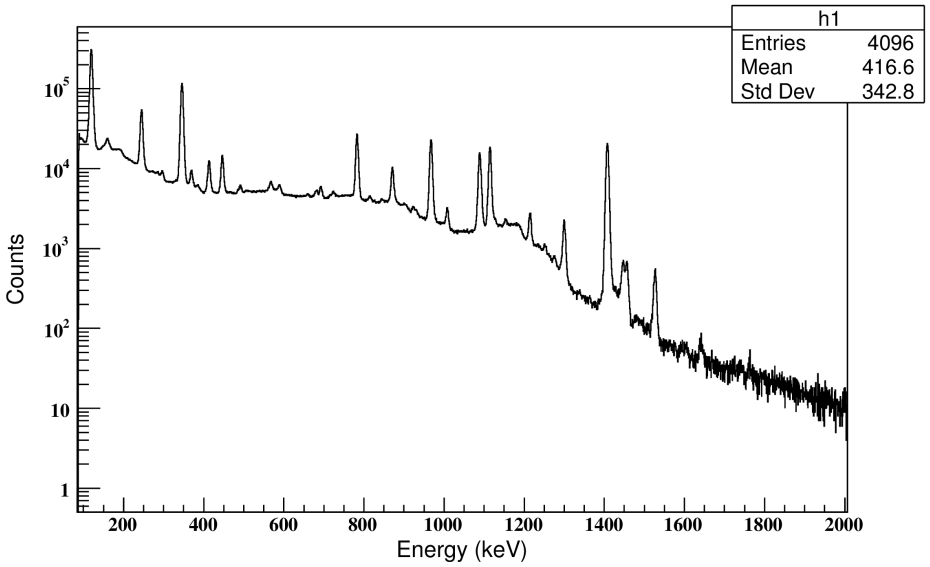

Figure 4.1: Energy spectrum of the ^{152}Eu decay at 7cm from the window of the 16% HPGe detector.

In order to create the efficiency curves of the 16% HPGe detector for several distances, the absolute peak efficiency ε of the detector should be calculated, for every photon energy. The efficiency is given by the formula:

$$\varepsilon = \frac{cps}{emissions} = \frac{\frac{counts}{livetime}}{A \cdot I} \qquad (4.1)$$

where, the activity A of the ^{152}Eu source was calculated using the equation :

$$A = A_o \cdot e^{-\lambda t} \qquad (4.2)$$

where, A_0 is the reference activity of the point source and
t is the time interval between the reference date and the date of the measurement.

^{152}Eu	
A_o (Bq)	217000
σ_{Ao} (Bq)	3000
Reference Date	01/01/2011
Experiment Date	01/07/2014
Duration (days)	1277
Duration (years)	3.4986
Half-life (years)	13.517
$\sigma_{Half-life}$ (years)	0.014
λ(years^{-1})	0.051280
σ_{λ}(years^{-1})	0.000053
A(Bq)	181361
$\sigma_{A(Bq)}$	2508

Table 4.1: Activity of the ^{152}Eu point source for the spectra at 7 and 10 cm.

E (keV)	σ_E (keV)	I	σ_I	Counts	σ_{Counts}	ε	σ_ε
244.6974	0.0008	0.07550	0.00040	435778	1093	0.009197	0.000138
344.2785	0.0012	0.26590	0.00200	1079590	1254	0.006470	0.000102
443.9606	0.0016	0.02827	0.00014	93887	619	0.005292	0.000085
778.9045	0.0024	0.12930	0.00080	220385	696	0.002716	0.000042
964.0570	0.0050	0.14510	0.00070	205805	603	0.002260	0.000034
1112.0760	0.0030	0.13670	0.00080	17375	567	0.002025	0.000031
1408.0130	0.0030	0.20870	0.00090	208469	481	0.001592	0.000023

Table 4.2: Efficiencies from a spectrum with livetime= 3460.378 s where the ^{152}Eu is placed at 7 cm distance from the 16% HPGe detector's window [Mar13].

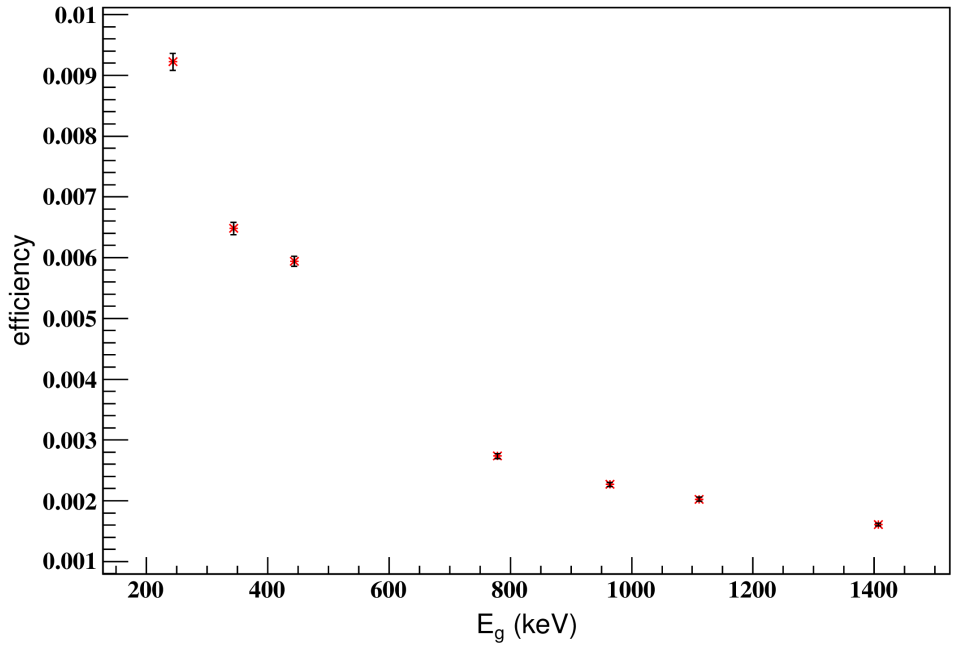

Figure 4.2: Calibration Curve for the 16% HPGe at 7 cm.

E (keV)	σ_E (keV)	I	σ_I	Counts	σ_{Counts}	ε	σ_ε
244.6974	0.0008	0.07550	0.00040	270207	864	0.005586	0.000085
344.2785	0.0012	0.26590	0.00200	652810	968	0.003832	0.000061
443.9606	0.0016	0.02827	0.00014	58006	478	0.003203	0.000054
778.9045	0.0024	0.12930	0.00080	134907	539	0.001629	0.000026
964.0570	0.0050	0.14510	0.00070	128150	476	0.001379	0.000021
1112.0760	0.0030	0.13670	0.00080	102699	414	0.001173	0.000018
1408.0130	0.0030	0.20870	0.00090	129395	372	0.000968	0.000014

Table 4.3: Efficiencies from a spectrum with livetime= 3532.468 s where the ^{152}Eu is placed at 10 cm distance from the 16% HPGe detector's window [Mar13].

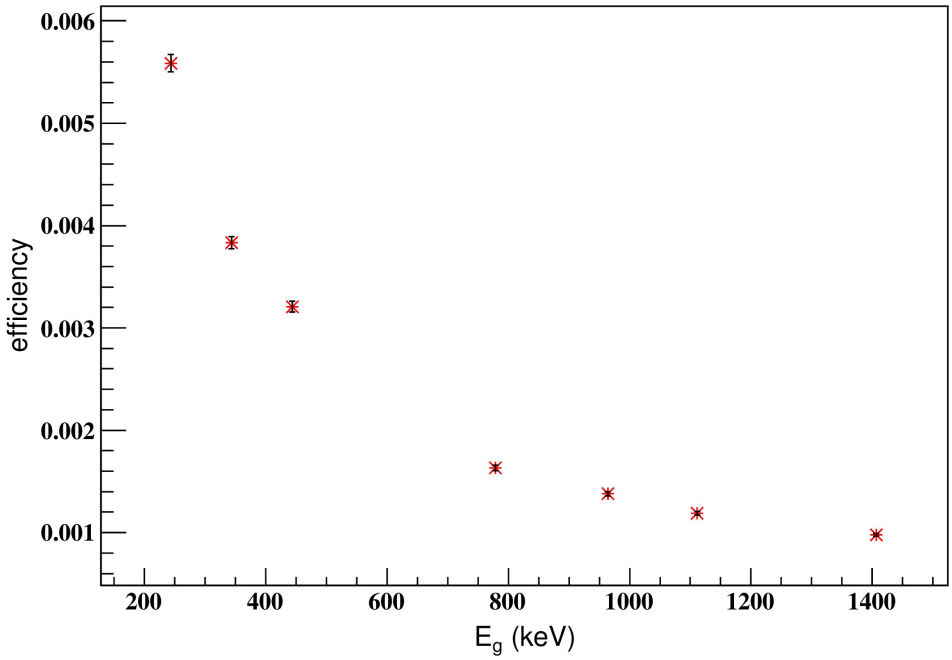

Figure 4.3: Calibration Curve for the 16% HPGe detector at 10 cm.

^{152}Eu	
A_o (Bq)	217000
σ_{Ao} (Bq)	3000
Reference Date	01/01/2011
Experiment Date	30/06/2014
Duration (days)	1276
Duration (years)	3.4959
Half-life (years)	13.517
$\sigma_{Half\text{-}life}$ (years)	0.014
λ(years^{-1})	0.051280
σ_{λ}(years^{-1})	0.000053
A(Bq)	181386
$\sigma_{A(Bq)}$	2508

Table 4.4: Activity of the ^{152}Eu point source for the spectrum at 13.4 cm.

E (keV)	σ_E (keV)	I	σ_I	Counts	σ_{Counts}	ε	σ_ε
244.6974	0.0008	0.07550	0.00040	32680	322	0.003455	0.000061
344.2785	0.0012	0.26590	0.00200	77662	354	0.002331	0.000038
443.9606	0.0016	0.02827	0.00014	7256	173	0.002049	0.000058
778.9045	0.0024	0.12930	0.00080	16107	194	0.000994	0.000019
964.0570	0.0050	0.14510	0.00070	15574	167	0.000857	0.000016
1112.0760	0.0030	0.13670	0.00080	11947	144	0.000698	0.000013
1408.0130	0.0030	0.20870	0.00090	15910	130	0.000609	0.000010

Table 4.5: Efficiencies from a spectrum with livetime= 690.661 s where the ^{152}Eu is placed at 13.4 cm distance from the 16% HPGe detector's window [Mar13].

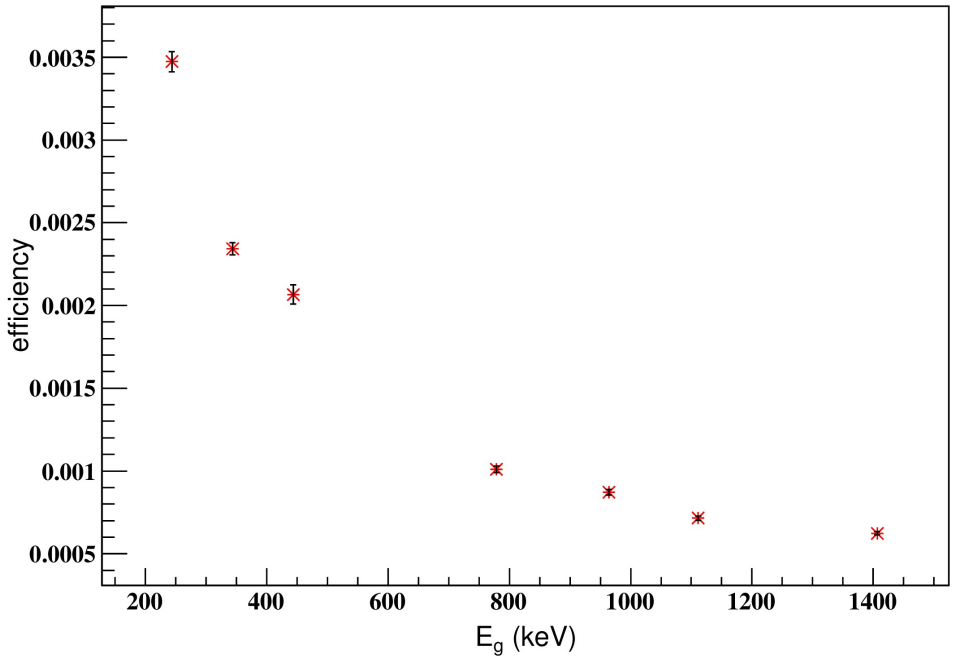

Figure 4.4: Calibration Curve for the 16% HPGe detector at 13.4 cm.

4.2 Efficiency of the Reference Foils

In order to simplify the interpolation procedure and to get a valid efficiency curve for the energy range of interest, the experimentally deduced efficiency points were presented graphically in the form: **ln efficiency=f (lnE)**. In this way, through the implementation of a linear fit (least squares method) and by adopting 68% confidence level bands, we are able to get the absolute peak efficiency at 7 cm for the characteristic γ-rays from the decay of the monitor foils. (Figure 4.5)

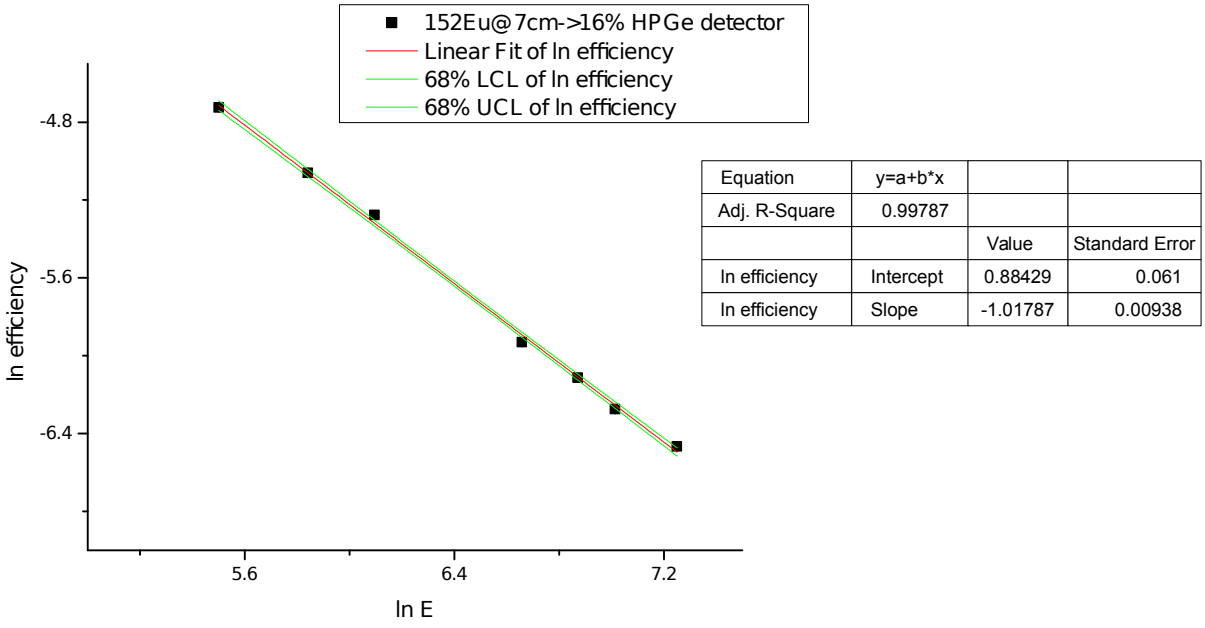

Figure 4.5: Graphical Representation of lnε=f (lnE) of the 16% HPGe detector at 7 cm.

The results are shown in the following table:

Target Nucleus	Decay Nucleus	Decay Radiation	efficiency	σ efficiency
^{197}Au	^{196}Au	333.03 keV	0.06554	0.00013
^{93}Nb	^{92m}Nb	934.44 keV	0.002293	0.000035
^{27}Al	^{24}Na	1368.626 keV	0.001554	0.000032

Table 4.6: Reference foils' efficiency for 7 cm distance from the window of the 16% HPGe detector [Xia07],[Bag12],[Fir07].

4.3 Determination of the ^{54}Mn Activity

For the efficiency determination of the two 100% HPGe detectors at close detection geometry, the ^{152}Eu point source was not suitable because of its complicated γ-ray cascade scheme. In such a close geometry as the one finally adopted, considering also the high relative efficiency of each detector, the complexity of the decay scheme would impose significant correction factors for the coincidence summing effects. For this reason, for the calibration of the two 100% HPGe detectors used for the measurement of the erbium samples, was finally utilized using a weak ^{54}Mn source that emits only one strong γ-ray at 834.848 keV (Figure 4.6) which is very close to the one at 826.6 keV from the ^{161}Er decay.

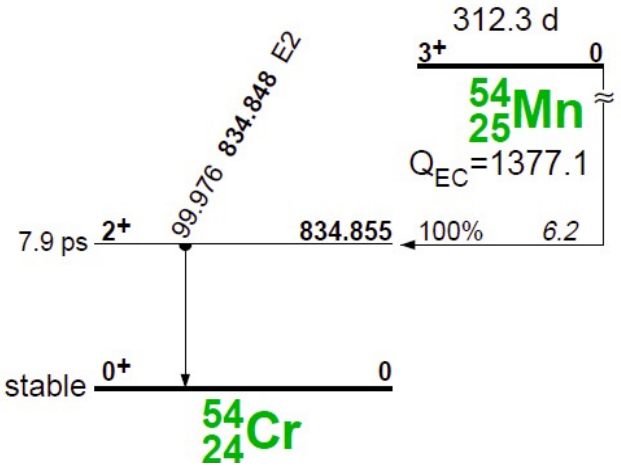

Figure 4.6: ^{54}Mn decay scheme.

To overcome the fact that the ^{54}Mn point source was not calibrated, the spectrum of the 16% HPGe detector, from the measurement of the ^{152}Eu source at 13.4 cm was used as to determine the efficiency of the detector at 834.848 keV- the characteristic decay line of ^{54}Mn. This relatively large distance was used as to minimize as possible the relative uncertainty concerning the placement of the source relative to the detector's window (Figure 4.7). Having determined the absolute peak detection efficiency, the ^{54}Mn point source activity was obtained in an accurate way.

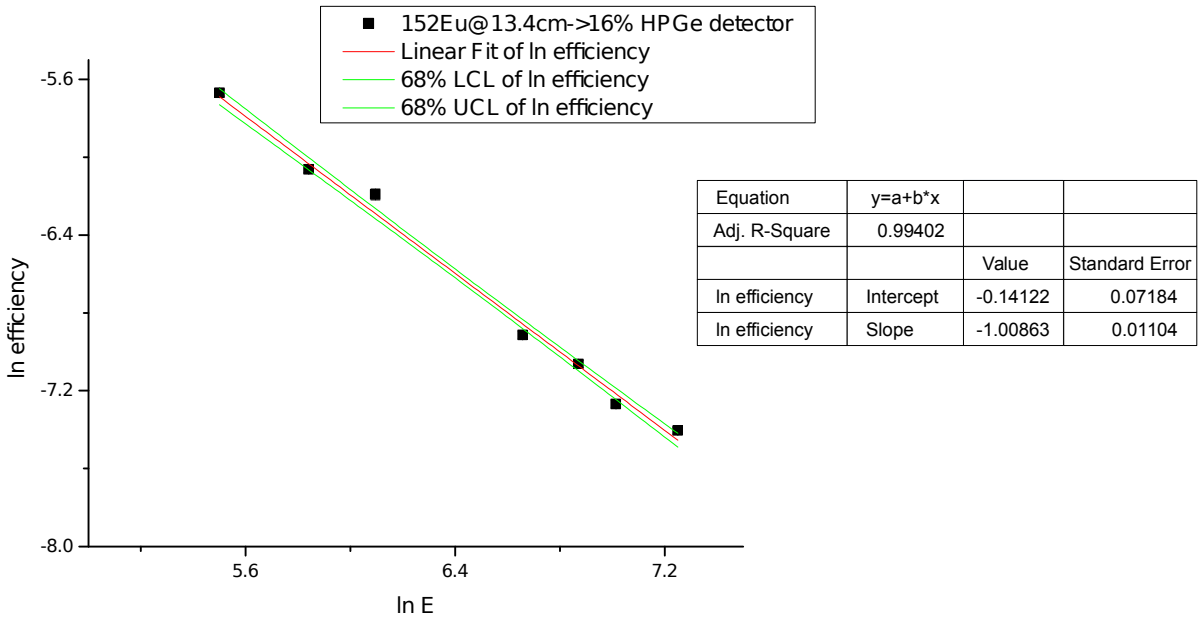

Figure 4.7: Graphical Representation of lnε=f (lnE) of the 16% HPGe detector at 13.4 cm.

The results are shown in the following table:

Parent Nucleus	Daughter Nucleus	Decay Radiation	efficiency	$\sigma_{efficiency}$
^{54}Mn	**^{54}Cr**	834.848 keV	0.000981	0.000024

Table 4.7: ^{54}Mn source's efficiency for 13.4 cm distance from the window of the 16% HPGe detector [DJ14].

The activity of the ^{54}Mn monoenergetic point source can be found using the formula (4.1).

E (keV)	σ_E (keV)	I	σ_I	Counts	σ_{Counts}	A (Bq)	σ_A (Bq)
834.848	0.003	0.99976	0.00001	1442	42	408	16

Table 4.8: Activity of the ^{54}Mn source extracted from a spectrum with livetime=3599.494 s where the source is placed at 13.4 cm distance from the 16% HPGe detector's window [DJ14].

4.4 Efficiency of the 2 x 100% HPGe Detectors' at Close Geometry

The absolute peak detection efficiency of the 2x100% HPGe detection setup had to be determined at the 826.6 keV γ-ray energy. Accordingly, the usage of the ^{54}Mn source is optimum for three reasons already mentioned in the text but summarized also below:

- The energy of interest is very close to the one of the ^{54}Mn calibrated source
- The ^{54}Mn source is monoenergetic. For this reason, there is no need for coincidence summing effect corrections. The same holds also for the actual measurements
- The ^{54}Mn source is weak enough as to keep as low as possible, probable implications of pile-up and/or dead time issues

For the calibration procedure the same geometry was implemented as the one of the actual Erbium sample measurements. The results of the calibration procedure are given in the tables 4.9-4.11.

	E (keV)	σ_E (keV)	I	σ_I	Counts	σ_{Counts}	A (Bq)	σ_A (Bq)	ε	σ_ε
ADC1	834.848	0.003	0.99976	0.00001	23975	157	408	16	0.0052	0.0020

Table 4.9: Efficiency of the first HPGe detector at 834.848 keV at close geometry extracted from a spectrum with livetime= 1136.31 s.

	E (keV)	σ_E (keV)	I	σ_I	Counts	σ_{Counts}	A (Bq)	σ_A (Bq)	ε	σ_ε
ADC2	834.848	0.003	0.99976	0.00001	23248	154	408	16	0.0051	0.0019

Table 4.10: Efficiency of the second HPGe detector at 834.848 keV at close geometry extracted from a spectrum with livetime= 1136.233 s.

In order to find the total efficiency, there spectra are summed and the livetime of the spectrum arising is defined as:

$$live\,time = \frac{live\,time_{ADC\,1} + live\,time_{ADC2}}{2} = 1136.2715\,s$$

	E (keV)	σ_E (keV)	I	σ_I	Counts	σ_{Counts}	A (Bq)	σ_A (Bq)	ε	σ_ε
Final	834.848	0.003	0.99976	0.00001	47176	220	408	16	0.1017	0.0039

Table 4.11:Total Efficiency of the 2 x100% HPGe detectors at 834.848 keV at close geometry extracted from a spectrum with livetime= 1136.2715 s.

4.5 Correction Factors

4.5.1 The f_b Correction Factor

The f_b factor is the correction factor by which the balance between the production and the decay of nuclei during irradiation is calculated. As mentioned in the previous chapter fb is expressed as:

$$f_b = \frac{\int_0^{t_{irr}} e^{\lambda t} \cdot f(t)\, dt}{\int_0^{t_{irr}} f(t)\, dt} \cdot e^{-\lambda t_{irr}} \qquad (4.3)$$

Depending on whether the neutron beam flux is constant or not the fb correction factor can take two forms:

- **<u>Constant Flux:</u>** means that $f(t) \rightarrow f_{ct}$ and the fb factor has the analytical solution

$$f_b = \frac{(1 - e^{-\lambda t_{ir}})}{\lambda t_{ir}} \qquad (4.4)$$

- **<u>Non-Constant Flux</u>:** the fb factor can be determined via the relation:

$$f_b = \frac{e^{-\lambda t_{ir}} \sum_{i=1} f_i \left(e^{(i+1)\lambda dt} - e^{i \lambda dt} \right)}{\lambda\, dt \sum_{i=1} f_i} \qquad (4.5)$$

  where the intervals of the previous formula (4.3) are now calculated from the corresponding channels of the neutron beam fluctuations spectra.

During all irradiations the BF_3 detector was monitoring the fluctuations of the neutron flux and the recorded spectra were used as input to a program developed in C++ that calculates the f_b correction factor for each target nucleus participating in the activations (see Appendix).

In the following table the f_b correction factor for each irradiation setup is given.

Decay Nucleus	E_n=17.1 MeV	E_n=18.1 MeV	E_n=19 MeV
	fb correction factor		
^{161}Er	0.41384	0.396773	0.392012
^{167}Ho	0.403491	0.38648	0.381562
^{24}Na	0.803986	0.79495	0.794199
^{196}Au	0.97739	0.976229	
^{92m}Nb			0.985438

Table 4.12: fb correction factor results.

4.5.2 The CF_{SA} Correction Factor

During the detection process of γ-radiation, a part of γ-rays emitted by the sample is absorbed or attenuated by the sample itself and therefore does not register under the detection peak. The extent of self-absorption and self-attenuation depends upon the energy of γ-rays, physical characteristics (Z atomic number), chemical composition of the material (density, mixtures), sample geometry (size, shape) and sample's position relative to the detector (solid angle dependence). For this reason, the estimation of the CF_{SA} correction factor is crucial.

To investigate the influence of the self-attenuation and self-absorption in the activity measurements, detailed Geant4 Monte Carlo simulations were performed (See Appendix).

Firstly, the manufacturer geometry was adopted using the appropriate framework and classes of the Geant4 detector simulation toolkit [Ago03]. The performance of the simulations with respect different distances for the calibrated point sources was tested with respect the experimental results. Having ensured that the simulation reproduces successfully the point source calibration spectra for different source to detector distances the same detector geometry was implemented for the monitor foils and erbium samples.

The CF_{SA} correction factor for every reference foil was tracked down via the formula:

$$CF_{SA} = \frac{efficiency_{PS}}{efficiency_{ES}} \qquad (4.6)$$

where $efficiency_{PS}$ is the point source detection efficiency and
$efficiency_{ES}$ is the detection efficiency for the sample material ans actual dimensions

By considering the CFSA as the ratio of the detection efficiencies for a point source and for the actual detection source, any systematic uncertainties from Geant4 MC calculation were canceled out and the detection efficiency was based on experimental results.

In the following table, the correction factors for self-attenuation concerning the reference foils can be seen.

Reference Foils	Eγ (keV)	CF_{SA}	σ CF_{SA}
En=17.1 MeV			
Al_B	1368.626	1.005	0.005
Al_A	1368.626	1.005	0.005
Au_2	333.03	1.128	0.002
Au_11	333.03	1.0550	0.0014
En=18.1 MeV			
Al_1	1368.626	1.005	0.005
Al_10	1368.626	1.005	0.005
Au_62	333.03	1.0550	0.0014
Au_92	333.03	1.0550	0.0014
En=19 MeV			
Al_8	1368.626	1.005	0.005
Al_F	1368.626	1.005	0.005
Nb_11	934.44	1.007	0.004
Nb_2	934.44	1.007	0.004

Table 4.13: CF_{SA} correction factors for the reference foils as retrieved from the Geant4 MC calculations.

For the case of the decay of the ^{161}Er, the correction factor CF_{SA} took into account not only the self-attenuation but in addition the fact that the detection set-up system of the 2x100 % HPGe detectors was calibrated at the 834.848 KeV gamma-ray of the monoenergetic point source of ^{54}Mn. Unlike the efficiency measurements for the reference foils, in the detection set-up used for the measurement of erbium samples' activity, the efficiency value for the 826.6 keV gamma-ray is not possible to be experimentally known. This is because the use of ^{152}Eu point source for the calibration curve design in such a close geometry would be subject to extended coincidence summing effects.

The CF_{SA} correction factor for the ^{161}Er case was calculated via the formula:

$$CF_{SA} = \frac{efficiency_{^{54}Mn}}{efficiency_{^{161}Er}} \qquad (4.7)$$

where $efficiency_{^{54}Mn}$ is the experimental efficiency of the ^{54}Mn monoenergetic point source at 834.848 KeV and

$efficiency_{^{161}Er}$ is the efficiency taken from the Geant4 MC simulations for the extended source of ^{161}Er at 826.6 KeV

The result of this calculation can be seen in the following table.

Nucleus	Eγ (keV)	ε	σ ε	CF_{SA}	σ CF_{SA}
^{161}Er	826.6	0.1017	0.0039	1.023	0.005

Table 4.14: CF_{SA} correction factor for the ^{161}Er decay as retrieved from the Geant4 MC calculations along with the experimental efficiency that was taken into account in the calculations.

For the case of the decay of the ^{167}Ho, the absolute peak efficiency was directly determined from Geant4 MC calculations where the coincidence summing effects, self-attenuation corrections as well as solid angle corrections for the extended erbium sample geometry were included in the calculated efficiency (Table 4.15).

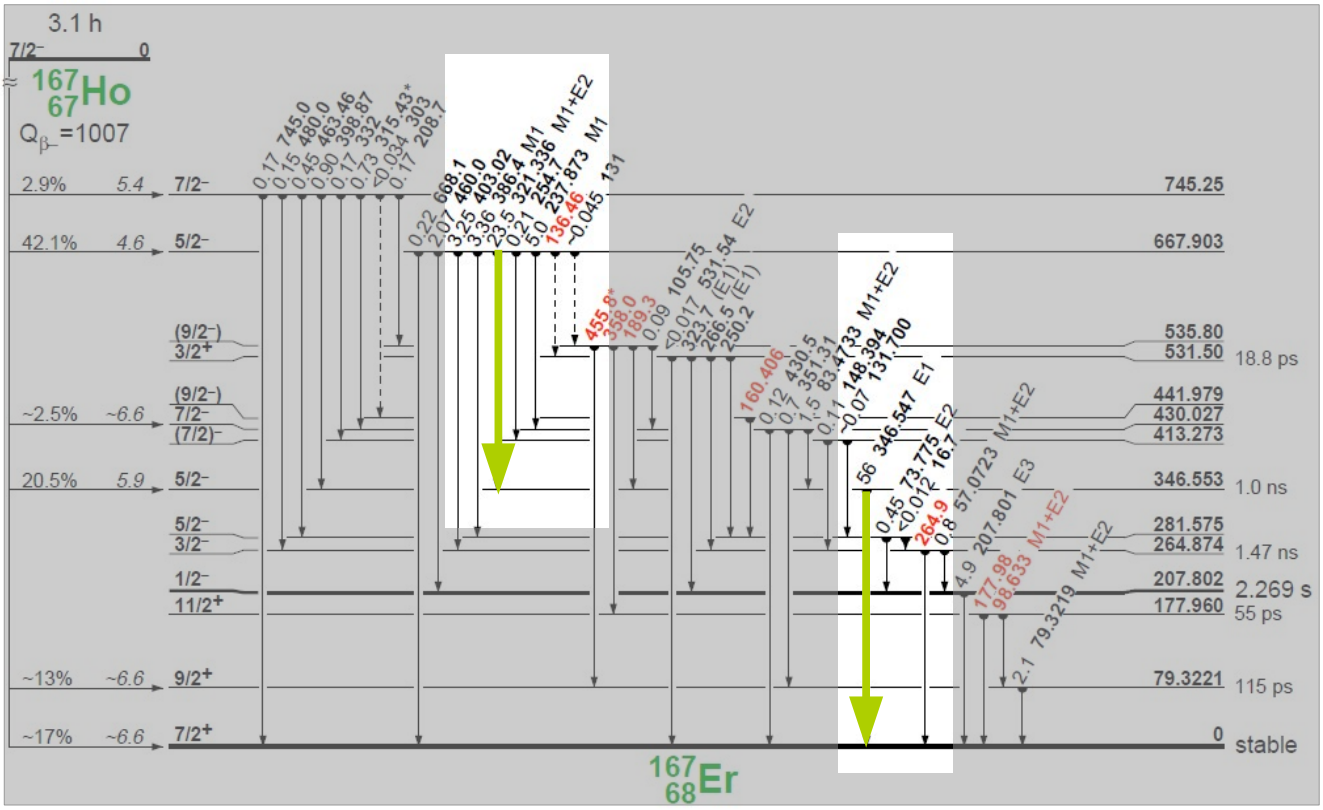

Figure 4.8: Decay scheme of ^{167}Ho highlighting the summing coincidence effect.

Coincidence summing effects:

Coincidence summing corrections are necessary when radioactive nucleus emits two or more photons within the resolving time of the detector. The importance of this effect depends on the detection geometry and the decay scheme of the radioactive source. For instance, when the first photon γ_1 with energy $E_{\gamma 1}$ deposits all its energy in the Ge crystal and if a second photon γ_2 with $E_{\gamma 2}$ is also detected, a sum pulse is recorded at the energy $E_{sum}= E_{\gamma 1}+ E_{\gamma 2}$ [DH88]. In this scenario some counting rate is lost for the first peak and at the same time additional artificial counts are recorded to the summing peak. In this way, when the multiplicity of a decay event is higher than 1 and if the solid angle covered from the γ-ray detector is large enough, then the contribution of the summing effect to the overall recorded intensity of each peak may be subject of important corrections. At larger source to detector distances, when the expected counting rate allows so, the summing effect contribution is expected to be negligible.

For the case of ^{161}Er activity, the coincidence summing effect correction factor was not considered given that the decay scheme for the most intense line at 826.6 keV is very simple with a multiplicity very close to 1. On the other hand, for the decay of ^{167}Ho this correction has to be taken into account in the efficiency value at 346.5 KeV. For this reason, the full isotopic decay was followed in the Geant4 MC calculations by using appropriate classes(G4IonTable, G4ParticleDefinition).

The results for the coincidence summing out correction are summarized in the next table.

Nucleus	Eγ (keV)	ε	σ_ε	CF_{SA}	σCF_{SA}
^{167}Ho	346.5	0.15	0.00	1	0

Table 4.15: Efficiency for the ^{167}Ho decay as retrieved from the Geant4 MC simulations taking into account the coincidence summing effects from the decay of ^{167}Ho nucleus.

4.5.3 The CF_{DT} Correction Factor

The dead time of a detector is defined as the minimum time interval that two consecutive counts must be separated in order to be recorded as two different events. The effect of having a dead time in a detector used to monitor counting rates is that the measured counting rates will be lower than the real ones. However, the correction factor for the dead time of the detector can be determined via the relation:

$$CF_{DT}=\frac{real\,time}{live\,time} \qquad (4.8)$$

where $realtime$ stands for the actual duration of the measurement and
$livetime$ stands for the time period where the Data Acquisition System (DAQ) was

really active and able to accept, process and record the produced pulses

4.6 Cross section of Reference Reactions

As mentioned above, the monitor foils were placed in front and back of the erbium sample utilizing the neutron flux determination in the sample. As can be seen in the following figures, the excitation function of the monitor reactions ^{197}Au(n,2n)^{196}Au, ^{27}Al(n,a)^{24}Na and ^{93}Nb(n,2n)^{92m}Nb is accurately known, allowing the neutron flux estimation of the reactions under study ^{162}Er(n,2n)^{161}Er and ^{167}Er(n,p)^{167}Ho by means of activation technique.

The reference cross sections used were retrieved from the IRDFF v. 1.05 data base (October 2014) [IRD14] and the results are summarized in the Table 4.16.

Reference Reaction	cross section (barns)	$\sigma_{\text{cross section}}$ (barns)
En=17.1 MeV		
^{197}Au(n,2n)^{196}Au	**1.982**	**0.041**
^{27}Al(n,a)^{24}Na	**0.07472**	**0.00062**
En=18.1 MeV		
^{197}Au(n,2n)^{196}Au	**1.660**	**0.032**
^{27}Al(n,a)^{24}Na	**0.05990**	**0.00059**
En=19 MeV		
^{93}Nb(n,2n)^{92m}Nb	**0.3759**	**0.0045**
^{27}Al(n,a)^{24}Na	**0.04852**	**0.00058**

Table 4.16: cross sections of reference reactions as retrieved from the IRDFF v. 1.05 data base.

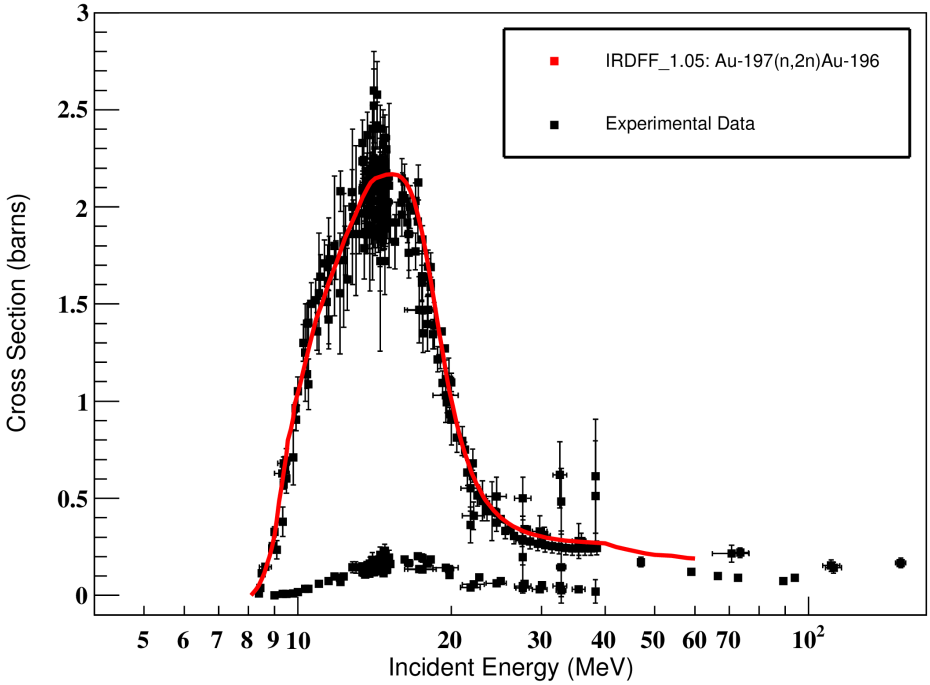

Figure 4.9: Excitation function of the $^{197}Au(n,2n)^{196}Au$ reaction as retrieved from the IRDFF v. 1.05 data base.

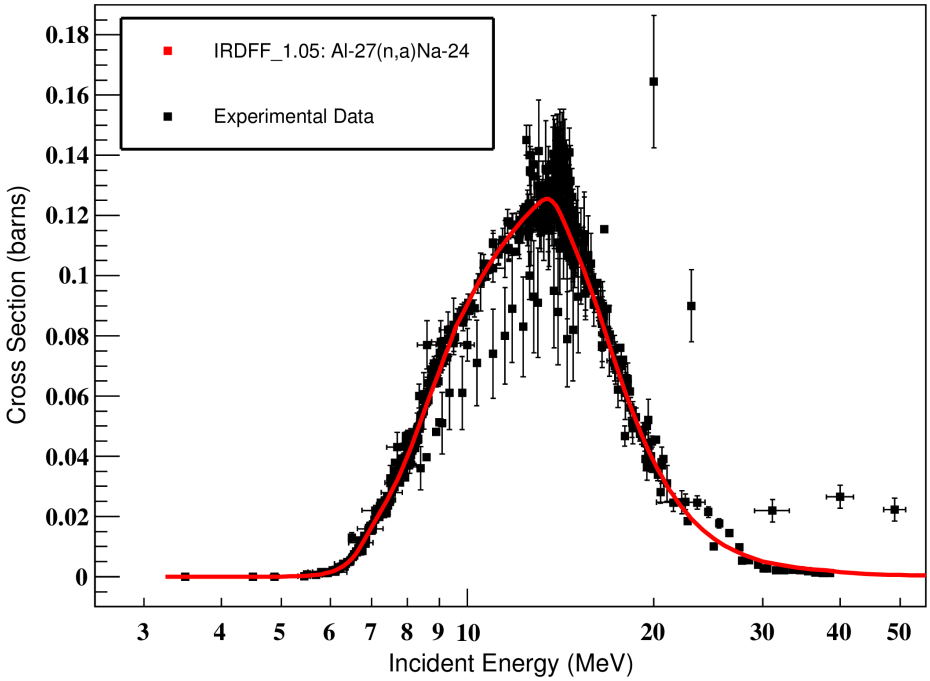

Figure 4.10: Excitation function of the $^{27}Al(n,a)^{24}Na$ reaction as retrieved from the IRDFF v. 1.05 data base.

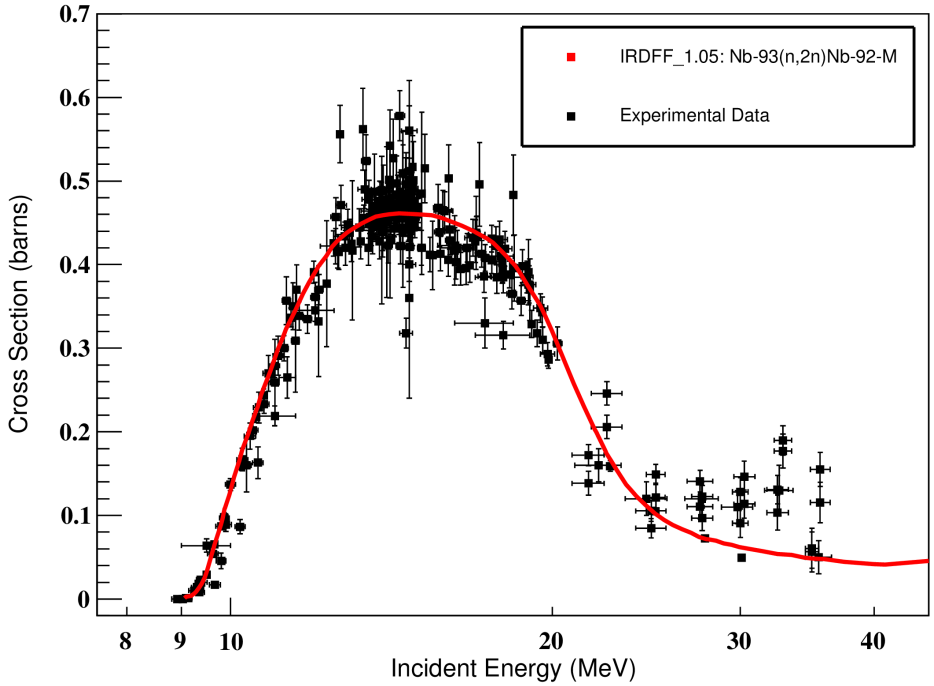

Figure 4.11: Excitation function of the ^{93}Nb(n,2n)^{92m}Nb reaction as retrieved from the IRDFF v. 1.05 data base.

4.7 Neutron Flux

In order to determine the neutron flux at each irradiation, the relation 4.8 as reported in the previous chapter will be used.

$$\Phi = \frac{counts \cdot CF_{SA} \cdot CF_{DT}}{\varepsilon \cdot I_{\gamma} \cdot \sigma \cdot N_T \cdot e^{-\lambda t_w} \left(1 - e^{-\lambda t_m}\right) \cdot f_b} \qquad (4.8)$$

The neutron flux will be calculated as the result of the mean value of the recorded neutron flux from the foil placed in front and in back position with respect to the erbium pellet target. The uncertainty of the mean neutron flux for every irradiation has been estimated equal to 7% of the its value.

$$\Phi = \frac{\Phi_{front\,foil} + \Phi_{back\,foil}}{2} \qquad (4.9) \qquad \sigma_{\Phi} = 0.07 \cdot \Phi \qquad (4.10)$$

Reference Reaction	En=17.1 MeV $^{197}Au(n,2n)^{196}Au$	
	Front Foil	Back Foil
Mass (gr)	0.6791	1.4374
σ_{Mass} (gr)	0.0002	0.0002
Atomic Weight	196.966568786	196.966568786
# of atoms in the target	1	1
Natural Abundance of target isotope	1	1
Half-life (h)	148.0056	148.0056
Irradiation time (s)	36240	36240
σ (barns)	0.07472	0.07472
σ_{σ} (barns)	0.00062	0.00062
Waiting time (s)	2.48340	148892
$\sigma_{Waiting\ time}$ (s)	60	60
Measuring time (s)	18014	18016
efficiency	0.06554	0.06554
$\sigma_{efficiency}$	0.00013	0.00013
Gamma Intensity	0.22881	0.22881
$\sigma_{Gamma\ Intensity}$	0.00946	0.00946
Counts	1247	2514
σ_{Counts}	57	76
CF_{SA}	1.0550	1.128
σ_{CFSA}	0.0014	0.002
CF_{DT}	1.0009	1.0010
f_b	0.97739	0.97739
Φ (neutrons/cm^2)	**1.30 E+10**	**1.17 E+10**

Table 4.17: Neutron flux data analysis for the first irradiation.

Reference Reaction	En=18.1 MeV $^{197}Au(n,2n)^{196}Au$	
	Front Foil	Back Foil
Mass (gr)	0.6466	0.6548
σ_{Mass} (gr)	0.0002	0.0002
Atomic Weight	196.966568786	196.966568786
# of atoms in the target	1	1
Natural Abundance of target isotope	1	1
Half-life (h)	148.0056	148.0056
Irradiation time (s)	36000	36000
σ (barns)	1.660	1.660
σ_{σ} (barns)	0.032	0.032
Waiting time (s)	220687	185034
$\sigma_{Waiting\ time}$ (s)	60	60
Measuring time (s)	34233	28826
efficiency	0.06554	0.06554
$\sigma_{efficiency}$	0.00013	0.00013
Gamma Intensity	0.22881	0.22881
$\sigma_{Gamma\ Intensity}$	0.00946	0.00946
Counts	1894	1147
σ_{Counts}	103	73
CF_{SA}	1.0550	1.0550
σ_{CFSA}	0.0014	0.0014
CF_{DT}	1.0011	1.0010
f_b	0.976229	0.976229
Φ (neutrons/cm^2)	**1.27 E+10**	**8.61 E+09**

Table 4.18: Neutron flux data analysis for the second irradiation.

Reference Reaction	En=19 MeV $^{93}Nb(n,2n)^{92m}Nb$	
	Front Foil	Back Foil
Mass (gr)	0.3026	0.3375
σ_{Mass} (gr)	0.0002	0.0002
Atomic Weight	92.906373004	92.906373004
# of atoms in the target	1	1
Natural Abundance of target isotope	1	1
Half-life (h)	243.6	243.6
Irradiation time (s)	35940	35940
σ (barns)	0.3759	0.3759
σ_{σ} (barns)	0.0045	0.0045
Waiting time (s)	222089	165575
$\sigma_{Waiting\ time}$ (s)	60	60
Measuring time (s)	25211	25212
efficiency	0.002293	0.002293
$\sigma_{efficiency}$	0.000035	0.000035
Gamma Intensity	0.9915	0.9915
$\sigma_{Gamma\ Intensity}$	0	0
Counts	294	277
σ_{Counts}	21	21
CF_{SA}	1.007	1.007
σ_{CFSA}	0.004	0.004
CF_{DT}	1.0000	1.0006
f_b	0.985438	0.985438
Φ (neutrons/cm^2)	**1.05 E+10**	**9.46 E+09**

Table 4.19: Neutron flux data analysis for the third irradiation.

Φ (neutrons/cm^2)	σ $_\Phi$ (neutrons/cm^2)
En=17.1 MeV	
1.23 E+10	8.64 E+08
En=18.1 MeV	
1.07 E+10	7.47 E+08
En=19 MeV	
9.46 E+09	6.62 E+08

Table 4.20: Neutron fluxes results for each irradiation.

4.8 Investigation of (n,x) Reactions for Erbium Isotopes

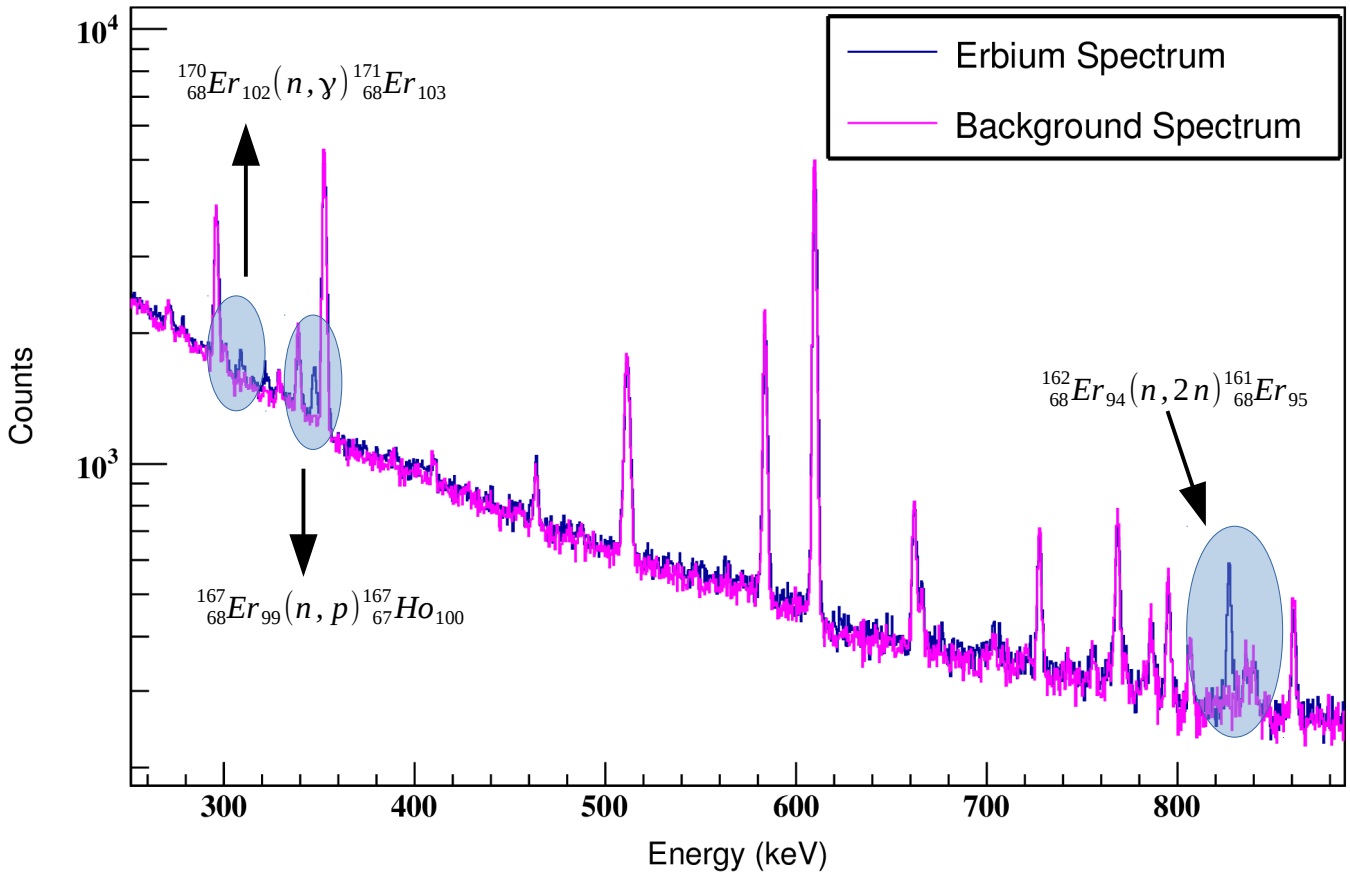

Figure 4.12: Neutron induced reactions for Erbium Isotopes based on 7 hours spectra.

According to the above spectrum taken from the 10 hours of neutron irradiation at En=17.1 MeV, three are the reactions that are triggered for the Erbium isotopes. The features of these reactions are listed on the Table 4.21. The same reactions take place in the other two neutron irradiations at 18.1 and 19 MeV as well.

Reaction	$E_{threshold}$ (MeV)	$T_{1/2}$ (h) of radioactive nucleus	Eγ (keV)	Iγ (%)
$^{162}Er(n,2n)^{161}Er$	9.262 ± 0.009	3.21 ± 0.03	826.6 ± 0.1	64 ± 4
$^{167}Er(n,p)^{167}Ho$	0.23 ± 0.06	3.1 ± 0.1	346.5 ± 0.2	57 ± 15
$^{170}Er(n,\gamma)^{171}Er$	0	7.516 ± 0.002	308.291 ± 0.018	64 ± 3

Table 4.21: Characteristics of (n,x) reactions at neutron energies higher than 17 MeV, for Erbium isotopes [Bag00], [Bag02], [Rei11].

4.9 Experimental Cross section Calculation for Erbium Isotopes

The experimental cross section of the reactions under study was obtained using the relation 4.11 (mentioned also in the previous chapter).

$$\sigma = \frac{counts \cdot CF_{SA} \cdot CF_{DT}}{\varepsilon \cdot I_{\gamma} \cdot \Phi \cdot N_T \cdot e^{-\lambda t_w}\left(1 - e^{-\lambda t_m}\right) \cdot f_b} \qquad (4.11)$$

The total uncertainty for each cross section will be obtained by combing the individual uncertainties in quadrature, according to the law of error propagation.

4.9.1 Cross section of the $^{162}_{68}Er_{94}(n,2n)^{161}_{68}Er_{93}$ Nuclear Reaction

Reaction	^{162}Er(n,2n)^{161}Er		
	En=17.1 MeV	En=18.1 MeV	En=19 MeV
Mass (gr)	1.0597	0.9944	1.0597
σ_{Mass} (gr)	0.0005	0.0005	0.0005
Molecular Weight	382.52	382.52	382.52
# of atoms in the target	2	2	2
Natural Abundance of target isotope	0.00139	0.00139	0.00139
Half-life (h)	3.21	3.21	3.21
Irradiation time (s)	36240	36000	35940
Φ (neutrons/cm^2)	1.23 E+10	1.07 E+10	9.46 E+09
σ_{Φ} (neutrons/cm^2)	8.64 E+08	7.47 E+08	6.62 E+08
Waiting time (s)	2816	3203	2349
$\sigma_{Waiting\ time}$ (s)	60	60	60
Measuring time (s)	36034	18017	25225
efficiency	0.1017	0.1017	0.1017
$\sigma_{efficiency}$	0.0039	0.0039	0.0039
Gamma Intensity	0.6405	0.6405	0.6405
$\sigma_{Gamma\ Intensity}$	0.0370	0.0370	0.0370
Counts	2210	1178	1418
σ_{Counts}	121	88	99
CF_{SA}	1.023	1.023	1.023
σ_{CFSA}	0.005	0.005	0.005
CF_{DT}	1.0018	1.0015	1.0016
f_b	0.41384	0.396773	0.392012
σ (barns)	**1.96**	**1.84**	**1.92**
σ_{σ} (barns)	**0.22**	**0.23**	**0.23**

Table 4.22: cross section results for the ^{162}Er(n,2n)^{161}Er nuclear reaction.

4.9.2 Cross section of the $^{167}_{68}Er_{99}(n,p)^{167}_{67}Ho_{100}$ Nuclear Reaction

Reaction	^{167}Er(n,p)^{167}Ho		
	En=17.1 MeV	En=18.1 MeV	En=19 MeV
Mass (gr)	1.0597	0.9944	1.0597
σ_{Mass} (gr)	0.0005	0.0005	0.0005
Molecular Weight	382.52	382.52	382.52
# of atoms in the target	2	2	2
Natural Abundance of target isotope	0.22869	0.22869	0.22869
Half-life (h)	3.1	3.1	3.1
Irradiation time (s)	36240	36000	35940
Φ (neutrons/cm^2)	1.23 E+10	1.07 E+10	9.46 E+09
σ_{Φ} (neutrons/cm^2)	8.64 E+08	7.47 E+08	6.62 E+08
Waiting time (s)	2816	3203	2349
$\sigma_{Waiting\ time}$ (s)	60	60	60
Measuring time (s)	18017	27027	30629
efficiency	0.15	0.15	0.15
$\sigma_{efficiency}$	0	0	0
Gamma Intensity	0.57	0.57	0.57
$\sigma_{Gamma\ Intensity}$	0.15	0.15	0.15
Counts	1786	1786	2393
σ_{Counts}	93	105	114
CF_{SA}	1	1	1
σ_{CFSA}	0	0	0
CF_{DT}	1.0021	1.0016	1.0015
f_b	0.403491	0.38648	0.381562
σ (barns)	**0.0097**	**0.0106**	**0.0146**
σ_{σ} (barns)	**0.0027**	**0.0030**	**0.0040**

Table 4.23: cross section results for the ^{167}Er(n,p)^{167}Ho nuclear reaction.

4.9.2.1 Contribution of the Interfering Reaction $^{170}_{68}Er_{102}(n,a)^{167}_{66}Dy_{101}$

As the target material used was erbium of natural isotopes composition, the possibility that some of the studied activation products might be formed not only with direct way but also via other interfering reactions, must be definitely be examined [Luo13]. In the case of ^{167}Er(n,p)^{167}Ho reaction, it is necessary to correct for this effect via the ^{170}Er(n,a)^{167}Dy process. When de-excited, the nucleus ^{167}Dy leads to the formation of the ^{167}Ho nucleus as can be seen in the following figure.

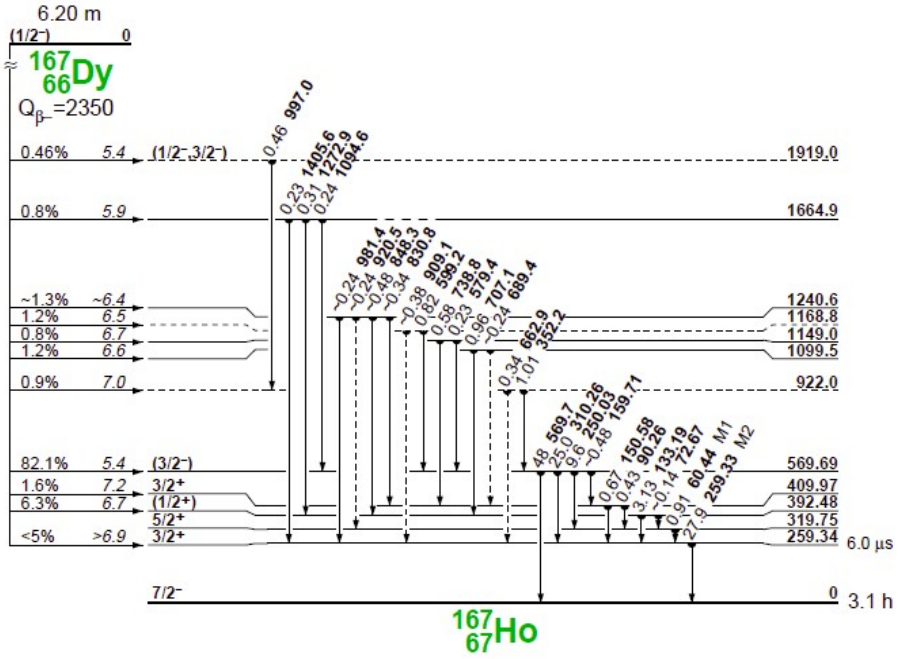

Figure 4.13: Formation of the ^{167}Ho nucleus via the ^{170}Er(n,a)^{167}Dy neutron induced reaction.

Taking into account the contamination of this channel to the ^{167}Er(n,p)^{167}Ho reaction under study, the cross section of the ^{170}Er(n,a)^{167}Dy nuclear reaction should be subtracted. The problem is that from the already taken data, the extraction of the cross section for this channel is not possible due to the short half-life of the ^{167}Dy nucleus ($T_{1/2}$= 6.20 s) in relation with the long waiting time from the end of the irradiations until the start of the erbium's activity measurement (>40 min which is longer than 3 times the nucleus's half-life). On the other hand, a new measurement in the Tandem Van der Graaf 5.5 MV accelerator of the Institute of Nuclear and Particle Physics of N.C.S.R. “Demokritos” is not feasible due to low cross section of the ^{170}Er(n,a)^{167}Dy reaction (mbarn region) and the short half-life time of the product nucleus.

Therefore, for the necessary correction in the cross section the ENDF/B-VII.1 data base will be used as there are no experimental data in the energy region of interest above 17 MeV. Additionally, the excitation function will be rescaled before the extraction of the cross section as all the existing experimental data are divergent in relation with the given excitation function. The uplift of the line was calculated based on the more recent measurements and more specifically those of *Dzysiuk et al. ,2012* and *Luo et al. ,2011*.

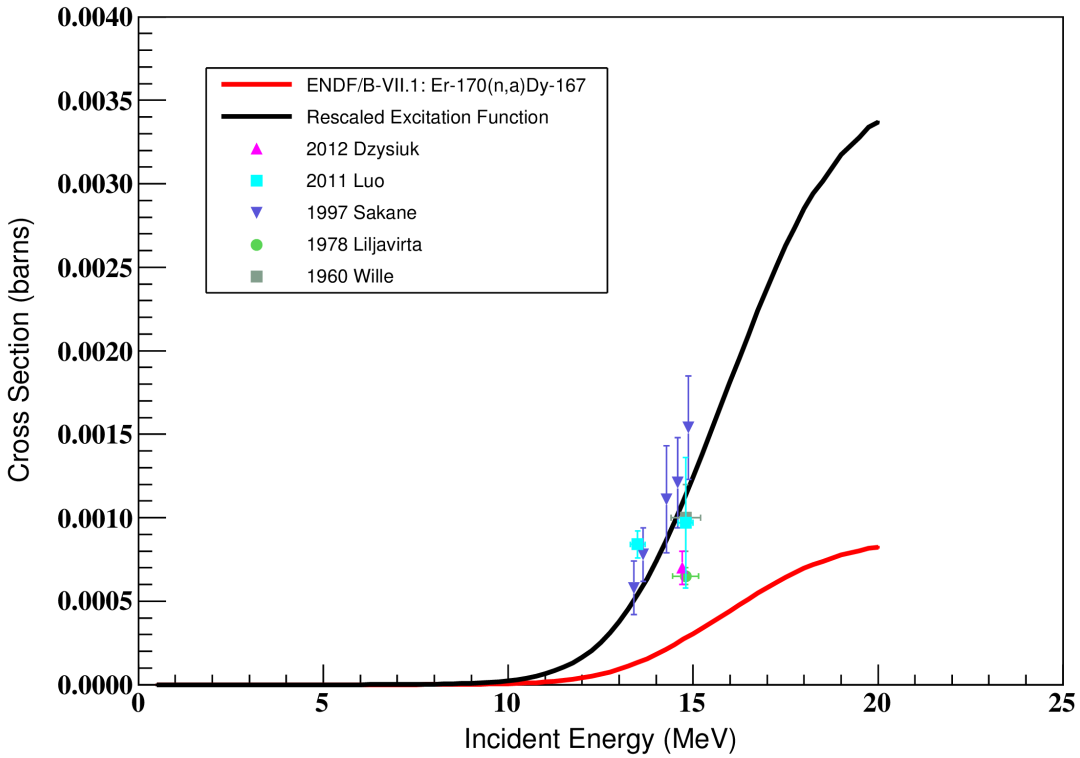

Figure 4.14: Excitation function of the ^{170}Er(n,a)^{167}Dy reaction with the measured data as retrieved from the ENDF/B-VII.1 data base [Dzy12] [Luo11] [Sak97] [LT78] [WF60].

The results from the interpretation of the above rescaled excitation function are presented in the following table.

En (MeV)	cross section (barns)
17.1	0.0025
18.1	0.0029
19	0.0032

Table 4.24: Estimation of the cross section for the reaction ^{170}Er(n,a)^{167}Dy for the energy region of interest.

4.9.2.2 Final Cross section Estimation of the $^{167}_{68}Er_{99}(n,p)^{167}_{67}Ho_{100}$ Reaction

En (MeV)	cross section (barns)	$\sigma_{\text{cross section}}$ (barns)
17.1	0.0072	0.0027
18.1	0.0077	0.0030
19	0.0114	0.0040

Table 4.25: Cross sections of the ^{167}Er(n,p)^{167}Ho neutron induced reaction.

4.9.3 The Case of the $^{170}_{68}Er_{102}(n,\gamma)^{171}_{68}Er_{103}$ Reaction

It is not possible to extract the ^{170}Er(n,γ)^{171}Er cross section from this experiment because the reaction has zero threshold and the reaction is activated by low energy neutrons.

CHAPTER 5
RESULTS AND DISCUSSION

5.1 Experimental Cross section Results

The results of the experimental cross sections of the present work for the reactions $^{162}Er(n,2n)^{161}Er$ and $^{167}Er(n,p)^{167}Ho$ at neutron energies of 17.1, 18.1 and 19 MeV along with previous experimental data points are depicted in the following figures.

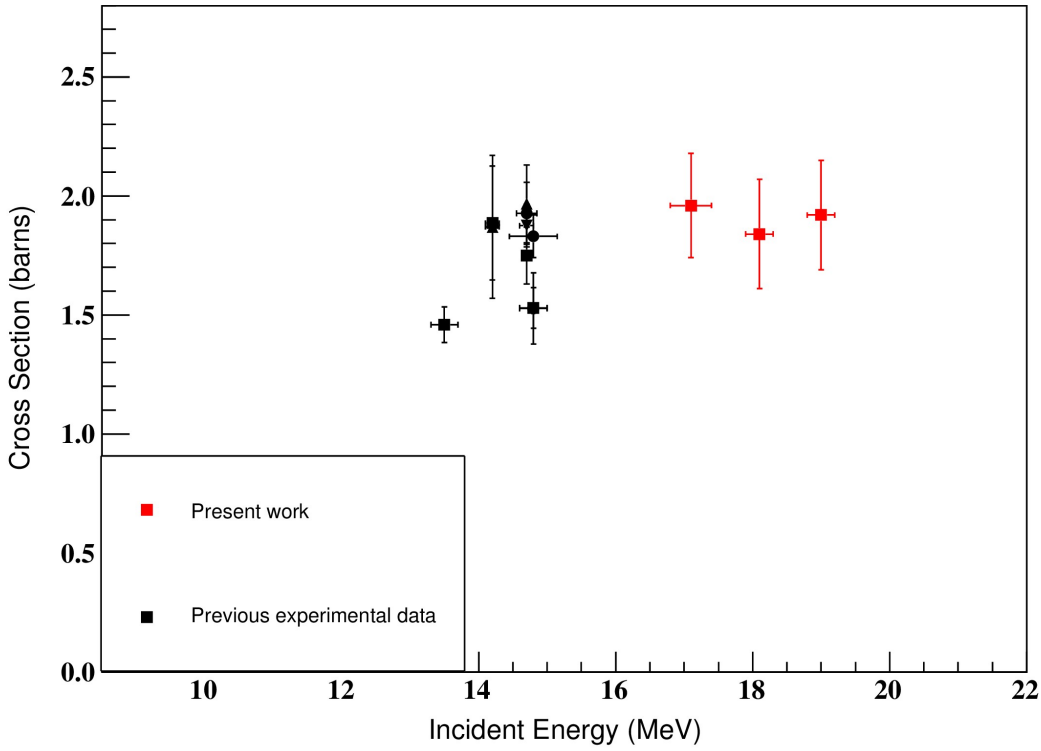

Figure 5.1: Cross section data points of the excitation function for the $^{162}Er(n,2n)^{161}Er$ nuclear reaction.

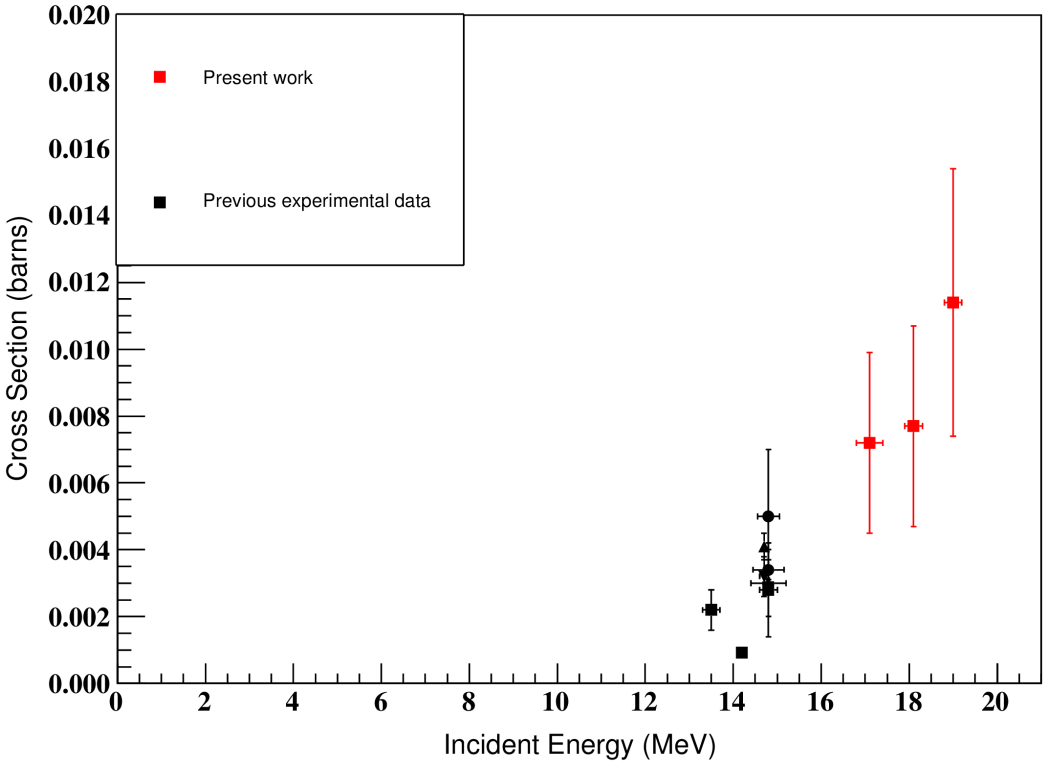

Figure 5.2: Cross section data points of the excitation function for the $^{167}Er(n,p)^{167}Ho$ nuclear reaction.

5.2 Summary and Final Conclusions

- The aim of the present work was the experimental study of the (n,x) reactions for Erbium isotopes at neutron energies higher than 17 MeV.
- Within the present work, **for the first time** the cross sections of the nuclear reactions ^{162}Er(n,2n)^{161}Er and ^{167}Er(n,p)^{167}Ho at 17.1, 18.1 and 19 MeV quasi-monoenergetic neutron beam energies were measured.
- The cross sections of the pre- mentioned nuclear reactions, have been measured by means of activation technique compared to those of reference reactions ^{197}Au(n,2n)^{196}Au, ^{27}Al(n,a)^{24}Na and ^{93}Nb(n,2n)^{92m}Nb.
- Especially, in the case of the ^{162}Er(n,2n)^{161}Er, the high sensitivity of the activation technique was demonstrated given that the natural abundance of the ^{162}Er isotope in the irradiated samples was only 0.139%.
- The neutron beams were produced in the Tandem Van der Graaf 5.5 MV accelerator of the Institute of Nuclear and Particle Physics of N.C.S.R. “Demokritos”, by using the reaction ^{3}H(d,n)^{4}He, with a solid Titanium -Tritide (TiT).
- For the measurement of the gamma-ray activity of the Erbium samples, were used two HPGe detectors with 100% relative efficiency in close geometry and for the monitor foils one with 16% relative efficiency.
- The contribution of the interfering reaction ^{170}Er(n,a)^{167}Dy to the cross section of the ^{167}Er(n,p)^{167}Ho reaction under study was subtracted.
- The final results for the experimental cross sections at the three neutron energies for the ^{162}Er and ^{167}Er Erbium isotopes, are summarized in Table 5.1.
- For the 162Er(n,2n)161Er reaction the dominant sources of the overall uncertainty was the counting rate statistics, while for the reaction 167Er(n,p)167Ho the most important contribution in the reported cross section values uncertainty is the error of the given intensity and the counting rate statistics.

Reaction	En (MeV)	Cross section (barns)	$\sigma_{\text{Cross section}}$ (barns)
^{162}Er(n,2n)^{161}Er	17.1	1.96	0.22
	18.1	1.84	0.23
	19	1.92	0.23
^{167}Er(n,p)^{167}Ho	17.1	0.0072	0.0027
	18.1	0.0077	0.0030
	19	0.0114	0.0040

Table 5.1: Final cross section results of the present work.

As an extension of this study:

- More measurements have been scheduled for the $^{162}Er(n,2n)^{161}Er$ compound nuclear reaction at near threshold energies at 10.7, 11 and 11.3 MeV neutron energy via the $^{2}H(d,n)^{3}He$ reaction, so as to have a complete overview of how the cross section progresses across the energy region that the reaction takes place.
- Improved decay and nuclear structure data are urgently needed for the 167Ho β- given that the dominant uncertainty in the presently reported $^{167}Er(n,p)^{167}Ho$ reaction cross section values are originated from the uncertainty in th γ-ray intensity (26.3%).
- As a next step of the present work, are planned theoretical calculations based on the statistical decay of the compound nucleus using the TALYS code. In this way, a better understanding of the role of the pre-equilibrium reaction mechanism, as well as more detailed parameterization of the compound nucleus model will result.

Appendix A

Neutron beam distribution using NeuSDesc Code

Neutron field production characteristics based including detector area Energy loss based on SRIM
Date: 2016-11-25 Time: 15:26:51

--- Neutrons ---
Reaction: T(d,n)4He, T/Ti target
Ion energy (keV): 2500
Neutron emission angle (degrees): 0
Solid target used
Target thickness (ug/cm2): 2123
OH/Li, H/Ti or D/Ti ratio: 1.543
Entrance window foil: Molybdenum
Entrance window thickness (nm) : 10000
Ion energy loss in target (keV): 464.170
Beam current (uA): 1
Fluence calculation at target distance (mm): 20
Fluence calculation at target radius (mm): 6.5
Angular straggling used
Ion energy (keV): 2500
Entrance window foil: Molybdenum
Entrance window thickness (nm) : 10000
Angular straggling used
Number of points to estimate average fluence: 200

For the reaction:
T(d,n)4He, T/Ti target
OH/Li, H/Ti or D/Ti ratio: 1.5430
Minimum neutron energy (MeV):16.0675
Maximum neutron energy (MeV):17.8156
Average neutron energy (MeV):17.1047
Centroid neutron energy (MeV):16.9415
Median neutron energy (MeV):17.1042
Standard deviation of neutron energy distribution (MeV): 0.2719
Total fluence (n/cm2 s): 0.1090E+07
Energy bin width of histogram (MeV): 0.2033E-01

------ Neutron spectrum ------

Neutron energy (MeV)	Fluence (n/(cm2 s)
15.9048	0.00000E+00
15.9252	0.00000E+00
15.9455	0.00000E+00
15.9658	0.00000E+00
15.9862	0.00000E+00
16.0065	0.00000E+00
16.0268	0.00000E+00
16.0471	0.00000E+00
16.0675	0.97013E+00
16.0878	0.17263E+02

16.1081	0.39515E+02
16.1284	0.53010E+02
16.1488	0.65731E+02
16.1691	0.75609E+02
16.1894	0.84077E+02
16.2098	0.91411E+02
16.2301	0.10377E+03
16.2504	0.12701E+03
16.2707	0.15485E+03
16.2911	0.19225E+03
16.3114	0.25882E+03
16.3317	0.35316E+03
16.3520	0.50001E+03
16.3724	0.77136E+03
16.3927	0.11833E+04
16.4130	0.16006E+04
16.4334	0.20389E+04
16.4537	0.25313E+04
16.4740	0.30365E+04
16.4943	0.36402E+04
16.5147	0.44095E+04
16.5350	0.52003E+04
16.5553	0.60285E+04
16.5756	0.69026E+04
16.5960	0.76724E+04
16.6163	0.85853E+04
16.6366	0.95081E+04
16.6570	0.10270E+05
16.6773	0.11251E+05
16.6976	0.12417E+05
16.7179	0.13560E+05
16.7383	0.14772E+05
16.7586	0.15920E+05
16.7789	0.16908E+05
16.7992	0.17684E+05
16.8196	0.18372E+05
16.8399	0.19176E+05
16.8602	0.20078E+05
16.8806	0.21054E+05
16.9009	0.22018E+05
16.9212	0.23028E+05
16.9415	0.24144E+05
16.9619	0.25377E+05
16.9822	0.26505E+05
17.0025	0.27596E+05
17.0228	0.28660E+05
17.0432	0.29466E+05
17.0635	0.30129E+05
17.0838	0.30638E+05
17.1042	0.30967E+05
17.1245	0.31086E+05
17.1448	0.30891E+05
17.1651	0.30606E+05
17.1855	0.30227E+05

17.2058	0.29817E+05
17.2261	0.29310E+05
17.2464	0.28620E+05
17.2668	0.27689E+05
17.2871	0.26724E+05
17.3074	0.25794E+05
17.3278	0.24857E+05
17.3481	0.23674E+05
17.3684	0.22336E+05
17.3887	0.21052E+05
17.4091	0.19669E+05
17.4294	0.18080E+05
17.4497	0.16658E+05
17.4701	0.15320E+05
17.4904	0.14037E+05
17.5107	0.12835E+05
17.5310	0.11585E+05
17.5514	0.10209E+05
17.5717	0.86835E+04
17.5920	0.71191E+04
17.6123	0.57120E+04
17.6327	0.44882E+04
17.6530	0.32805E+04
17.6733	0.22206E+04
17.6937	0.13672E+04
17.7140	0.71469E+03
17.7343	0.31560E+03
17.7546	0.12030E+03
17.7750	0.28021E+02
17.7953	0.48925E+00
17.8156	0.00000E+00
17.8359	0.00000E+00
17.8563	0.00000E+00
17.8766	0.00000E+00
17.8969	0.00000E+00
17.9173	0.00000E+00
17.9376	0.00000E+00
17.9579	0.00000E+00

==========

==========

The sum of the spectra from the reaction(s):
T(d,n)4He, T/Ti target

Total summed fluence (n/cm2 s): 0.1090E+07

------ Neutron spectrum ------

Neutron energy (MeV)	Fluence (n/(cm2 MeV s)
15.9353	0.00000E+00
15.9557	0.00000E+00
15.9760	0.00000E+00
15.9963	0.00000E+00
16.0166	0.00000E+00

16.0370	0.00000E+00
16.0573	0.00000E+00
16.0776	0.47725E+02
16.0980	0.84925E+03
16.1183	0.19439E+04
16.1386	0.26078E+04
16.1589	0.32336E+04
16.1793	0.37195E+04
16.1996	0.41362E+04
16.2199	0.44970E+04
16.2402	0.51048E+04
16.2606	0.62482E+04
16.2809	0.76177E+04
16.3012	0.94577E+04
16.3216	0.12733E+05
16.3419	0.17374E+05
16.3622	0.24598E+05
16.3825	0.37947E+05
16.4029	0.58211E+05
16.4232	0.78743E+05
16.4435	0.10030E+06
16.4638	0.12453E+06
16.4842	0.14938E+06
16.5045	0.17908E+06
16.5248	0.21692E+06
16.5452	0.25583E+06
16.5655	0.29657E+06
16.5858	0.33957E+06
16.6061	0.37744E+06
16.6265	0.42235E+06
16.6468	0.46775E+06
16.6671	0.50522E+06
16.6874	0.55351E+06
16.7078	0.61085E+06
16.7281	0.66710E+06
16.7484	0.72673E+06
16.7688	0.78319E+06
16.7891	0.83176E+06
16.8094	0.86995E+06
16.8297	0.90380E+06
16.8501	0.94336E+06
16.8704	0.98775E+06
16.8907	0.10358E+07
16.9110	0.10832E+07
16.9314	0.11328E+07
16.9517	0.11878E+07
16.9720	0.12484E+07
16.9924	0.13039E+07
17.0127	0.13576E+07
17.0330	0.14099E+07
17.0533	0.14496E+07
17.0737	0.14822E+07
17.0940	0.15072E+07
17.1143	0.15234E+07

17.1346	0.15293E+07
17.1550	0.15197E+07
17.1753	0.15057E+07
17.1956	0.14870E+07
17.2160	0.14669E+07
17.2363	0.14419E+07
17.2566	0.14080E+07
17.2769	0.13621E+07
17.2973	0.13147E+07
17.3176	0.12689E+07
17.3379	0.12228E+07
17.3582	0.11646E+07
17.3786	0.10988E+07
17.3989	0.10357E+07
17.4192	0.96763E+06
17.4396	0.88945E+06
17.4599	0.81947E+06
17.4802	0.75365E+06
17.5005	0.69053E+06
17.5209	0.63140E+06
17.5412	0.56992E+06
17.5615	0.50222E+06
17.5819	0.42718E+06
17.6022	0.35022E+06
17.6225	0.28100E+06
17.6428	0.22079E+06
17.6632	0.16139E+06
17.6835	0.10924E+06
17.7038	0.67260E+05
17.7241	0.35159E+05
17.7445	0.15526E+05
17.7648	0.59183E+04
17.7851	0.13785E+04
17.8055	0.24069E+02
17.8258	0.00000E+00
17.8461	0.00000E+00
17.8664	0.00000E+00
17.8868	0.00000E+00
17.9071	0.00000E+00
17.9274	0.00000E+00
17.9477	0.00000E+00
17.9528	0.00000E+00

Neutron field production characteristics based including detector area Energy loss based on SRIM
Date: 2016-11-25 Time: 17:08:47

--- Neutrons ---
Reaction: T(d,n)4He, T/Ti target
Ion energy (keV): 3000
Neutron emission angle (degrees): 0
Solid target used
Target thickness (ug/cm2): 2123
OH/Li, H/Ti or D/Ti ratio: 1.543
Entrance window foil: Molybdenum
Entrance window thickness (nm) : 10000
Ion energy loss in target (keV): 359.085
Beam current (uA): 1
Fluence calculation at target distance (mm): 20
Fluence calculation at target radius (mm): 6.5
Angular straggling used
Ion energy (keV): 3000
Entrance window foil: Molybdenum
Entrance window thickness (nm) : 10000
Angular straggling used
Number of points to estimate average fluence: 200

For the reaction:
T(d,n)4He, T/Ti target
OH/Li, H/Ti or D/Ti ratio: 1.5430
Minimum neutron energy (MeV):17.3261
Maximum neutron energy (MeV):18.6570
Average neutron energy (MeV):18.1036
Centroid neutron energy (MeV):17.9915
Median neutron energy (MeV):18.1063
Standard deviation of neutron energy distribution (MeV): 0.1866
Total fluence (n/cm2 s): 0.8542E+06
Energy bin width of histogram (MeV): 0.1530E-01

------ Neutron spectrum ------

Neutron energy (MeV)	Fluence (n/(cm2 s)
17.2037	0.00000E+00
17.2190	0.00000E+00
17.2343	0.00000E+00
17.2496	0.00000E+00
17.2649	0.00000E+00
17.2802	0.00000E+00
17.2955	0.00000E+00
17.3108	0.00000E+00
17.3261	0.11184E+00
17.3414	0.14576E+01
17.3567	0.53208E+01
17.3720	0.89471E+01
17.3873	0.12700E+02
17.4026	0.15838E+02

17.4179	0.18407E+02
17.4332	0.22065E+02
17.4485	0.31611E+02
17.4638	0.46461E+02
17.4790	0.73207E+02
17.4943	0.10903E+03
17.5096	0.14919E+03
17.5249	0.18905E+03
17.5402	0.23764E+03
17.5555	0.32514E+03
17.5708	0.44279E+03
17.5861	0.57664E+03
17.6014	0.73198E+03
17.6167	0.93139E+03
17.6320	0.11896E+04
17.6473	0.15226E+04
17.6626	0.19264E+04
17.6779	0.24234E+04
17.6932	0.29744E+04
17.7085	0.35948E+04
17.7238	0.43091E+04
17.7391	0.51323E+04
17.7544	0.60638E+04
17.7697	0.70459E+04
17.7850	0.80487E+04
17.8003	0.90989E+04
17.8156	0.10178E+05
17.8309	0.11319E+05
17.8462	0.12402E+05
17.8615	0.13523E+05
17.8768	0.14606E+05
17.8921	0.15715E+05
17.9074	0.16869E+05
17.9227	0.17969E+05
17.9380	0.19022E+05
17.9533	0.20030E+05
17.9686	0.21024E+05
17.9839	0.21893E+05
17.9992	0.22716E+05
18.0145	0.23437E+05
18.0298	0.24083E+05
18.0451	0.24664E+05
18.0604	0.25191E+05
18.0757	0.25647E+05
18.0910	0.25982E+05
18.1063	0.26109E+05
18.1216	0.26078E+05
18.1369	0.25904E+05
18.1522	0.25619E+05
18.1674	0.25202E+05
18.1827	0.24672E+05
18.1980	0.24066E+05
18.2133	0.23295E+05
18.2286	0.22387E+05

18.2439	0.21340E+05
18.2592	0.20251E+05
18.2745	0.19120E+05
18.2898	0.18002E+05
18.3051	0.16798E+05
18.3204	0.15566E+05
18.3357	0.14364E+05
18.3510	0.13114E+05
18.3663	0.11855E+05
18.3816	0.10570E+05
18.3969	0.92736E+04
18.4122	0.80030E+04
18.4275	0.67707E+04
18.4428	0.56190E+04
18.4581	0.45982E+04
18.4734	0.36518E+04
18.4887	0.28070E+04
18.5040	0.20865E+04
18.5193	0.14395E+04
18.5346	0.94444E+03
18.5499	0.57512E+03
18.5652	0.34307E+03
18.5805	0.17812E+03
18.5958	0.87057E+02
18.6111	0.22762E+02
18.6264	0.23542E+01
18.6417	0.24343E-01
18.6570	0.00000E+00
18.6723	0.00000E+00
18.6876	0.00000E+00
18.7029	0.00000E+00
18.7182	0.00000E+00
18.7335	0.00000E+00
18.7488	0.00000E+00

==========

==========
The sum of the spectra from the reaction(s):
T(d,n)4He, T/Ti target

Total summed fluence (n/cm2 s): 0.8542E+06

------ Neutron spectrum ------

Neutron energy (MeV)	Fluence (n/(cm2 MeV s)
17.2266	0.00000E+00
17.2419	0.00000E+00
17.2572	0.00000E+00
17.2725	0.00000E+00
17.2878	0.00000E+00
17.3031	0.00000E+00
17.3184	0.00000E+00
17.3337	0.73108E+01
17.3490	0.95281E+02

17.3643	0.34782E+03
17.3796	0.58486E+03
17.3949	0.83017E+03
17.4102	0.10353E+04
17.4255	0.12032E+04
17.4408	0.14423E+04
17.4561	0.20664E+04
17.4714	0.30371E+04
17.4867	0.47855E+04
17.5020	0.71271E+04
17.5173	0.97524E+04
17.5326	0.12358E+05
17.5479	0.15534E+05
17.5632	0.21254E+05
17.5785	0.28945E+05
17.5938	0.37694E+05
17.6091	0.47849E+05
17.6244	0.60884E+05
17.6397	0.77764E+05
17.6550	0.99529E+05
17.6703	0.12592E+06
17.6856	0.15842E+06
17.7009	0.19443E+06
17.7162	0.23499E+06
17.7315	0.28168E+06
17.7468	0.33550E+06
17.7621	0.39638E+06
17.7774	0.46059E+06
17.7927	0.52614E+06
17.8080	0.59479E+06
17.8232	0.66530E+06
17.8385	0.73990E+06
17.8538	0.81073E+06
17.8691	0.88398E+06
17.8844	0.95481E+06
17.8997	0.10273E+07
17.9150	0.11027E+07
17.9303	0.11746E+07
17.9456	0.12434E+07
17.9609	0.13094E+07
17.9762	0.13743E+07
17.9915	0.14311E+07
18.0068	0.14849E+07
18.0221	0.15321E+07
18.0374	0.15743E+07
18.0527	0.16123E+07
18.0680	0.16467E+07
18.0833	0.16765E+07
18.0986	0.16984E+07
18.1139	0.17067E+07
18.1292	0.17047E+07
18.1445	0.16933E+07
18.1598	0.16747E+07
18.1751	0.16474E+07

18.1904	0.16128E+07
18.2057	0.15732E+07
18.2210	0.15228E+07
18.2363	0.14634E+07
18.2516	0.13950E+07
18.2669	0.13238E+07
18.2822	0.12499E+07
18.2975	0.11768E+07
18.3128	0.10981E+07
18.3281	0.10175E+07
18.3434	0.93895E+06
18.3587	0.85728E+06
18.3740	0.77495E+06
18.3893	0.69095E+06
18.4046	0.60621E+06
18.4199	0.52315E+06
18.4352	0.44259E+06
18.4505	0.36731E+06
18.4658	0.30058E+06
18.4811	0.23871E+06
18.4964	0.18349E+06
18.5116	0.13639E+06
18.5269	0.94102E+05
18.5422	0.61737E+05
18.5575	0.37595E+05
18.5728	0.22426E+05
18.5881	0.11644E+05
18.6034	0.56908E+04
18.6187	0.14879E+04
18.6340	0.15389E+03
18.6493	0.15913E+01
18.6646	0.00000E+00
18.6799	0.00000E+00
18.6952	0.00000E+00
18.7105	0.00000E+00
18.7258	0.00000E+00
18.7411	0.00000E+00
18.7449	0.00000E+00

Neutron field production characteristics based including detector area Energy loss based on SRIM
Date: 2016-11-25 Time: 18:06:27

--- Neutrons ---
Reaction: T(d,n)4He, T/Ti target
Ion energy (keV): 3550
Neutron emission angle (degrees): 0
Solid target used
Target thickness (ug/cm2): 2123
OH/Li, H/Ti or D/Ti ratio: 1.543
Entrance window foil: Molybdenum
Entrance window thickness (nm) : 10000
Ion energy loss in target (keV): 297.516
Beam current (uA): 2
Fluence calculation at target distance (mm): 20
Fluence calculation at target radius (mm): 6.5
Angular straggling used
Ion energy (keV): 3550
Entrance window foil: Molybdenum
Entrance window thickness (nm) : 10000
Angular straggling used
Number of points to estimate average fluence: 200

For the reaction:
T(d,n)4He, T/Ti target
OH/Li, H/Ti or D/Ti ratio: 1.5430
Minimum neutron energy (MeV):18.2528
Maximum neutron energy (MeV):19.4900
Average neutron energy (MeV):19.0031
Centroid neutron energy (MeV):18.8714
Median neutron energy (MeV):18.9979
Standard deviation of neutron energy distribution (MeV): 0.1569
Total fluence (n/cm2 s): 0.1768E+07
Energy bin width of histogram (MeV): 0.1406E-01

------ Neutron spectrum ------

Neutron energy (MeV)	Fluence (n/(cm2 s)
18.1404	0.00000E+00
18.1544	0.00000E+00
18.1685	0.00000E+00
18.1826	0.00000E+00
18.1966	0.00000E+00
18.2107	0.00000E+00
18.2247	0.00000E+00
18.2388	0.00000E+00
18.2528	0.29937E+00
18.2669	0.13357E+01
18.2810	0.34400E+01
18.2950	0.69919E+01
18.3091	0.12447E+02
18.3231	0.16061E+02

18.3372	0.21068E+02
18.3513	0.33233E+02
18.3653	0.49309E+02
18.3794	0.71687E+02
18.3934	0.99296E+02
18.4075	0.12163E+03
18.4215	0.14399E+03
18.4356	0.17326E+03
18.4497	0.21737E+03
18.4637	0.27756E+03
18.4778	0.36728E+03
18.4918	0.46750E+03
18.5059	0.58781E+03
18.5200	0.73712E+03
18.5340	0.92162E+03
18.5481	0.11517E+04
18.5621	0.14406E+04
18.5762	0.17947E+04
18.5902	0.22564E+04
18.6043	0.28451E+04
18.6184	0.35965E+04
18.6324	0.45454E+04
18.6465	0.56667E+04
18.6605	0.69332E+04
18.6746	0.83413E+04
18.6887	0.99641E+04
18.7027	0.11813E+05
18.7168	0.13886E+05
18.7308	0.16145E+05
18.7449	0.18656E+05
18.7590	0.21358E+05
18.7730	0.24130E+05
18.7871	0.27039E+05
18.8011	0.30034E+05
18.8152	0.33044E+05
18.8292	0.35912E+05
18.8433	0.38684E+05
18.8574	0.41563E+05
18.8714	0.44386E+05
18.8855	0.47076E+05
18.8995	0.49624E+05
18.9136	0.51963E+05
18.9277	0.54188E+05
18.9417	0.56144E+05
18.9558	0.57729E+05
18.9698	0.58880E+05
18.9839	0.59768E+05
18.9979	0.60380E+05
19.0120	0.60359E+05
19.0261	0.60048E+05
19.0401	0.59350E+05
19.0542	0.58137E+05
19.0682	0.56673E+05
19.0823	0.54972E+05

19.0964	0.52891E+05
19.1104	0.50414E+05
19.1245	0.47654E+05
19.1385	0.44860E+05
19.1526	0.41899E+05
19.1666	0.38612E+05
19.1807	0.35187E+05
19.1948	0.31988E+05
19.2088	0.28746E+05
19.2229	0.25562E+05
19.2369	0.22476E+05
19.2510	0.19330E+05
19.2651	0.16375E+05
19.2791	0.13673E+05
19.2932	0.11315E+05
19.3072	0.92403E+04
19.3213	0.73357E+04
19.3353	0.55232E+04
19.3494	0.39092E+04
19.3635	0.26475E+04
19.3775	0.17466E+04
19.3916	0.11162E+04
19.4056	0.62168E+03
19.4197	0.31465E+03
19.4338	0.14097E+03
19.4478	0.45376E+02
19.4619	0.34821E+01
19.4759	0.73513E-03
19.4900	0.00000E+00
19.5041	0.00000E+00
19.5181	0.00000E+00
19.5322	0.00000E+00
19.5462	0.00000E+00
19.5603	0.00000E+00

==========

==========
The sum of the spectra from the reaction(s):
T(d,n)4He, T/Ti target

Total summed fluence (n/cm2 s): 0.1768E+07

------ Neutron spectrum ------

Neutron energy (MeV)	Fluence (n/(cm2 MeV s)
18.1615	0.00000E+00
18.1755	0.00000E+00
18.1896	0.00000E+00
18.2036	0.00000E+00
18.2177	0.00000E+00
18.2318	0.00000E+00
18.2458	0.00000E+00
18.2599	0.21295E+02
18.2739	0.95012E+02

18.2880	0.24469E+03
18.3020	0.49734E+03
18.3161	0.88537E+03
18.3302	0.11424E+04
18.3442	0.14986E+04
18.3583	0.23639E+04
18.3723	0.35074E+04
18.3864	0.50992E+04
18.4005	0.70631E+04
18.4145	0.86519E+04
18.4286	0.10242E+05
18.4426	0.12325E+05
18.4567	0.15462E+05
18.4708	0.19744E+05
18.4848	0.26125E+05
18.4989	0.33254E+05
18.5129	0.41812E+05
18.5270	0.52432E+05
18.5410	0.65556E+05
18.5551	0.81922E+05
18.5692	0.10247E+06
18.5832	0.12766E+06
18.5973	0.16050E+06
18.6113	0.20238E+06
18.6254	0.25583E+06
18.6395	0.32332E+06
18.6535	0.40308E+06
18.6676	0.49317E+06
18.6816	0.59333E+06
18.6957	0.70876E+06
18.7097	0.84028E+06
18.7238	0.98772E+06
18.7379	0.11484E+07
18.7519	0.13270E+07
18.7660	0.15192E+07
18.7800	0.17164E+07
18.7941	0.19233E+07
18.8082	0.21364E+07
18.8222	0.23505E+07
18.8363	0.25545E+07
18.8503	0.27517E+07
18.8644	0.29565E+07
18.8784	0.31572E+07
18.8925	0.33486E+07
18.9066	0.35299E+07
18.9206	0.36962E+07
18.9347	0.38545E+07
18.9487	0.39936E+07
18.9628	0.41064E+07
18.9769	0.41882E+07
18.9909	0.42514E+07
19.0050	0.42949E+07
19.0190	0.42934E+07
19.0331	0.42713E+07

19.0472	0.42217E+07
19.0612	0.41354E+07
19.0753	0.40313E+07
19.0893	0.39102E+07
19.1034	0.37622E+07
19.1174	0.35860E+07
19.1315	0.33897E+07
19.1456	0.31910E+07
19.1596	0.29803E+07
19.1737	0.27465E+07
19.1877	0.25029E+07
19.2018	0.22754E+07
19.2159	0.20448E+07
19.2299	0.18182E+07
19.2440	0.15988E+07
19.2580	0.13750E+07
19.2721	0.11648E+07
19.2861	0.97260E+06
19.3002	0.80487E+06
19.3143	0.65727E+06
19.3283	0.52180E+06
19.3424	0.39288E+06
19.3564	0.27806E+06
19.3705	0.18832E+06
19.3846	0.12424E+06
19.3986	0.79396E+05
19.4127	0.44221E+05
19.4267	0.22381E+05
19.4408	0.10027E+05
19.4548	0.32276E+04
19.4689	0.24769E+03
19.4830	0.52291E-01
19.4970	0.00000E+00
19.5111	0.00000E+00
19.5251	0.00000E+00
19.5392	0.00000E+00
19.5533	0.00000E+00
19.5568	0.00000E+00

Appendix B

Calculation of fb Correction Factor for non-constant flux

```
# include <iostream>
# include <cmath>
# include <fstream>
using namespace std;

int main ()
{
  char filename[80];
  double half_life;
  double lamda;
  double Irradiation_time;
  double dt;
  double flux[5000];
  double sum_1=0., sum_2=0.;
  int number_of_channels;
  cout<<"give the half life in second: ";
  cin>>half_life;
  lamda=log(2)/half_life;
  cout<<"give the name of the BF3 file: ";
  cin>>filename;
  cout<<"give the number of channels: ";
  cin>>number_of_channels;
  cout<<"give the Irradiation time is second :" ;
  cin>>Irradiation_time;
  cout<<"give the dt of each channel: ";
  cin>>dt;
  double fb, fb_constant,TotCor;

ifstream infile;
infile.open(filename);
for (int i=0;i<number_of_channels;i++){
infile>>flux[i];
}
for(int j=0;j<number_of_channels;j++){
sum_2=sum_2+flux[j];
 sum_1=sum_1+flux[j]*(exp((j+1)*lamda*dt)-exp((j)*lamda*dt));
}
 fb=(exp(-lamda*Irradiation_time)/(lamda*dt))*(sum_1/sum_2);
 TotCor=sum_2*lamda*dt/(sum_1*exp(-lamda*Irradiation_time));
 fb_constant=(1-exp(-lamda*Irradiation_time))/(lamda*Irradiation_time);
 cout<<"the correction factor for non constant flux is: ";
 cout<<fb<<"\n";
 cout<<"the correction factor for constant flux is: ";
 cout<<fb_constant<<"\n";
 cout<<"the 1/fb for non constant flux is: ";
 cout<<TotCor<<"\n";
}
```

Appendix C

Calculation of Self-Attenuation Correction Factor for the Erbium targets

```
#include "XriDetectorConstruction.hh"
#include "G4SDManager.hh"
#include "G4Element.hh"
#include "G4Material.hh"
#include "G4Box.hh"
#include "G4Tubs.hh"
#include "G4Cons.hh"
#include "G4LogicalVolume.hh"
#include "G4ThreeVector.hh"
#include "G4PVPlacement.hh"

#include "G4UnitsTable.hh"
#include "globals.hh"

#include "G4SystemOfUnits.hh"
#include "G4PhysicalConstants.hh"

#include "G4VisAttributes.hh"
#include "G4Colour.hh"

#include "G4SystemOfUnits.hh"
#include "G4PhysicalConstants.hh"

XriDetectorConstruction::XriDetectorConstruction()
{;}

XriDetectorConstruction::~XriDetectorConstruction()
{;}

G4VPhysicalVolume* XriDetectorConstruction::Construct()
{

  G4UnitDefinition::BuildUnitsTable();

      //================================ materials ====================================//

  G4double a;
  G4double z;
  G4int iz, in;
  G4double density;
  G4String name, symbol;
  G4int ncomponents;
  G4double fractionmass;
  G4int natoms;

// ---------- plexiglass of Eu source

  a = 12.011*g/mole;
  G4Element* elC  = new G4Element(name="Carbon",symbol=" C" , z= 6., a);
```

```
 a = 1.008*g/mole;
 G4Element *elH  = new G4Element(name="Hydrogen",  symbol=" H" , z= 1., a);

 a = 15.999*g/mole;
 G4Element *elO  = new G4Element(name="Oxygen",  symbol=" O" , z= 8., a);

  // ERBIUM TARGET
   a=167.259*g/mole;

  G4Element *elEr  = new G4Element(name="Erbium",  symbol="Er" , z= 68., a);
 density = 8.64*g/cm3;
 G4Material* Er2O3 = new G4Material(name="Erbium_oxide",density,ncomponents=2);

 Er2O3->AddElement(elEr, natoms=2);
 Er2O3->AddElement(elO,  natoms=3);

 density = 1.5*g/cm3;
G4Material* Cellulose = new G4Material("Cellulose" , density, ncomponents=3);
Cellulose->AddElement(elH, natoms=10);
Cellulose->AddElement(elC, natoms=6);
Cellulose->AddElement(elO, natoms=5);

density = 3.9*g/cm3;
G4Material* ErTarget = new G4Material(name="ErTarget",density,ncomponents=2);
ErTarget->AddMaterial(Cellulose,fractionmass=9.1*perCent);
ErTarget->AddMaterial(Er2O3,fractionmass=90.9*perCent);

/*  //POINT SOURCE
 density = 1.19*g/cm3;
 G4Material* Plexiglass = new G4Material(name="Plexiglass",density,ncomponents=3);
 Plexiglass->AddElement(elC, natoms=5);
 Plexiglass->AddElement(elH, natoms=8);
 Plexiglass->AddElement(elO, natoms=2); */



//  -------  defining Ge crystal

 a = 72.61*g/mole;
 density = 5.323*g/cm3;
 G4Material* Ge = new G4Material(name="Ge",z=32., a, density);

// ------- defining Mg housing

 a = 24.305*g/mole;
 density = 1.738*g/cm3;
 G4Material* Mg = new G4Material(name="Mg", z=12., a, density);



// ------- defining Al housing

 a = 26.981539*g/mole;
```

```
  density = 2.70*g/cm3;
  G4Material* Al = new G4Material(name="Al", z=13., a, density);


//--------- defining Air

  a = 14.007*g/mole;
  G4Element* elN  = new G4Element(name="Nitrogen",symbol=" N" , z= 7., a);

// a = 15.999*g/mole;
// G4Element *elO  = new G4Element(name="Oxygen",  symbol=" O" , z= 8., a);

  density = 1.29*mg/cm3;
  G4Material *Air = new G4Material(name="Air ",density,ncomponents=2);
  Air->AddElement(elO, fractionmass=30.0*perCent);
  Air->AddElement(elN, fractionmass=70.0*perCent);

//  -----   defining vacuum

  G4double pressure, temperature;
  density = universe_mean_density;
  pressure = 3.0E-18*pascal;
  temperature = 2.73*kelvin;
  G4Material *Vacuum = new G4Material(name="Vacuum", z=1.0, a=1.01*g/mole,
                              density, kStateGas, temperature, pressure);


  G4cout << "\n\n ####------------------------------------------------------#### \n";
  G4cout << "\n\t\t#### List of isotopes used #### \n";
//  G4cout << *(G4Isotope::GetIsotopeTable());
  G4cout << "\n\n\n\n\t\t #### List of elements used #### \n";
  G4cout << *(G4Element::GetElementTable());
  G4cout << "\n\n\n\n\t\t #### List of materials used #### \n";
  G4cout << *(G4Material::GetMaterialTable());
  G4cout << "\n\n ####------------------------------------------------------#### \n";


          //================================== volumes ============================//

//------------------------------ beam line along z axis

  G4double startFi = 0.0*deg;
  G4double endFi = 360.0*deg;

//------------------------------ world volume

  G4double WorldOutR = 20.0*cm;
  G4double WorldInR = 0.0*cm;
  G4double WorldHalfh = 30.0*cm;

  G4Tubs *World_tub
    = new G4Tubs("World_tub",WorldInR,WorldOutR,WorldHalfh,
                                    startFi,endFi);
```

```
  G4LogicalVolume *World_log
    = new G4LogicalVolume(World_tub,Air,"World_log",0,0,0);

  G4VPhysicalVolume *World_phys
    = new G4PVPlacement(0,G4ThreeVector(),"World",
                        World_log,0,false,0);


//---------------- Mg entrance window

  G4double SD = 1.75*cm;//1.75*cm;     // SD=Source-Detector distance, set equal to 7cm+0.5mm to the source
centre
  G4double MgWOutR = 4.5*cm;
  G4double MgWInR = 0.*cm;
  G4double MgWHalfh = (1.5/2)*mm;

  G4Tubs *MgW_tube
    = new G4Tubs("MgW_tube",MgWInR,MgWOutR,MgWHalfh,
                                       startFi,endFi);

  G4LogicalVolume *MgW_log
    = new G4LogicalVolume(MgW_tube,Mg,"MgW_log",0,0,0);

  G4double Pos_x = 0.0*cm;
  G4double Pos_y = 0.0*cm;
  G4double Pos_z = -SD-MgWHalfh;
  G4VPhysicalVolume *MgWTube_phys
    = new G4PVPlacement(0,
            G4ThreeVector(Pos_x,Pos_y,Pos_z),
            MgW_log,"MgWTube",World_log,false,0);

//---------------- Mg entrance window 2


   G4LogicalVolume *MgW_log2
  = new G4LogicalVolume(MgW_tube,Mg,"MgW_log2",0,0,0);

   Pos_x = 0.0*cm;
   Pos_y = 0.0*cm;
   Pos_z = SD+MgWHalfh;
  G4VPhysicalVolume *MgWTube_phys2
   = new G4PVPlacement(0,
          G4ThreeVector(Pos_x,Pos_y,Pos_z),
            MgW_log2,"MgWTube2",World_log,false,0);


//------------------- Mg housing

  G4double MgThickness = 1.5*mm;
  G4double MgOutR = MgWOutR;
  G4double MgInR = 0.*cm;
  G4double MgHalfh = (16.4/2.)*cm;

  G4Tubs *Mg_tube
```

```
    = new G4Tubs("Mg_tube",MgInR,MgOutR,MgHalfh,
                                    startFi,endFi);

  G4LogicalVolume *Mg_log
    = new G4LogicalVolume(Mg_tube,Mg,"Mg_log",0,0,0);

  Pos_x = 0.0*cm;
  Pos_y = 0.0*cm;
  Pos_z = -SD-2.*MgWHalfh-MgHalfh;
  G4VPhysicalVolume *MgTube_phys
    = new G4PVPlacement(0,
          G4ThreeVector(Pos_x,Pos_y,Pos_z),
          Mg_log,"MgTube",World_log,false,0);

//------------------ Mg housing 2

  G4LogicalVolume *Mg_log2
    = new G4LogicalVolume(Mg_tube,Mg,"Mg_log2",0,0,0);

  Pos_x = 0.0*cm;
  Pos_y = 0.0*cm;
  Pos_z = SD+2.*MgWHalfh+MgHalfh;
  G4VPhysicalVolume *MgTube_phys2
    = new G4PVPlacement(0,
          G4ThreeVector(Pos_x,Pos_y,Pos_z),
          Mg_log2,"MgTube2",World_log,false,0);


//--------------- Vacuum between Mg window and Mg housing

  G4double VacuumOutR = MgOutR - MgThickness;
  G4double VacuumInR = 0.*cm;
  G4double VacuumHalfh = MgHalfh - MgThickness/2.;

  G4Tubs *Vacuum_tube
    = new G4Tubs("Vacuum_tube",VacuumInR,VacuumOutR,VacuumHalfh,
                                    startFi,endFi);

  G4LogicalVolume *Vacuum_log
    = new G4LogicalVolume(Vacuum_tube,Vacuum,"Vacuum_log",0,0,0);

  Pos_x = 0.0*cm;
  Pos_y = 0.0*cm;
  Pos_z = MgThickness/2.;
  G4VPhysicalVolume *VacuumTube_phys
    = new G4PVPlacement(0,
          G4ThreeVector(Pos_x,Pos_y,Pos_z),
          Vacuum_log,"VacuumTube",Mg_log,false,0);

//--------------- Vacuum between Mg window2 and Mg housing2


  G4LogicalVolume *Vacuum_log2
    = new G4LogicalVolume(Vacuum_tube,Vacuum,"Vacuum_log2",0,0,0);
```

```
  Pos_x = 0.0*cm;
  Pos_y = 0.0*cm;
  Pos_z = -MgThickness/2.;
  G4VPhysicalVolume *VacuumTube_phys2
    = new G4PVPlacement(0,
            G4ThreeVector(Pos_x,Pos_y,Pos_z),
            Vacuum_log2,"VacuumTube2",Mg_log2,false,0);

//---------------- Al mylar entrance window

  G4double gapMg_Al = 3.95*mm;
  G4double AlWOutR = 3.956*cm;
  G4double AlWInR = 0.*cm;
  G4double AlWHalfh = (0.05/2)*mm;

  G4Tubs *AlW_tube
    = new G4Tubs("AlW_tube",AlWInR,AlWOutR,AlWHalfh,
                                        startFi,endFi);

  G4LogicalVolume *AlW_log
    = new G4LogicalVolume(AlW_tube,Al,"AlW_log",0,0,0);

  Pos_x = 0.0*cm;
  Pos_y = 0.0*cm;
  Pos_z = VacuumHalfh-gapMg_Al-AlWHalfh;
  G4VPhysicalVolume *AlWTube_phys
    = new G4PVPlacement(0,
            G4ThreeVector(Pos_x,Pos_y,Pos_z),
            AlW_log,"AlWTube",Vacuum_log,false,0);


//---------------- Al mylar entrance window2


  G4LogicalVolume *AlW_log2
    = new G4LogicalVolume(AlW_tube,Al,"AlW_log2",0,0,0);

  Pos_x = 0.0*cm;
  Pos_y = 0.0*cm;
  Pos_z = -(VacuumHalfh-gapMg_Al-AlWHalfh);
  G4VPhysicalVolume *AlWTube_phys2
    = new G4PVPlacement(0,
            G4ThreeVector(Pos_x,Pos_y,Pos_z),
            AlW_log2,"AlWTube2",Vacuum_log2,false,0);


//------------------- Al housing

  G4double AlThickness = 0.76*mm;
  G4double AlOutR = AlWOutR;
  G4double AlInR = 0.*cm;
  G4double AlHalfh = (12.68/2.)*cm;
```

```
  G4Tubs *Al_tube
    = new G4Tubs("Al_tube",AlInR,AlOutR,AlHalfh,
                                    startFi,endFi);

  G4LogicalVolume *Al_log
    = new G4LogicalVolume(Al_tube,Al,"Al_log",0,0,0);

  Pos_x = 0.0*cm;
  Pos_y = 0.0*cm;
  Pos_z = VacuumHalfh-gapMg_Al-2*AlWHalfh - AlHalfh;
  G4VPhysicalVolume *AlTube_phys
    = new G4PVPlacement(0,
          G4ThreeVector(Pos_x,Pos_y,Pos_z),
          Al_log,"AlTube",Vacuum_log,false,0);

//------------------ Al housing2


  G4LogicalVolume *Al_log2
    = new G4LogicalVolume(Al_tube,Al,"Al_log2",0,0,0);

  Pos_x = 0.0*cm;
  Pos_y = 0.0*cm;
  Pos_z = -(VacuumHalfh-gapMg_Al-2*AlWHalfh - AlHalfh);
  G4VPhysicalVolume *AlTube_phys2
    = new G4PVPlacement(0,
          G4ThreeVector(Pos_x,Pos_y,Pos_z),
          Al_log2,"AlTube2",Vacuum_log2,false,0);



//--------------- Vacuum between Al  window and Al housing

  G4double InVacuumOutR = AlOutR - AlThickness;
  G4double InVacuumInR = 0.*cm;
  G4double InVacuumHalfh = AlHalfh - AlThickness/2.;

  G4Tubs *InVacuum_tube
    = new G4Tubs("InVacuum_tube",InVacuumInR,InVacuumOutR,InVacuumHalfh,
                                    startFi,endFi);

  G4LogicalVolume *InVacuum_log
    = new G4LogicalVolume(InVacuum_tube,Vacuum,"InVacuum_log",0,0,0);

  Pos_x = 0.0*cm;
  Pos_y = 0.0*cm;
  Pos_z = AlThickness/2.;
  G4VPhysicalVolume *InVacuumTube_phys
    = new G4PVPlacement(0,
          G4ThreeVector(Pos_x,Pos_y,Pos_z),
          InVacuum_log,"InVacuumTube",Al_log,false,0);


//--------------- Vacuum between Al  window2  and Al housing2
```

```
  G4LogicalVolume *InVacuum_log2
    = new G4LogicalVolume(InVacuum_tube,Vacuum,"InVacuum_log2",0,0,0);

  Pos_x = 0.0*cm;
  Pos_y = 0.0*cm;
  Pos_z = -AlThickness/2.;
  G4VPhysicalVolume *InVacuumTube_phys2
    = new G4PVPlacement(0,
          G4ThreeVector(Pos_x,Pos_y,Pos_z),
          InVacuum_log2,"InVacuumTube2",Al_log2,false,0);


//--------------- Dead layer Window Ge cone front


  G4double FDLWConeRadiusUpMax = 3.58 *cm; //Front Dead Layer Window Uppper Max Radius
  G4double FDLWConeRadiusUpMin = 0.0 *cm; //Front Dead Layer Window Uppper Min Radius
  G4double FDLWConeRadiusBottomMax = 3.68 *cm; //Front Dead Layer Window Bottom Max Radius
  G4double FDLWConeRadiusBottomMin = 0.0 *cm; //Front Dead Layer Window Bottom Min Radius
  G4double FDLWConeHalfHeight = (0.00003/2.0)*cm; //Front Dead Layer thinkness

  G4Cons *FDLW_cone
    = new G4Cons("FDLW_cone", FDLWConeRadiusBottomMin, FDLWConeRadiusBottomMax,
                              FDLWConeRadiusUpMin,FDLWConeRadiusUpMax,
                              FDLWConeHalfHeight,
                        startFi,endFi);

  G4LogicalVolume *FDLW_log
    = new G4LogicalVolume(FDLW_cone,Ge,"FDLW_log",0,0,0);

  Pos_x = 0.0*cm;
  Pos_y = 0.0*cm;
  Pos_z = InVacuumHalfh-FDLWConeHalfHeight;
  G4VPhysicalVolume *FDLWCone_phys
    = new G4PVPlacement(0,
          G4ThreeVector(Pos_x,Pos_y,Pos_z),
          FDLW_log,"FDLWCone",InVacuum_log,false,0);


//--------------- Dead layer Window2 Ge cone front

  G4double FDLWConeRadiusUpMax2 = 3.68 *cm; //Front Dead Layer Window Uppper Max Radius
  G4double FDLWConeRadiusUpMin2 = 0.0 *cm; //Front Dead Layer Window Uppper Min Radius
  G4double FDLWConeRadiusBottomMax2 = 3.58 *cm; //Front Dead Layer Window Bottom Max Radius
  G4double FDLWConeRadiusBottomMin2 = 0.0 *cm; //Front Dead Layer Window Bottom Min Radius
  G4double FDLWConeHalfHeight2 = (0.00003/2.0)*cm; //Front Dead Layer thinkness

  G4Cons *FDLW_cone2
    = new G4Cons("FDLW_cone2", FDLWConeRadiusBottomMin2, FDLWConeRadiusBottomMax2,
                              FDLWConeRadiusUpMin2,FDLWConeRadiusUpMax2,
                              FDLWConeHalfHeight2,
                        startFi,endFi);
```

```
  G4LogicalVolume *FDLW_log2
    = new G4LogicalVolume(FDLW_cone2,Ge,"FDLW_log2",0,0,0);

  Pos_x = 0.0*cm;
  Pos_y = 0.0*cm;
  Pos_z = -(InVacuumHalfh-FDLWConeHalfHeight2);
  G4VPhysicalVolume *FDLWCone_phys2
    = new G4PVPlacement(0,
          G4ThreeVector(Pos_x,Pos_y,Pos_z),
          FDLW_log2,"FDLWCone2",InVacuum_log2,false,0);


//-------------- Front Ge cone


  G4double FrontGeConeRadiusUpMax = 3.68 *cm; // Ge cone upper max radius
  G4double FrontGeConeRadiusUpMin = 0.0 *cm; // Ge cone upper min radius
  G4double FrontGeConeRadiusBottomMax = 3.78 *cm; // Ge cone bottom max radius
  G4double FrontGeConeRadiusBottomMin = 0.0 *cm; // Ge cone bottom min radius
  G4double FrontGeConeHalfHeight = (0.1/2.0)*cm; //Front Dead Layer thinkness

  G4Cons *frontGe_cone
    = new G4Cons("frontGe_cone",FrontGeConeRadiusBottomMin, FrontGeConeRadiusBottomMax,
                                FrontGeConeRadiusUpMin,FrontGeConeRadiusUpMax,
                                FrontGeConeHalfHeight,
                        startFi,endFi);

  G4LogicalVolume *frontGeCone_log
    = new G4LogicalVolume(frontGe_cone,Ge,"frontGeCone_log",0,0,0);

  Pos_x = 0.0*cm;
  Pos_y = 0.0*cm;
  Pos_z = InVacuumHalfh-2*FDLWConeHalfHeight-FrontGeConeHalfHeight;
  G4VPhysicalVolume *frontGeCone_phys
    = new G4PVPlacement(0,
          G4ThreeVector(Pos_x,Pos_y,Pos_z),
          frontGeCone_log,"frontGeCone",InVacuum_log,false,0);

//-------------- Front Ge cone2

  G4double FrontGeConeRadiusUpMax2 = 3.78 *cm; // Ge cone upper max radius
  G4double FrontGeConeRadiusUpMin2 = 0.0 *cm; // Ge cone upper min radius
  G4double FrontGeConeRadiusBottomMax2 = 3.68 *cm; // Ge cone bottom max radius
  G4double FrontGeConeRadiusBottomMin2 = 0.0 *cm; // Ge cone bottom min radius
  G4double FrontGeConeHalfHeight2 = (0.1/2.0)*cm; //Front Dead Layer thinkness

  G4Cons *frontGe_cone2
    = new G4Cons("frontGe_cone2",FrontGeConeRadiusBottomMin2, FrontGeConeRadiusBottomMax2,
                                FrontGeConeRadiusUpMin2,FrontGeConeRadiusUpMax2,
                                FrontGeConeHalfHeight2,
                        startFi,endFi);
```

```
   G4LogicalVolume *frontGeCone_log2
    = new G4LogicalVolume(frontGe_cone2,Ge,"frontGeCone_log2",0,0,0);

  Pos_x = 0.0*cm;
  Pos_y = 0.0*cm;
  Pos_z = -(InVacuumHalfh-2*FDLWConeHalfHeight2-FrontGeConeHalfHeight2);
  G4VPhysicalVolume *frontGeCone_phys2
    = new G4PVPlacement(0,
            G4ThreeVector(Pos_x,Pos_y,Pos_z),
            frontGeCone_log2,"frontGeCone2",InVacuum_log2,false,0);

// ----------- Plexiglass or target

  G4double PlexiOutR = 1.295/2.*cm;//2.0/2.*cm;
  G4double PlexiInR = 0.*cm;
  G4double PlexiHalfh = 0.2/2.*cm;

  G4Tubs *Plexi_tube
    = new G4Tubs("Plexi_tube",PlexiInR,PlexiOutR,PlexiHalfh,
                                      startFi,endFi);

  G4LogicalVolume *Plexi_log
    = new G4LogicalVolume(Plexi_tube,ErTarget,"Plexi_log",0,0,0);

  Pos_x = 0.0*cm;
  Pos_y = 0.0*cm;
  Pos_z = 0.0*cm; //Here Christine had:    -PlexiHalfh/2.;
  G4VPhysicalVolume *PlexiTube_phys
    = new G4PVPlacement(0,
            G4ThreeVector(Pos_x,Pos_y,Pos_z),
            Plexi_log,"PlexiTube",World_log,false,0);


//--------------- Dead layer of crystal at the crystal sides: denoted as "outDead"


  G4double GeOutR = 3.77997*cm;  //***HTAN 50/2*
  G4double GeHalfh = 8.99/2.*cm;
  G4double outDeadThickness = 0.00003*cm;
  G4double outDeadOutR = GeOutR + outDeadThickness;
  G4double outDeadInR = 0.*mm;
  G4double outDeadHalfh = GeHalfh;

  G4Tubs *outDead_tube
    = new G4Tubs("outDead_tube",outDeadInR,outDeadOutR,outDeadHalfh,
                                      startFi,endFi);

  G4LogicalVolume *outDead_log
    = new G4LogicalVolume(outDead_tube,Ge,"outDead_log",0,0,0);

  Pos_x = 0.0*cm;
  Pos_y = 0.0*cm;
  Pos_z =InVacuumHalfh-2*FDLWConeHalfHeight-2*FrontGeConeHalfHeight-outDeadHalfh;
```

```
  G4VPhysicalVolume *outDeadTube_phys
    = new G4PVPlacement(0,
            G4ThreeVector(Pos_x,Pos_y,Pos_z),
            outDead_log,"outDeadTube",lnVacuum_log,false,0);


//---------- Dead layer 2  of crystal at the crystal sides: denoted as "outDead2"


  G4LogicalVolume *outDead_log2
  = new G4LogicalVolume(outDead_tube,Ge,"outDead_log2",0,0,0);

  Pos_x = 0.0*cm;
  Pos_y = 0.0*cm;
  Pos_z =-(lnVacuumHalfh-2*FDLWConeHalfHeight2-2*FrontGeConeHalfHeight2-outDeadHalfh);

  G4VPhysicalVolume *outDeadTube_phys2
  = new G4PVPlacement(0,
          G4ThreeVector(Pos_x,Pos_y,Pos_z),
          outDead_log2,"outDeadTube2",lnVacuum_log2,false,0);


//------------------ Ge crystal

  G4double GeInR = 0.*mm;

  G4Tubs *Ge_tube
    = new G4Tubs("Ge_tube",GeInR,GeOutR,GeHalfh,
                                      startFi,endFi);

  G4LogicalVolume *Ge_log
    = new G4LogicalVolume(Ge_tube,Ge,"Ge_log",0,0,0);

  Pos_x = 0.0*cm;
  Pos_y = 0.0*cm;
  Pos_z = 0.0*cm;
  G4VPhysicalVolume *GeTube_phys
    = new G4PVPlacement(0,
            G4ThreeVector(Pos_x,Pos_y,Pos_z),
            Ge_log,"GeTube",outDead_log,false,0);

//------------------ Ge crystal 2


  G4LogicalVolume *Ge_log2
  = new G4LogicalVolume(Ge_tube,Ge,"Ge_log2",0,0,0);

  Pos_x = 0.0*cm;
  Pos_y = 0.0*cm;
  Pos_z = 0.0*cm;
  G4VPhysicalVolume *GeTube_phys2
  = new G4PVPlacement(0,
          G4ThreeVector(Pos_x,Pos_y,Pos_z),
          Ge_log2,"GeTube2",outDead_log2,false,0);
```

```
//---------- Dead layer in borehole: denoted as inDead

  G4double BoreholeHalfh = 84/2.*mm;
  G4double BoreholeOutR = 10.1/2.*mm;
  G4double inDeadThickness =0.7*mm;
  G4double inDeadOutR = BoreholeOutR + inDeadThickness;
  G4double inDeadInR = 0.*mm;
  G4double inDeadHalfh = BoreholeHalfh + inDeadThickness/2.;

  G4Tubs *inDead_tube
    = new G4Tubs("inDead_tube",inDeadInR,inDeadOutR,inDeadHalfh,
                                    startFi,endFi);

  G4LogicalVolume *inDead_log
    = new G4LogicalVolume(inDead_tube,Ge,"inDead_log",0,0,0);

  Pos_x = 0.0*cm;
  Pos_y = 0.0*cm;
  Pos_z = - GeHalfh + inDeadHalfh;
  G4VPhysicalVolume *inDeadTube_phys
    = new G4PVPlacement(0,
          G4ThreeVector(Pos_x,Pos_y,Pos_z),
          inDead_log,"inDeadTube",Ge_log,false,0);



//---------- Dead layer 2 in borehole 2: denoted as inDead2


  G4LogicalVolume *inDead_log2
    = new G4LogicalVolume(inDead_tube,Ge,"inDead_log2",0,0,0);

  Pos_x = 0.0*cm;
  Pos_y = 0.0*cm;
  Pos_z = -(- GeHalfh + inDeadHalfh);
  G4VPhysicalVolume *inDeadTube_phys2
    = new G4PVPlacement(0,
          G4ThreeVector(Pos_x,Pos_y,Pos_z),
          inDead_log2,"inDeadTube2",Ge_log2,false,0);

//--------------- Borehole

  G4double BoreholeInR = 0.*mm;

  G4Tubs *Borehole_tube
    = new G4Tubs("Borehole_tube",BoreholeInR,BoreholeOutR,BoreholeHalfh,
                                    startFi,endFi);

  G4LogicalVolume *Borehole_log
    = new G4LogicalVolume(Borehole_tube,Vacuum,"Borehole_log",0,0,0);

  Pos_x = 0.0*cm;
  Pos_y = 0.0*cm;
```

```
  Pos_z = - inDeadThickness/2.;
  G4VPhysicalVolume *BoreholeTube_phys
    = new G4PVPlacement(0,
            G4ThreeVector(Pos_x,Pos_y,Pos_z),
            Borehole_log,"BoreholeTube",inDead_log,false,0);


//---------------- Borehole 2


  G4LogicalVolume *Borehole_log2
    = new G4LogicalVolume(Borehole_tube,Vacuum,"Borehole_log2",0,0,0);

  Pos_x = 0.0*cm;
  Pos_y = 0.0*cm;
  Pos_z =-(- inDeadThickness/2.);
  G4VPhysicalVolume *BoreholeTube_phys2
    = new G4PVPlacement(0,
            G4ThreeVector(Pos_x,Pos_y,Pos_z),
            Borehole_log2,"BoreholeTube2",inDead_log2,false,0);



      //========================== Visualization attributes
=======================================//

  World_log->SetVisAttributes (G4VisAttributes::Invisible);
  G4VisAttributes *MgWTubeAttr = new G4VisAttributes(G4Colour(0.,0.,1.));         //Blue
  G4VisAttributes *AlWTubeAttr = new G4VisAttributes(G4Colour(0.,0.,1.));         //Blue
  G4VisAttributes *MgTubeAttr = new G4VisAttributes(G4Colour(1.,0.,0.));         //Red

G4VisAttributes *AlTubeAttr = new G4VisAttributes(G4Colour(1.,0.,0.));         //Red
  G4VisAttributes *VacuumTubeAttr = new G4VisAttributes(G4Colour(0.3,0.3,0.3));  //light gray
 G4VisAttributes *InVacuumTubeAttr = new G4VisAttributes(G4Colour(0.3,0.3,0.3));  //light gray
  G4VisAttributes *outDeadTubeAttr = new G4VisAttributes(G4Colour(0.,1.,0.));    //green
  G4VisAttributes *GeTubeAttr = new G4VisAttributes(G4Colour(0.8,0.8,0.8));      //grey
  G4VisAttributes *inDeadTubeAttr = new G4VisAttributes(G4Colour(0.,0.4,0.3));   //tale
  G4VisAttributes *BoreholeTubeAttr = new G4VisAttributes(G4Colour(0.,0.,1.));   //blue
  G4VisAttributes *PlexiTubeAttr = new G4VisAttributes(G4Colour(0.8,0.8,1.));   //gray
//  G4VisAttributes *VerticalPbAttr = new G4VisAttributes(G4Colour(1.,1.,1.));
//  G4VisAttributes *HorizontalPbAttr = new G4VisAttributes(G4Colour(1.,1.,1.));
 G4VisAttributes *FDLWConeAttr = new G4VisAttributes(G4Colour(0.,1.,0.));    //gree
 G4VisAttributes *FrontGeConeAttr = new G4VisAttributes(G4Colour(0.,1.,0.));    //gree
/*  VerticalPbAttr->SetVisibility(true);
  VerticalPbAttr->SetForceWireframe(true);
  vertPb_log->SetVisAttributes(VerticalPbAttr);

  HorizontalPbAttr->SetVisibility(true);
  HorizontalPbAttr->SetForceWireframe(true);
  horPb_log->SetVisAttributes(HorizontalPbAttr);
*/

  PlexiTubeAttr->SetVisibility(true);
  PlexiTubeAttr->SetForceWireframe(true);
```

```
Plexi_log->SetVisAttributes(PlexiTubeAttr);

MgWTubeAttr->SetVisibility(true);
MgWTubeAttr->SetForceWireframe(true);
MgW_log->SetVisAttributes(MgWTubeAttr);
MgW_log2->SetVisAttributes(MgWTubeAttr);

MgTubeAttr->SetVisibility(true);
MgTubeAttr->SetForceWireframe(true);
Mg_log->SetVisAttributes(MgTubeAttr);
Mg_log2->SetVisAttributes(MgTubeAttr);

AlTubeAttr->SetVisibility(true);
AlTubeAttr->SetForceWireframe(true);
Al_log->SetVisAttributes(AlTubeAttr);
Al_log2->SetVisAttributes(AlTubeAttr);

AlWTubeAttr->SetVisibility(true);
AlWTubeAttr->SetForceWireframe(true);
AlW_log->SetVisAttributes(AlWTubeAttr);
AlW_log2->SetVisAttributes(AlWTubeAttr);

VacuumTubeAttr->SetVisibility(true);
VacuumTubeAttr->SetForceWireframe(true);
Vacuum_log->SetVisAttributes(VacuumTubeAttr);
Vacuum_log2->SetVisAttributes(VacuumTubeAttr);

InVacuumTubeAttr->SetVisibility(true);
InVacuumTubeAttr->SetForceWireframe(true);
InVacuum_log->SetVisAttributes(InVacuumTubeAttr);
InVacuum_log2->SetVisAttributes(InVacuumTubeAttr);

FDLWConeAttr->SetVisibility(true);
FDLWConeAttr->SetForceWireframe(true);
FDLW_log->SetVisAttributes(FDLWConeAttr);
FDLW_log2->SetVisAttributes(FDLWConeAttr);

FrontGeConeAttr->SetVisibility(true);
FrontGeConeAttr->SetForceWireframe(true);
frontGeCone_log->SetVisAttributes(FrontGeConeAttr);
frontGeCone_log2->SetVisAttributes(FrontGeConeAttr);

outDeadTubeAttr->SetVisibility(true);
outDeadTubeAttr->SetForceWireframe(true);
outDead_log->SetVisAttributes(outDeadTubeAttr);
outDead_log2->SetVisAttributes(outDeadTubeAttr);

GeTubeAttr->SetVisibility(true);
GeTubeAttr->SetForceWireframe(true);
Ge_log->SetVisAttributes(GeTubeAttr);
Ge_log2->SetVisAttributes(GeTubeAttr);

inDeadTubeAttr->SetVisibility(true);
inDeadTubeAttr->SetForceWireframe(true);
```

```
  inDead_log->SetVisAttributes(inDeadTubeAttr);
  inDead_log2->SetVisAttributes(inDeadTubeAttr);

  BoreholeTubeAttr->SetVisibility(true);
  BoreholeTubeAttr->SetForceWireframe(true);
  Borehole_log->SetVisAttributes(BoreholeTubeAttr);
  Borehole_log2->SetVisAttributes(BoreholeTubeAttr);


  return World_phys;
}
```

References

[1] [http://www.nndc.bnl.gov/chart/

[2] https://www-nds.iaea.org/relnsd/vcharthtml/VChartHTML.html

[Ago03] S. Agostinelli et al., Nuclear Instruments and Methods in Physics Research A, 506 (2003) 250-303

[Ass81] Π. Ασημακόπουλος, Εισαγωγή στην Πυρηνική Φυσική, Τόμος ΙΙ, Εκδόσεις Φάσμα, 1981

[Bag00] Coral M. Baglin, Nuclear Data Sheets for A=167*, Nuclear Data Sheets 90 431 (2000)

[Bag02] Coral M. Baglin, Nuclear Data Sheets for A=171, Nuclear Data Sheets 96 (2002) 399-610

[Bag12] Coral M. Baglin, Nuclear Data Sheets for A=92*, Nuclear Data Sheets 113 (2012) 2187-2389

[Bar72] A. Bari, 14.8 MeV neutron activation cross sections of rubidium, strontium, zirconium, niobium and rare-earth nuclides, Dissertation Abstracts B 32 (1972) 5091

[BW91] J. M. Blatt and V. F. Weisskopf, Theoretical nuclear physics, Dover Publications, Inc., New York, 1991.

[Col00] A. J. Cole, Statistical models for nuclear decay - from evaporation to vaporization, Fundamental and Applied Nuclear Physics Series, Institute of Physics Publishing, Bristol and Philadelphia, 2000.

[DH88] K. Debertin and R. G. Helmer, Gamma- and X-ray spectrometry with semiconductor detectors, North-Holland Press,1988

[DJ14] Yang Dong and Huo Junde, Nuclear Data Sheets for A=54, Nuclear Data Sheets 121 (2014) 1-142

[Dzy12] N. Dzysiuk, A. Kadenko, I. Kadenko, G. Primenko, Measurement and systematic study of (n,x) cross sections for dysprosium (Dy), erbium (Er) and ytterbium (Yb) isotopes at 14.7 MeV neutron energy, Phys. Rev. C 86 (2012) p 034609

[Fir07] R. B. Firestone, Nuclear Data Sheets for A=24, Nuclear Data Sheets 108 (2007) 2319-2392

[GH92] E. Gadioli and P. E. Hodgson, Pre- equilibrium nuclear reactions, Oxford Studies in Nuclear Physics, vol. 15, Clarendon Press, Oxford, New York, 1992.

[Hav71] E. Havlik, Messung von (n,p), (n,a) and (n,2n) Wirkungsquerschnitten an schweven

Kernen, Acta Physica Austriaca 34 (1971) 209

[IAE87] Handbook on nuclear activation data, Tech. Report 273, IAEA, Vienna, 1987.

[IRD14] International Reactor Dosimetry and Fusion File IRDFF v.1.05, 09 October, 2014

[Kal13] Μεταπτυχιακή Διπλωματική Εργασία, Καλαμαρά Αντιγόνη, "Εφαρμογή της αντίδρασης $^{3}H(d,n)^{4}He$ στην παραγωγή υψηλοενεργειακής δέσμης νετρονίων για τη μελέτη της αντίδρασης $^{241}Am(n,2n)^{240}Am$.", 2013

[Kno00] G. F. Knoll, Radiation detection and measurement, 3 ed., John Wiley and sons, Inc., New York, 2000.

[Kon98] X. Kong, Y. Wang, J. Yang, Cross sections for (n,2n), (n,p) and (n,a) reactions on rare-earth isotopes at 14.7 MeV, Appl. Radiat. Isot. 49 (1998) 1529

[Lak74] N. Lakshmana Das, C.V. Srinivase Rao, B.V. Thirumala Rao, J.R. Rao, Pre- compound decay in (n,2n) reactions at 14.2 MeV, 17. Nucl. and Solid State Physics Symp.,Bombay (1974) vol2 p105

[Lak78] N. Lakshmana Das, C.V. Srinivasa Rao, B.V. Thirumala Rao, J. Rama Rao, Ge(Li) measurement of some neutron activation cross-sections at (14.2 ± 0.2) MeV, Nuovo Cimento A 48 (1978) 500

[Lov02] G. Lövestam, EnergySet- a programme to calculate accelerator settings and neutron yield data for the IRMM VdG laboratory, Institute for Reference Materials and Measurements Internal Report No. GER/NP/2/2002/06/20 (2002).

[LT78] H. Liljavirta, T. Tuurnala, Cross Sections of Er isotopes for Neutron Induced Reactions at 14.8 MeV, Physica Scripta 18 (1978) 75-77

[Luo11] J. Luo, R. Liu, L. Jiang, Z. Liu, Cross sections for fast-neutron interaction with erbium isotopes, Journal of Radiaoanalytical and Nuclear Chemistry 289 (2011) 455-459

[Luo13] J. Luo, J. Liu, L. Jiang, R. Liu, S. Ge, Z. Liu, Measurement of $^{167}Er(n,p)^{167}Ho$ reaction at 13.5 and 14.8 MeV, Radiation Physics and Chemistry 92 (2013) 28-31

[Mar13] M. J. Martin, Nuclear Data Sheets for A=152*, Nuclear Data Sheets 114 (2013) 1497-1847

[Pat04] N. Patronis, S. Dababneh, P. A. Assimakopoulos, R. Gallino, M. Heil, F. Käppeler, D. Karamanis, P. E. Koehler, A. Mengoni, and R. Plag,Neutron capture studies on unstable ^{135}Cs for nucleosynthesis and transmutation, Phys. Rev. C **69**, 025803, 2004

[Pra69] P.R. Prasad, J.R. Rao, E.Kondaiah, Cross sections for (n,2n), (n,a) and (n,p) reactions in rare- earth isotopes at 14.2 MeV, Nuclear Physics A 125 (1969) 57-64

[PS71] R. Prasad and D.C Sarkat, Measured (n,p) reaction cross-sections and their predicted values at 14.8 MeV, Nuovo Cimento A 3 (1971) 467

[Qai74] S.M. Qaim, Total (n,2n) cross sections and isomeric cross section ratios at 14.7 MeV in the region of rare earths, Nucl. Physics A 224 (1974) 319

[Rei11] C. W. Reich, Nuclear Data Sheets for A=161*, Nuclear Data Sheets 112 (2011) 2497-2713

[Sak97] H. Sakane, H. Yamamoto, K. Kawade, I. Iida, A.Takahashi, Measurement of formation cross sections of short-lived nuclei by 14 MeV neutron, Nd, Sm, Dy, Er, Yb, (1997) JAERI-Conf. Japan

[WF60] R.G. Wille and R.W. Fink, Activation Cross Sections for 14.8 MeV Neutrons and some new Radioactive Nuclides in the Rare Earth Region, Physical Review 118 (1960) 242

[Xia07] Huang Xiaolong, Nuclear Data Sheets for A=196*, Nuclear Data Sheets 108 (2007) 1093-1286

[Zie08] J. F. Ziegler and J. P. Biersack, SRIM-2008. Available from http://www.srim.org.